Research Department

Technical Report No. 66

The calculation of geopotential and the pressure gradient in the ECMWF atmospheric model: influence on the simulation of the polar atmosphere and on temperature analyses

A.J. Simmons

Chen Jiabin *

ECMWF
LIBRARY
25 NOV 1992
No. C

* Current affiliation:
Institute of Atmospheric physics, Beijing, China

July 1990

Abstract

The spectral atmospheric model used for prediction at ECMWF is modified to change the spectrally-represented thermodynamic variable from temperature to the deviation of temperature from a reference profile which depends analytically on pressure. There is only a minor change to the form of the thermodynamic equation, and the calculation of the pressure gradient is modified to eliminate some of the cancellation between the $\nabla\varphi$ and $RT\nabla\ell np$ terms which occurs in the standard formulation. At T42 resolution the revised scheme significantly improves southern hemispheric forecasts, with differences originating over Antarctica. There is also a small improvement over the Arctic. Sensitivity is much less at T106 resolution, but a minor advantage can still be seen in high southern latitudes, and there is a reduction in noise in the vertical velocity field near the Andes at tropical latitudes.

The benefit of the revised scheme at high latitudes is also captured by a simpler revision which retains temperature as the spectrally-represented variable, and uses a reference temperature only in the computation of the pressure-gradient terms in gridpoint space. Results indicate that much of the systematic difference in behaviour between T42 and T106 simulations at high latitudes can be removed by changing the pressure-gradient calculation. In particular, the new schemes correct a systematic tendency for erroneously high pressures east of the Ross Ice Shelf over Antarctica in lower resolution simulations at medium and longer time ranges. Improvement occurs because the schemes reduce an inconsistent treatment of the $\nabla\varphi$ and $RT\nabla\ell np$ terms in the model's semi-implicit treatment of the vorticity equation.

A small beneficial impact of the revised pressure-gradient calculation is found in a two-day data-assimilation experiment at T106 resolution. A more substantial improvement comes from using the reference temperature to reduce a systematic error in the calculation of first-guess geopotential heights at standard pressure levels. The resulting height analyses agree slightly better with radiosonde measurements, and initialization causes less of a degradation of the fit to observed data. Temperatures are systematically warmer in the upper troposphere (by almost 0.5K in the global mean at 200hPa) and cooler in the lower troposphere, and are closer to observed values. Results from forecasts carried out after one and two days of assimilation show small improvements in the short and early medium range, and are inconclusive at longer time ranges.

Tests of the version with modified thermodynamic variable have also been carried out using p_s rather than ℓnp_s as the spectrally-represented pressure variable. The reference atmosphere is utilized to reduce the aliasing that occurs in a standard spectral formulation when p_s is used as the basic prognostic variable. The p_s scheme has the advantage of mass conservation, but the stability of the semi-implicit time-integration is somewhat reduced. Little impact is seen on the quality of medium-range forecasts or longer-term simulations.

CONTENTS

1. INTRODUCTION

Mountains exert a significant influence on atmospheric motion on a variety of scales. In the development of numerical models for weather prediction and the simulation of climate, much attention has been devoted in recent years to the better representation of the effects of unresolved orographic variations on the larger scales of motion, both through enhancement of the explicitly resolved orography, as in the "envelope" orography introduced by Wallace et al. (1983), and through parametrization of gravity-wave drag (Boer et al., 1984; Palmer et al., 1986). In addition, there has been continuing study of the numerical problems that arise in solving the primitive equations in regions in which the model orography slopes steeply. This report is concerned with the latter aspect.

The "sigma" coordinate, pressure normalized by its surface value, proposed by Phillips (1957) has become widely used in models as a way of conveniently incorporating variations in the height of the earth's surface. Its popularity is perhaps indicative of its general suitability, but the use of this and other terrain-following vertical coordinates is not without problems. Much attention has been devoted to achieving an accurate computation of the two terms which form the net pressure gradient in the horizontal momentum equations, and which are large and cancelling over steep mountain slopes (e.g. Kurihara, 1968; Corby et al., 1972; Gary, 1973; Sundqvist, 1976; Janjic, 1977; Nakamura, 1978; Simmons and Burridge, 1981; Mesinger, 1982; Arakawa and Suarez, 1983; Mesinger and Janjic, 1987). Cancellation can also occur between the "horizontal" and "vertical" advection of any variable which varies rapidly with height, such as specific humidity. An example is given by Simmons (1987). Among other problems, we note a potential for spurious convective orographic precipitation arising from application of "horizontal" diffusion of temperature along sloping coordinate surfaces (see also Simmons (1987) for an example). The use of hybrid coordinates which change from a terrain-following sigma-like coordinate at low levels to a pressure coordinate at upper tropospheric or stratospheric levels (e.g. Fels et al., 1980; Simmons and Burridge, 1981; Mechoso et al., 1982) offers some improvements, but problems remain at lower levels. A novel alternative approach based on "block" mountains whose heights are restricted to coincide with coordinate surfaces has been developed by Mesinger (1984) and Mesinger et al. (1988).

In this report we examine alternative formulations for the dynamical calculation within the spectral model developed for operational medium-range prediction at ECMWF (Simmons et al., 1989). Most results are presented for the hybrid coordinate used routinely with this model (Simmons and Burridge, 1981; Simmons and Strüfing, 1983), although some discussion is given for the sigma coordinate. The initial motivation for this study was to test further a scheme based on a spectral representation not of temperature, but of the

deviation of temperature from a reference temperature which is a particular analytic function of pressure, as proposed by Chen et al. (1987), based on the work of Zeng (1963, 1965). The new prognostic variable exhibits less variation along the terrain-following coordinate surfaces of the model than does temperature, and the pressure-gradient terms are rewritten to remove much of the cancellation between them. The scheme, which we refer to as the "TR" scheme, is described in the following section.

It will be seen later in the report that the TR scheme has a significant beneficial impact on the performance of the model at T42 horizontal resolution in the vicinity of Antarctica, and to a lesser extent at Arctic latitudes. The source of the improvement is the changed representation of the pressure gradient, and section 3 describes a much simpler scheme, referred to as the "PG" scheme. In this scheme the standard set of prognostic variables is used, but there is a revised calculation of the pressure-gradient terms which again makes use of a reference temperature profile, following in effect previous suggestions by Gary(1973) and Phillips(1973). A related revision to the post-processing of model-level variables to produce pressure-level geopotentials for use in data assimilation and in the dissemination and diagnosis of forecasts is presented in section 4.

Idealized tests of the TR and PG schemes are reported in section 5, and sections 6 and 7 present objective and subjective assessments of their performance in medium-range predictions using T42 and T106 resolutions, and in longer-term simulations using T42. Results from T106 data assimilation tests are presented in section 8.

It is usual in spectral models to use the natural logarithm of surface pressure, $\ell n p_s$, rather than surface pressure, p_s, as one of the spectrally represented prognostic variables. This is computationally convenient in sigma-coordinate models, but violates the mass-conservation that occurs if p_s is used as the basic variable (Gordon, 1981), and can give rise to problems in long-term integrations of spectral models unless corrected (see Laprise, 1985, for example). Use of p_s as a prognostic variable does, however, introduce a much more substantial aliasing in the calculation of the pressure gradient (Simmons, 1987). As part of the present study we have carried out a number of tests using p_s in conjunction with the alternative thermodynamic variable of the TR scheme. Results are presented in section 9, which is followed by a concluding discussion.

2. THE TR SCHEME

a) The prognostic variable

Temperature, T, is replaced as the basic spectrally represented variable by $\tilde{T}$, the deviation of temperature from a reference state of the form proposed by Chen et al. (1987):

$$\tilde{T} = T - T_o - T_1 (p/p_o)^{\kappa} \qquad (1)$$

Here p is pressure, p_o is a constant reference pressure, chosen to be 1013.2hPa, and κ denotes as usual R_d/C_{pd}, where R_d and C_{pd} are respectively the gas constant and specific heat at constant pressure for dry air. The values T_o and T_1 are specified in terms of reference values of temperature, T_{oo}, and lapse rate, Λ, at the reference surface pressure p_o:

$$T_1 = \frac{\Lambda T_{oo} C_{pd}}{g} \qquad T_o = T_{oo} - T_1$$

where g is the acceleration due to gravity. The values 288K and 6.5K(km)$^{-1}$ have been chosen for T_{oo} and Λ, which makes the reference temperature and its gradient match those of the ICAO(1964) reference atmosphere (see section 3) at pressure p_o.

It should be noted that the reference temperature profile does not exhibit any change in gradient to represent a stratosphere, and thus the vertical temperature gradient of the reference atmosphere will tend to be opposite in sign to that of the actual atmosphere at stratospheric levels. This has not been found to be a cause of serious problems in practice, but this may be in part because most of this study has been carried out using the hybrid vertical coordinate adopted routinely at ECMWF. This coordinate reduces continuously from sigma to pressure as the pressure decreases, and the reference profile exhibits little variation in the horizontal at upper levels. Zhang et al. (1990) discuss extensions of this scheme for more general reference states.

b) The thermodynamic equation

The thermodynamic equation, as applied in the standard version of the model, is written:

$$\frac{D\tilde{T}}{Dt} - \frac{\kappa T_v \omega}{(1+(\delta-1)q)p} = P_T + K_T \qquad (2)$$

where D/Dt denotes the usual material derivative, T_v is virtual temperature:

$$T_v = (1 + (\frac{1}{\varepsilon} - 1)q)\, T$$

q is specific humidity, $\omega = Dp/Dt$, ε is R_d/R_v and δ is C_{pv}/C_{pd}, where R_v and C_{pv} are the gas constant and specific heat for water vapour. P_T denotes the rate of change of temperature due to parametrized processes and K_T the change due to horizontal diffusion.

With the new variable defined by (1), there is only a marginal increase in complexity of this equation:

$$\frac{D\tilde{T}}{Dt} - \frac{\kappa\omega}{p}\left(T_0 + \tilde{T} + \frac{qT(\frac{1}{\varepsilon} - \delta)}{1+(\delta-1)q}\right) = P_T + K_{\tilde{T}} \qquad (3)$$

In particular, there is no increase in aliasing when a conventional spectral transform method is used to solve (3) instead of (2). The vertical discretization applied to (3) directly parallels that applied to (2) (Simmons and Burridge, 1981), with T replaced by $\tilde{T}$ in the vertical advection term, and $T_v/(1+(\delta-1)q)$ replaced by $T_0 + \tilde{T} + qT(\frac{1}{\varepsilon} - \delta)/(1+(\delta-1)q)$ in the energy conversion term.

c) The pressure gradient

The geopotential, φ, is given by

$$\varphi = \varphi_s + \int_p^{p_s} \frac{R_d T_v}{p}\, dp \qquad (4)$$

where φ_s is the surface geopotential. Defining $\tilde{T}_v$ by

$$\tilde{T}_v = \tilde{T} + (\frac{1}{\varepsilon} - 1)\, Tq = T_v - T_0 - T_1 (p/p_0)^{\kappa} \qquad (5)$$

the pressure gradient

$$\nabla(\varphi_s + \int_p^{p_s} \frac{R_d T_v}{p}\, dp) + R_d T_v \nabla \ell np \qquad (6)$$

can be rewritten as

$$\nabla(\varphi_s + \int_p^{p_s} \frac{R_d \tilde{T}_v}{p}\, dp) + R_d \tilde{T}_v \nabla \ell np +$$

$$+ R_d \nabla \{\int_p^{p_s} \frac{1}{p} (T_0 + T_1 (p/p_0)^{\kappa})\, dp\} + \frac{R_d}{p} (T_0 + T_1 (p/p_0)^{\kappa}) \nabla p$$

or

$$\nabla(\tilde{\varphi}_s + \int_p^{p_s} \frac{R_d \tilde{T}_v}{p}\, dp) + R_d \tilde{T}_v \nabla \ell n p \qquad (7)$$

where

$$\tilde{\varphi}_s = \varphi_s + R_d T_o \ell n\, p_s/p_o + C_{pd} T_1 ((p_s/p_o)^\kappa - 1) \qquad (8)$$

Equation (8) can also be written

$$\tilde{\varphi}_s = R_d T_o \ell n\, (p_s/p_{sr}) + C_{pd} T_1 ((p_s/p_o)^\kappa - (p_{sr}/p_o)^\kappa) \qquad (9)$$

where

$$\varphi_s + R_d T_o \ell n\, (p_{sr}/p_o) + C_{pd} T_1 ((p_{sr}/p_o)^\kappa - 1) = 0 \qquad (10)$$

p_{sr} is the surface pressure which ensures a balanced state for the reference atmosphere $T_o + T_1 (p/p_o)^\kappa$ in the presence of a surface geopotential φ_s.

The discretization of (7) in the TR scheme is carried out in exactly the same way as (6) in the standard model. There is here, however, some additional aliasing in the calculation of the spectral components of $\tilde{\varphi}_s$. When $\ell n p_s$ is the spectrally represented pressure variable, this aliasing is small, since (8) can be written

$$\tilde{\varphi}_s = \varphi_s + R_d (T_o + T_1) \ell n\, (p_s/p_o) + \tfrac{1}{2} C_{pd} T_1 (\kappa \ell n (p_s/p_o))^2 + O((\kappa \ell n (p_s/p_o))^3)$$

and only the $O((\kappa \ell n (p_s/p_o))^3)$ term will be aliased. Aliasing is much larger, however, when p_s is the prognostic variable, it being transferred from the $\frac{R_d T_v}{p} \nabla p$ term in the usual spectral approach to the $\nabla \varphi_s$ term in the TR scheme.

Much of the aliasing has been removed by introducing a small modification to φ_s. Let φ_{sg} denote the grid-point values of the basic, spectrally fitted orography. The equation

$$\varphi_{sg} + R_d T_o \ell n\, (p_{sg}/p_o) + C_{pd} T_1 ((p_{sg}/p_o)^\kappa - 1) = 0$$

is solved iteratively for p_{sg}. Modified values of p_{sg}, the p_{sr} values to be used in form (9), are computed by first performing a spectral fit of either ℓnp_{sg} or p_{sg} (depending on the choice of ℓnp_s or p_s as spectral variable) and by then reevaluating grid-point values of surface pressure from the spectral fit. Finally, the value of φ_s to be used in (8) is determined as

$$\varphi_s = - R_d T_o \ell n (p_{sr}/p_o) - C_{pd} T_1 ((p_{sr}/p_o)^\kappa - 1)$$

Using the operational T106 ECMWF orography for φ_{sg}, the modified surface geopotential φ_s hardly differs from φ_{sg} when ℓnp_s is the prognostic variable. The maximum height difference is under 2m, and occurs over the Himalayas. A maximum difference of just under 30m is found in the same region when p_s is the prognostic variable.

The modification of φ_s may be unnecessary in practice, since initialization of model fields will lead to small adjustments in surface pressure which will largely balance the pressure gradient terms. These adjustments are estimated from the above height changes to be of the order of 0.2hPa for ℓnp_s as variable, and 3hPa for p_s. Further discussion is given by Simmons(1987) in the context of using p_s as the prognostic variable in an otherwise conventional spectral formulation.

d) Calculation of $(p/p_o)^\kappa$ and $\frac{\partial T}{\partial t}$

Values of $(p/p_o)^\kappa$ are needed in the model to compute T from $\tilde{T}$ for virtual temperature terms in the dynamical equations and for input to parametrization schemes. We write

$$(p/p_o)^\kappa = e^{\kappa(\ell np - \ell np_o)}$$

and evaluate this at model level k (k>1) using

$$\ell np_k = (\frac{\partial}{\partial p} (p \ell np) - 1)_k$$

$$= \frac{1}{\Delta p_k} (p_{k+½} \ell np_{k+½} - p_{k-½} \ell np_{k-½}) - 1 \qquad (11)$$

where $p_{k+½}$ is the pressure at the half-level k+½ and $\Delta p_k = p_{k+½} - p_{k-½}$. This form is consistent with the expressions for $\nabla \ell np_k$ and ω used in the model (Simmons and Burridge, 1981). For the uppermost level we set $p_1 = \frac{1}{2} p_{1½}$.

In addition, values of $\frac{\partial T}{\partial t}$ are needed for input to the parametrization schemes. The dynamical calculation provides values of $\frac{\partial \tilde{T}}{\partial t}$, and we use the relation

$$\frac{\partial T}{\partial t} = \frac{\partial \tilde{T}}{\partial t} + \kappa T_1 (p/p_o)^{\kappa} \frac{\partial \ell np}{\partial p_s} \frac{\partial p_s}{\partial t}$$

Here $\partial \ell np/\partial p_s$ is computed in the same way as in the evaluation of the pressure gradient term, using (11):

$$\left(\frac{\partial \ell np}{\partial p_s}\right)_k = \frac{\partial}{\partial p_s} \left\{ \frac{p_{k+\frac{1}{2}} \ell np_{k+\frac{1}{2}} - p_{k-\frac{1}{2}} \ell np_{k-\frac{1}{2}}}{\Delta p_k} \right\}$$

$$= \frac{1}{\Delta p_k} \left\{ (B_{k+\frac{1}{2}} - B_{k-\frac{1}{2}}) + \frac{A_{k+\frac{1}{2}} B_{k-\frac{1}{2}} - A_{k-\frac{1}{2}} B_{k+\frac{1}{2}}}{\Delta p_k} \ell n \frac{p_{k+\frac{1}{2}}}{p_{k-\frac{1}{2}}} \right\}$$

where the $A_{k+\frac{1}{2}}$ and $B_{k+\frac{1}{2}}$ define the pressure $p_{k+\frac{1}{2}}$ in terms of the surface pressure:

$$p_{k+\frac{1}{2}} = A_{k+\frac{1}{2}} + B_{k+\frac{1}{2}} p_s$$

e) Horizontal diffusion

In the standard ECMWF model a linear ∇^4 horizontal diffusion of variables is applied in spectral space. The diffusion of temperature is modified by a term involving ℓnp_s to approximate a diffusion not of temperature but of the deviation of temperature from a reference atmosphere (Simmons, 1987). Thus, in the TR scheme we simply apply the fourth order diffusion to the spectrally represented variable $\tilde{T}$.

f) The semi-implicit scheme

The semi-implicit time integration scheme for the standard model makes use of an isothermal basic-state temperature to define the linearized gravity-wave terms to be treated implicitly. Working with the corresponding linearized form of the discretized equations for the TR scheme would have introduced additional calculation similar to that involved in introducing a vertically varying basic-state temperature into the standard scheme. Rather than do this, the operators used in the standard semi-implicit scheme are modified as indicated below.

The linearized gravity-wave equations for the standard model are:

$$\frac{\partial D'}{\partial t} = - \nabla^2 (\gamma T' + \delta(\ell n p_s)')$$

$$\frac{\partial T'}{\partial t} = - \tau D'$$

$$\frac{\partial(\ell n p_s)'}{\partial t} = - \nu D'$$

Reference should be made to Simmons et al. (1989) for a definition of the terminology, and to Simmons and Burridge (1981) for a specification of the matrices γ and τ, and row and column vectors ν and δ.

In the above equations, T' denotes the first-order deviation of temperature from an isothermal basic-state value, and if $\bar{T}'$ is the corresponding deviation of $\bar{T}$ from its basic-state value, then from (1),

$$\bar{T}' = T' - \sigma(\ell n p_s)'$$

where

$$\sigma = p_r \kappa T_1 \left[(p/p_0)^{\kappa} \frac{\partial \ell n p}{\partial p_s} \right]_{p_s = p_r}$$

and p_r is the constant surface pressure of the basic state. The first two gravity-wave equations become:

$$\frac{\partial D'}{\partial t} = - \nabla^2 (\gamma \bar{T}' + (\delta + \gamma\sigma) (\ell n p_s)')$$

and

$$\frac{\partial \bar{T}'}{\partial t} = - (\tau - \sigma\nu) D'$$

The semi-implicit time scheme for the TR scheme is thus given as for the standard model (Simmons et al., 1989), but with τ replaced by τ-$\sigma\nu$ and δ by δ+$\gamma\sigma$. In the above equations, $(\ell n p_s)'$ is replaced by p_s'/p_r to obtain the scheme when p_s is the spectrally represented variable.

g) Conservation properties

The vertical finite-difference scheme of Simmons and Burridge(1981), as used in the standard model, conserves angular momentum, although this conservation is formally lost when the spectral horizontal discretization is introduced. The similarity in form of (6) and (7) implies that the same is true for angular momentum conservation in the TR scheme.

The vertical discretization of the standard model also conserves the sum of kinetic and potential energies for adiabatic motion. The vertical advection of temperature is treated in such a way as to conserve the integral of the square of temperature, the finite-difference scheme preserving the continuous relation:

$$\int_0^1 T\dot{\eta}\,\frac{\partial T}{\partial \eta}\,\frac{\partial p}{\partial \eta}\,d\eta + \int_0^1 \frac{1}{2}\,T^2\,\frac{\partial}{\partial \eta}\,(\dot{\eta}\,\frac{\partial p}{\partial \eta})\,d\eta = 0$$

where η is the vertical coordinate and $\dot{\eta} = \frac{D\eta}{Dt} = 0$ at the boundaries η=0 and η=1. Because of the above properties, the vertical discretization of the TR scheme conserves the sum of kinetic energy and an available potential energy, in the sense shown below.

The momentum equations for the TR scheme are identical to those of the standard scheme, but with T_v replaced by $\tilde{T}_v$ and φ_s by $\tilde{\varphi}_s$. The adiabatic form of the thermodynamic equation, neglecting the small terms involving specific humidity, is (from Eq.(3))

$$\frac{D\tilde{T}}{Dt} = \frac{\kappa\omega}{p}\,(T_0 + \tilde{T})$$

which can be written

$$\frac{D}{Dt}\,(\frac{1}{2}\,\frac{C_{pd}\tilde{T}^2}{T_0}) = \frac{R_d\omega\tilde{T}}{p} + \frac{R_d\omega\tilde{T}^2}{pT_0} \qquad (12)$$

The corresponding form for the standard scheme is

$$\frac{D}{Dt}\,(C_{pd}\,T) = \frac{R_d\omega T}{p}$$

Thus, given the conservation properties of the standard scheme, if the second term on the right hand side of (12) can be neglected in comparison with the first (i.e. if $|\tilde{T}| << T_0$),

the vertical differencing in the TR scheme respects an energy conservation in the form

$$\frac{\partial}{\partial t}\left[\int\left(\int_0^1 \frac{1}{2}\left(u^2+v^2+\frac{C_{pd}\tilde{T}^2}{T_o}\right)\frac{\partial p}{\partial \eta}\,d\eta\right)dA\right] + \int \varphi_s \frac{\partial p_s}{\partial t}\,dA = 0$$

or

$$\frac{\partial}{\partial t}\left[\int\left(\int_0^1 \frac{1}{2}\left(u^2+v^2+\frac{C_{pd}\tilde{T}^2}{T_o}\right)\frac{\partial p}{\partial \eta}\,d\eta\right)dA\right] +$$

$$+\int\left(p_s \varphi_s + p_s\left\{R_d T_o\left(\ell n(p_s/p_o) - 1\right) + C_{pd} T_1\left(\frac{1}{\kappa+1}\left(p_s/p_o\right)^{\kappa} - 1\right)\right\}\right)dA$$

where u and v are the usual horizontal velocity components, and $\int$ ( )dA denotes an integral over the globe. The term

$$\int\left(\int_0^1 \frac{1}{2}\,\frac{C_{pd}\tilde{T}^2}{T_o}\,\frac{\partial p}{\partial \eta}\right)dA$$

can be recognized as equivalent in form to the classically defined available potential energy of Lorenz (1955). The reference temperature, T_{ref}, is given by

$$T_{ref} = T_o + T_1\left(p/p_o\right)^{\kappa}$$

and has a lapse rate, Γ_{ref}, given by $\Gamma_{ref} = \Gamma_d - \frac{g}{C_{pd}}\,\frac{T_0}{T_{ref}}$

where $\Gamma_d = \frac{g}{C_{pd}}$. Thus the term $\frac{1}{2}\,\frac{C_{pd}\,\tilde{T}^2}{T_0}$ can be written in the more familiar form given by Lorenz:

$$\frac{C_{pd}}{2}\left(\frac{\Gamma_d}{\Gamma_d - \Gamma_{ref}}\right)\frac{\tilde{T}^2}{T_{ref}}$$

3. THE PG SCHEME

The PG scheme was designed to reproduce the principal beneficial effect of the TR scheme with the minimum change to the standard model. There is no change from the standard model in the basic spectrally represented variables, and the only change (apart from a post-processing change discussed in the following section) is in the calculation of the pressure gradient. A deviation virtual temperature $\approx{T}_v$ is computed in grid-point space as

$$\approx{T}_v = T_v - T_{oo}\,(p/p_o)^{\alpha} \qquad (13)$$

where $\alpha = \dfrac{\Lambda R_d}{g}$ and p_o, T_{00} and Λ take the same values as for the TR scheme. The reference temperature used here is based on the tropospheric part of the ICAO(1964) standard atmosphere, and has a uniform lapse rate Λ. It is identical in value and lapse rate at $p = p_o$ to the reference atmosphere of the TR scheme, and differs little from the TR reference state at other tropospheric levels, the difference at 200hPa being 5.4K. The form (13) was chosen for the PG scheme as it gives a simpler computation for the geopotential term. The particular advantage of form (1) for the TR scheme is its simple modification of the thermodynamic equation. The term $(p/p_o)^{\alpha}$ in (13) is computed in the same way as the $(p/p_o)^{\kappa}$ term in the TR scheme.

Following the TR scheme, the pressure gradient (6) is replaced by the form

$$\nabla\Big(\approx{\varphi}_s + \int_p^{p_s} \frac{R_d \approx{T}_v}{p}\,dp\Big) + R_d \approx{T}_v \nabla \ell np \qquad (14)$$

where

$$\approx{\varphi}_s = \varphi_s + \frac{R_d T_{oo}}{\alpha}\left(\frac{p_s}{p_o}\right)^{\alpha} \qquad (15)$$

The surface geopotential φ_s in (15) is as used in the standard version of the model.

4. THE POST-PROCESSING OF GEOPOTENTIAL

Model variables are "post-processed" to provide output fields on standard pressure levels which are used as first-guess fields in data assimilation and for the dissemination and diagnosis of forecasts. In particular, the data assimilation makes use of postprocessed geopotential heights, and the calculation of these has been modified in a way similar to the changed dynamical calculation of φ.

The method adopted in the standard model comprises first integration of the hydrostatic equation to derive half-level values of geopotential:

$$\varphi_{k-½} = \varphi_{k+½} + R_d\,(T_v)_k\,\ell n\,\frac{p_{k+½}}{p_{k-½}}$$

$$\varphi_{NLEV-½} = \varphi_s + R_d\,(T_v)_{NLEV}\,\ell n\,\frac{p_s}{p_{NLEV-½}}$$

The half-level values of φ are then interpolated to pressure levels. We write this symbolically as

$$\varphi(p) = \varphi_s + \gamma_p\,T_v$$

For the schemes examined here, we first examined a treatment directly following that used in the calculation of the pressure gradient terms. For the TR scheme,

$$\tilde{T}_v = T_v - T_o - T_1\,(p/p_o)^\kappa$$

$$\varphi(p) = \varphi_s + R_d\,T_o\,\ell n\,(p_s/p) + C_{pd}\,T_1\,((p_s/p_o)^\kappa - (p/p_o)^\kappa) + \gamma_p\,\tilde{T}_v$$

and for the PG scheme,

$$\tilde{\tilde{T}}_v = T_v - T_{oo}\,(p/p_o)^\alpha$$

$$\varphi(p) = \varphi_s + \frac{R_d T_{oo}}{\alpha}\,((p_s/p_o)^\alpha - (p/p_o)^\alpha) + \gamma_p\,\tilde{\tilde{T}}_v$$

5. IDEALIZED TESTS

a) Cancellation between the pressure-gradient terms

Several idealized calculations of error in the evaluation of pressure-gradient terms have been carried out to compare the TR and PG schemes with the standard ECMWF scheme, which we label as the "control" in the following figures. To do such calculations, we define a dry atmosphere at rest with an analytically prescribed temperature profile which is a function of pressure alone, and which is of a form such that the balanced surface pressure can be computed analytically given the basic model orography φ_{sg}. The temperature field is evaluated at model grid-points for each model level, and the reference temperature is subtracted in the case of the TR scheme. The resulting model-level fields, together with ℓnp_s or p_s as appropriate, are fitted spectrally. They are then supplied as initial conditions to an adiabatic version of the model (in its standard, TR or PG formulation). The magnitudes of the initial tendencies of divergence and vorticity in the model provide measures of error in the numerical calculation of the net pressure-gradient term $\nabla\varphi + R_d T \nabla \ell np$, which vanishes for the exact solution. The operational hybrid coordinate, 19-level T106 resolution and orography were used for the tests shown here, unless otherwise stated.

Results are presented in Fig. 1 for the analytical temperature distribution given by the ICAO standard atmosphere as used with the PG scheme, with the isothermal stratosphere as used in the post-processing of geopotential. The definition of the PG and TR schemes means that this is not an unbiased test. For the PG scheme there would be no tropospheric pressure-gradient error were it not for the spectral fitting of the initial conditions, although the similarity shown below between the PG and standard schemes in fact suggests that this spectral fitting is the major source of error, rather than the vertical discretization. Results for two other temperature distributions will be presented subsequently.

The upper-left panel of Fig. 1 displays the magnitude of the maximum erroneous divergence tendency calculated separately for each model level over all points of the computational grid. The initial grid-point tendencies were first fitted spectrally, and then re-evaluated at model grid-points. The standard and TR schemes are compared, and for the TR scheme results are presented both for the full scheme as used in the forecast experiments to be reported subsequently, and for a version in which the surface geopotential φ_s was not modified to cancel aliasing (labelled "Unmodified phis"). The prognostic pressure variable is ℓnp_s. The solid curve denotes results from the standard scheme. As pressure decreases, the divergence tendency decreases to a minimum just below the tropopause, and there is then a sharp increase in error in moving from the troposphere to the stratosphere

When tested using analyzed atmospheric data (and the operational distribution of 19 levels in the vertical: see Simmons et al., 1989), differences were found to be only a few metres at tropospheric and lower stratospheric levels, but they increased sharply above 50hPa, approaching 100m at 10hPa. Tests of the type presented in the following section indicated that the new schemes were the more accurate in the troposphere, but were subject to severe error in post-processed heights for levels near the top of the model.

The large stratospheric differences were essentially independent of horizontal position, and were due to the stratospheric decrease of the reference temperatures as pressure decreases. For an isothermal stratosphere the standard scheme yields exact stratospheric thicknesses between half levels, and this exactness is lost when the reference atmosphere is introduced. It has already been noted that this is of little significance for the model dynamics, since differences become independent of horizontal position as pressure decreases, in the case of hybrid coordinates.

As a remedy, and for the purpose of post-processing only, the reference atmospheres were modified to be isothermal above pressure p_T. For pressures greater than p_T, the above expressions for $\tilde{T}_v$, $\approx{T}_v$ and $\varphi(p)$ are unchanged. For the TR scheme, p_T=200hPa, and for $p<p_T$,

$$\tilde{T}_v = T_v - T_T$$

$$T_T = T_o + T_1 (p_T/p_o)^{\kappa}$$

and

$$\varphi(p) = \varphi_s + R_d T_o \ell n (p_s/p_T) + C_{pd} T_1 ((p_s/p_o)^{\kappa} - (p_T/p_o)^{\kappa}) +$$

$$+ R_d T_T \ell n (p_T/p) + \gamma_p \tilde{T}_v$$

For the PG scheme, we choose p_T to give a stratospheric temperature, T_T, of 216.5K, this corresponding to the ICAO standard tropopause height of 11km. In this case, for $p<p_T$ we have

$$\approx{T}_v = T_v - T_T$$

and

$$\varphi(p) = \varphi_s + \frac{R_d T_{oo}}{\alpha} ((p_s/p_o)^{\alpha} - (p_T/p_o)^{\alpha}) + R_d T_T \ell n (p_T/p) + \gamma_p \approx{T}_v$$

(between levels 9 and 7). The reason for the latter is discussed by Sundqvist (1976). The dotted curve is for the TR scheme without modification of φ_s. In this case errors are lower near the ground and in the stratosphere than is the case for the standard model, and larger in the middle and upper troposphere. The dashed curve is the result for the full TR scheme. The reduction in error due to the adjustment of φ_s can be clearly seen.

The upper right-hand panel of Fig. 1 shows the corresponding result when p_s is the spectrally-fitted pressure variable. Also included here for reference is a repetition of the curve for ℓnp_s as variable for the standard model. The change in scale should be noted. Using p_s as the basic variable results in a large erroneous divergence tendency for both the standard scheme and the TR scheme with no modification of φ_s. Using the modified φ_s, the error is reduced substantially, to values lower than those from the standard ℓnp_s scheme for this particular temperature distribution.

The middle panels of Fig. 1 compare the standard, PG and full TR schemes, showing tendencies of vorticity as well as divergence. For both fields, the performance of the PG scheme approximates that of the standard scheme in the troposphere, and that of the TR scheme in the stratosphere. The reduced tropospheric error of the TR scheme holds for vorticity as well as divergence. All schemes produce a similar peak in the vorticity tendency around the tropopause (which comes only from the $R_d T \nabla \ell np$ term).

The lower panels present corresponding results for the sigma coordinate with levels defined to coincide with those of the hybrid coordinate at the surface pressure of 1013.2hPa. The generally larger erroneous divergence tendency in the stratosphere is as shown by Simmons and Burridge (1981). In the troposphere, results for divergence are much as found for the hybrid coordinate, apart from there being less of a decrease of error with increasing height. The sharp increase in error near the top of the model that can be seen for the TR and PG sigma-coordinate schemes arises because of the unrepresentative stratospheric decrease in reference temperature discussed earlier. For the sigma coordinate there is a particularly large spurious vorticity tendency at the tropopause (note the change in scale), although the tendency vanishes identically in the isothermal stratosphere for the standard scheme. The large values are spread over more levels than the corresponding, weaker peak for the hybrid coordinate because more model levels intersect the tropopause for the sigma coordinate.

Results for two other temperature distributions are presented in Fig. 2. The upper panels are for a profile comprising two segments in which the variation of temperature is linear in ℓnp; the profile is as illustrated and used in idealized testing by Simmons and Burridge (1981). The lower panel relates to a profile which is closer to conditions in very high latitudes, and results are presented only for maximum tendencies computed poleward

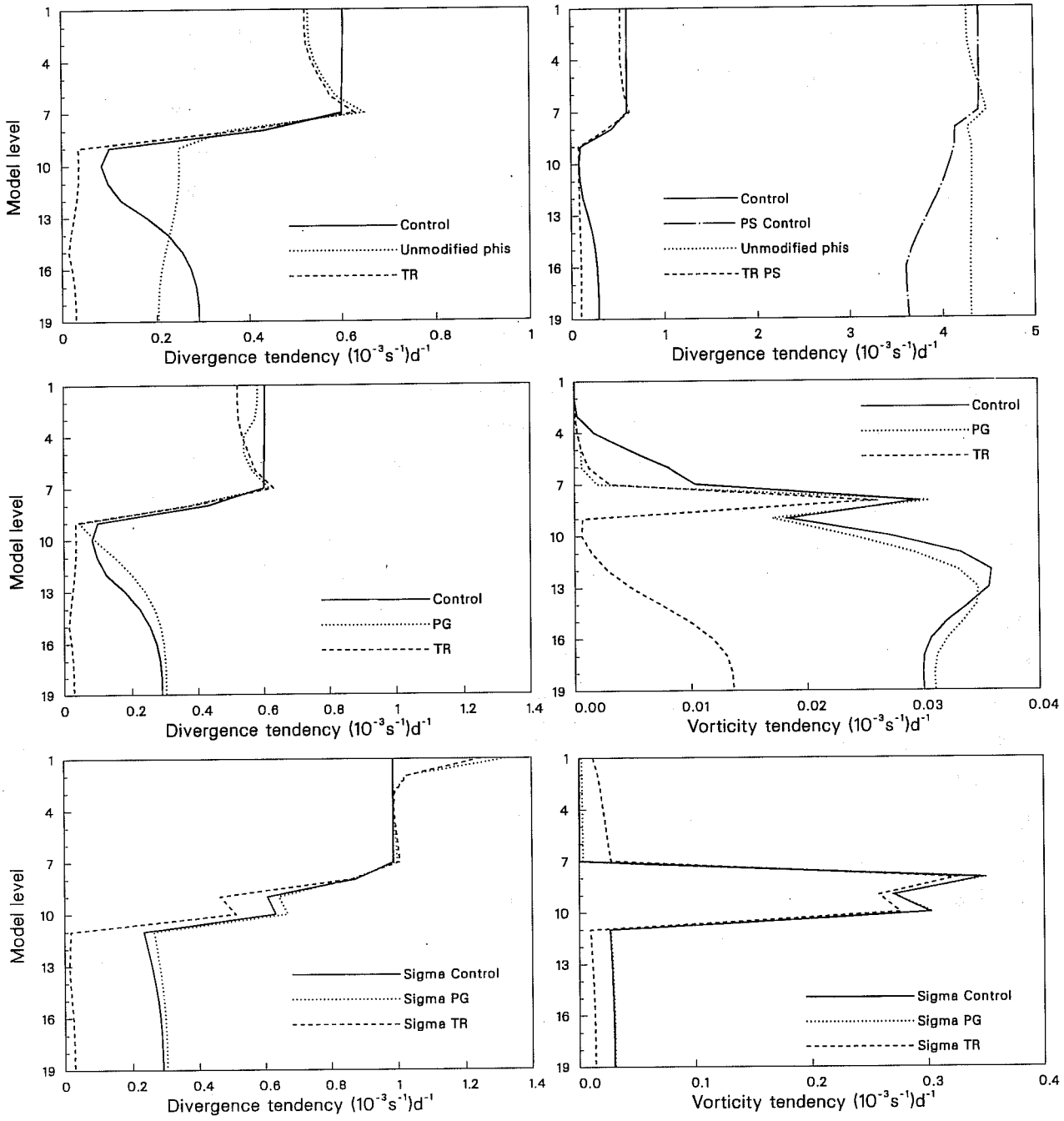

Fig. 1 Maximum spurious tendencies of divergence and vorticity for each model level, calculated for the ICAO standard atmosphere, using various model versions as specified in each panel.

of latitude 60° in the two hemispheres. The ICAO temperature distribution is modified so that T_{oo}=268K, T_T=200K, and the atmosphere is isothermal below 850hPa. Results are presented for the standard, PG and TR schemes, for both ℓnp_s and p_s as prognostic variable in the latter case.

The first point to note from Fig. 2 is that error is generally larger with the p_s scheme. This is confirmed by calculations for other temperature distributions. Comparison with Fig. 1 indicates that error is still less than in the absence of any adjustment of φ_s to reduce aliasing. However, the particularly low error seen in Fig. 1 for the full p_s scheme is a particular consequence of a close match between the reference temperature assumed by the scheme and the ICAO temperature distribution used in the test.

The logarithmic temperature distribution has a stratosphere in which the temperature increases with height, and for this distribution the TR and PG schemes exhibit slightly larger errors than does the standard scheme. There is also substantial sensitivity in the low-level vorticity tendency. For the "polar" profile these tendencies are particularly large, and are associated with the lapse-rate change at 850hPa. These large values are analogous to the large tropopause values shown for the sigma coordinate in Fig. 1; when a lapse rate change occurs at low levels there is little advantage of the hybrid over the sigma coordinate. The PG and standard schemes are particularly close for the "polar" profile at low levels.

The distribution of error in the horizontal has also been studied. Maximum values are larger in amplitude for the higher resolution, but (not surprisingly) smaller in scale. Over Antarctica they are more confined to the edge of the plateau. There is no outstanding difference between the standard and PG schemes. These results give no obvious hint of the striking sensitivity found in the forecast experiments to be presented subsequently.

b) Stability of the semi-implicit time scheme

The semi-implicit time differencing adopted for the TR and PG schemes differs from that for the standard scheme in that it is not based on a linearization of the discretized equations of the particular scheme for small-amplitude gravity-wave motion about a basic state at rest, but is based instead on a linearization of the discretized equations of the standard scheme. Stability properties of the time differencing have thus been examined for the TR and PG schemes in the way set out for the standard scheme by Simmons et al. (1989). A sample of results is presented in Table 1. For the cases shown, the isothermal basic-state temperature used in the scheme was 300K and the basic-state surface pressure was 800hPa. These are the values routinely used in the standard scheme. The "actual" temperature profile for which stability was examined is that based on logarithmic functions of pressure used by Simmons and Burridge (1981) and for the preceding pressure-gradient

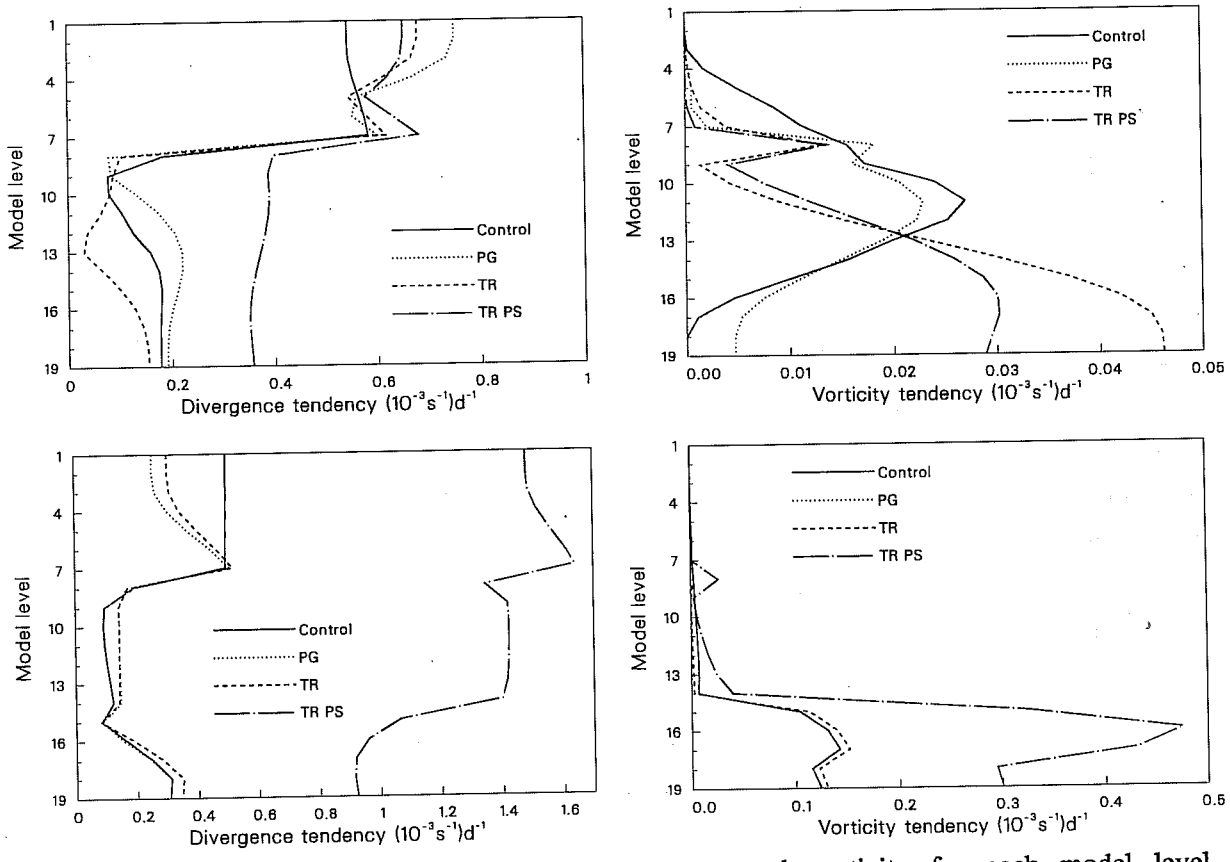

Fig. 2 Maximum spurious tendencies of divergence and vorticity for each model level, for the logarithmic (upper) and "polar" (lower) temperature profiles specified in the text.

calculations of Simmons et al. (1978). When p_s is used as the spectrally-fitted variable with the TR scheme, the semi-implicit time-differencing is stable for longer timesteps where the surface pressure is small. However, instability occurs in this case for some of the timesteps examined with an actual surface pressure of 1013.2hPa, for β=.75, although the unstable timesteps are longer than the 15 minutes used routinely for T106 resolution. A more severe instability is found at low surface pressures for a tropical temperature profile.

In practice, no case of instability has been found for the PG scheme or the TR scheme with ℓnp_s as the prognostic variable, using the standard ECMWF values of ε and β. The same is true of all T42 forecasts using the TR scheme with prognostic variable p_s. However, out of six corresponding T106 forecasts, three (May, July and September cases) were unstable. Forecasts for the latter cases were carried out successfully to day 10 using the semi-implicit scheme with β=1.

c) Accuracy of post-processed height fields

The accuracy of post-processed heights has been assessed using analytical temperature profiles for which exact heights at standard pressure levels can be found. As in the idealized calculation of pressure-gradient error, 19-level T106 datasets are constructed for a dry atmosphere at rest. The analytically-prescribed temperature profile (a function of pressure alone) is used to compute the balanced surface pressure at model grid-points, for the model orography used operationally. Once the surface pressure is known, the temperatures on model coordinate surfaces are computed, and fields are spectrally fitted. The datasets are then post-processed, and standard-level geopotentials are compared with corresponding analytically-computed values.

The post-processing used to obtain the results described below was the usual ECMWF scheme, which includes a spectral fit and packing of the standard-level data. Tests indicate that this makes a contribution to the net error which is small compared to the error introduced by the numerical integration of the hydrostatic equation and subsequent interpolation from model to pressure levels. The post-processing also includes extrapolation under the model orography. To avoid any significant effect of this, results are shown only for the 700hPa level and above.

Root mean square and mean errors have been computed over the globe for a number of temperature profiles, using the standard ECMWF scheme and the TR and PG schemes. Errors are dominated by the mean component, and the TR and PG schemes give similar results overall. Mean errors at standard pressure levels for the standard and PG schemes are shown in the upper panels of Fig. 3 for two temperature profiles. The left-hand panel is for the ICAO standard atmosphere, with isothermal stratosphere, and in this case the PG

calculations. Results are presented for three values of the actual surface pressure, for two values of the time filter ε, and for two values of the parameter β which determines the extent to which the central time level is included in the calculation of the linearized gravity-wave terms (ε=0.1 and β=0.75 in routine application of the model, and for most tests presented subsequently; β=1 corresponds to the classical semi-implicit scheme). Reference should be made to Simmons et al. (1989) for further detail.

It can be seen for the cases shown in Table 1 that the stability properties of the TR and PG schemes, with $\ell n p_s$ as the spectrally-fitted variable, are at least as good as those of the standard scheme, and rather better where the surface pressure is low. Similar conclusions are drawn for actual temperature profiles more representative of the tropics and polar regions. Instability occurs for rather shorter timesteps for the polar profile, and only for longer timesteps for the tropical profile, in accord with the original stability

	Standard Scheme				PG Scheme			
p_s (hPa)	β=1 ε=.1	β=.75 ε=.1	β=1 ε=.01	β=.75 ε=.01	β=1 ε=.1	β=.75 ε=.1	β=1 ε=.01	β=.75 ε=.01
1013.2	St	St	St	St	St	St	St	St
750	St	St	St	45	St	St	St	St
500	18	15	9	6	30	33	9	6

	TR Scheme				TR Scheme (p_s)			
p_s (hPa)	β=1 ε=.1	β=.75 ε=.1	β=1 ε=.01	β=.75 ε=.01	β=1 ε=.1	β=.75 ε=.1	β =1 ε=.01	β=.75 ε=.01
1013.2	St	St	St	St	St	39	St	24
750	St	St	St	St	St	St	St	St
500	24	24	12	9	St	St	36	36

Table 1 Stability of the semi-implicit time scheme. St denotes stability for all timesteps examined, and unstable cases are denoted by the smallest timestep (in minutes) for which instability is found for wavenumber 106. Analyses were carried out for timesteps in the range of 3 to 45 minutes, using a 3-minute interval.

scheme would give no error were it not for spectral fitting and packing. This is reflected in the low mean error seen at all levels for the PG scheme. The panel to the right is for the logarithmic profile utilized for the calculations shown in the preceding subsections. In this case the temperature increases with height in the stratosphere, and there is a quite substantial error of 25 to 30m at 10hPa (the top model level) for all schemes. Generally, no clear signal emerges from these calculations as to which of the schemes gives lower errors in the stratosphere.

Conversely, the PG and TR schemes give significantly lower errors for the troposphere. In particular, over the oceans and low-lying land the standard scheme has heights around 3 to 5 metres too low in the middle and upper troposphere. Corresponding error maps show horizontal variations of up to about 2m. These are related to the presence of orography, which causes variations in post-processing error because of variations in the distribution of pressure on model coordinate surfaces. The tropospheric post-processing biases essentially disappear with the TR and PG schemes, which suggests an advantage to these schemes when used in data assimilation to produce first guesses at standard pressure levels. Further discussion of this is given in section 8.

The lower panels of Fig. 3 show further calculations of mean height error for the ICAO temperature profile and the standard post-processing scheme. The lower left panel shows error for two alternative ways of specifying model-level temperatures. The results discussed above were for the case in which the analytical representation of the temperature profile was used directly to evaluate the temperature at the full model levels with pressures p_k defined by Eq.(11). The alternatives shown are the evaluation of the full-level temperature as the layer-mean:

$$T_k = \frac{1}{\Delta p_k} \int_{p_{k-\frac{1}{2}}}^{p_{k+\frac{1}{2}}} T \, dp$$

and the corresponding mean when the integral is taken with respect to $\ell n p$:

$$T_k = \frac{1}{\ell n \frac{p_{k+\frac{1}{2}}}{p_{k-\frac{1}{2}}}} \int_{p_{k-\frac{1}{2}}}^{p_{k+\frac{1}{2}}} \frac{T}{p} \, dp$$

Of these alternatives, the former is consistent with the interpretation of the model's vertical finite-difference scheme as a Galerkin scheme with piecewise-constant basis

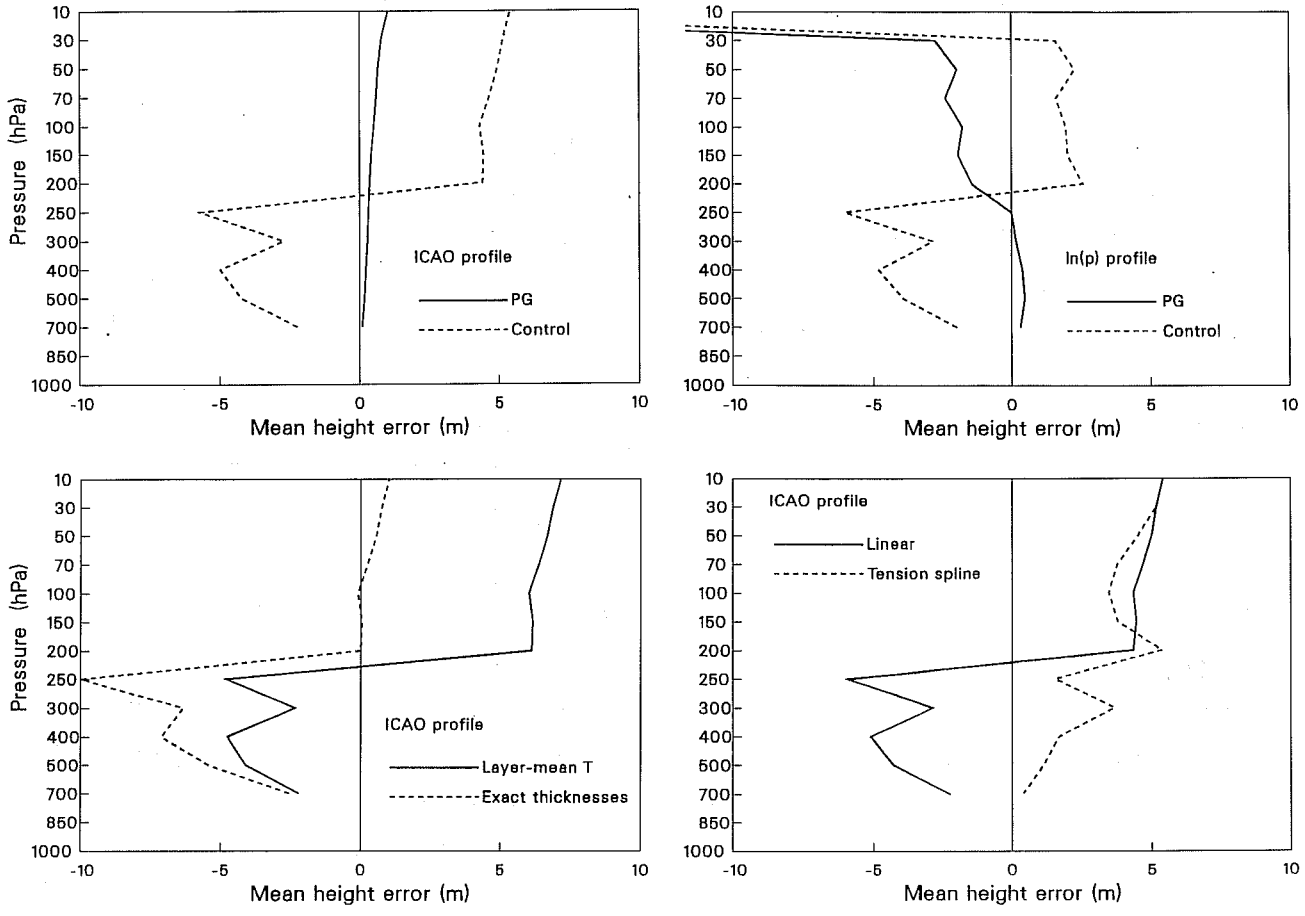

Fig. 3 Global-mean errors of post-processed pressure-level heights(m), for the standard (dashed) and PG (solid) schemes, and for the ICAO standard atmosphere (upper left) and the logarithmic temperature profile (upper right). Results for the ICAO atmosphere are also shown for alternative specifications of the model-level temperatures(lower left) and alternative vertical interpolation methods(lower right).

6. OBJECTIVE ASSESSMENT OF FORECAST EXPERIMENTS

a) Introduction

Forecast experiments were initially carried out using a version of the TR scheme which was not quite as described in section 2. A set of 12 cases was run using the standard 19-level vertical resolution and horizontal resolutions T21, T42 and T63. Four cases were also run at T106 resolution, but one became computationally unstable, due it is thought to the semi-implicit time scheme, which differed from that set out in section 2. The experiments showed a clear beneficial impact of the new scheme in the Southern Hemisphere. This impact was largest at T21, and decreased monotonically as resolution increased. Results were less clear-cut for the Northern Hemisphere, although some improvement was seen. Following these encouraging results, reported separately by Chen and Simmons (1990), the formulation of the scheme was revised, resulting in the TR scheme as specified in this report. The PG scheme was also developed. These schemes have been tested in series of 10-day forecast experiments using 19-level T42 and T106 resolutions, and we concentrate on these later experiments for presentation here. The T42 results with the TR scheme were largely similar to those obtained in the first set of experiments.

The T42 experiments were based on a set of 12 cases, one for each month of the year. The initial time and date were 12UTC and the 15th of each month, for April 1987, July 1987 to March 1988, and May and June 1988. The model parametrizations were those used operationally in mid-January 1988, and operational T106 analyses (produced using the standard scheme in the assimilating model) were truncated to T42 to provide initial conditions. The T42 forecasts were carried out for the standard, TR and PG schemes with the usual ℓnp_s as prognostic variable, and also for the TR scheme with p_s as prognostic variable. Results from the latter are discussed separately in section 9. Results from standard T106 forecasts were also available for these dates.

The T106 experiments with ℓnp_s as variable used 12 cases as above, but for a more recent set of months: March 1988, May 1988 to February 1989, and April 1989. The three 1989 cases used a slightly revised initialization and surface parametrization which were introduced operationally early in the year. Six cases (one every other month starting from March 1988) were also run with the TR scheme with p_s as prognostic variable. Operational analyses again provided the initial conditions.

b) T42 experiments

Figs. 4 and 5 present objective verification scores averaged over the set of 12 T42 cases, for the extratropical northern and southern hemispheres. Very little impact was found in the tropics (not shown). Anomaly correlations of the 500hPa height field (correlations between observed and forecast deviations from climatology) are shown in the upper panels

functions (Laprise and Girard, 1989). The latter gives exact thicknesses between model half-levels, and the dominant error is in this case due to vertical interpolation. Fig. 3 shows that the point and layer-mean definitions of T_k give basically similar errors. When the temperature decreases with height, the standard finite-difference scheme tends to overestimate heights if full-level temperatures are point or layer-mean values. The component of the error due to interpolation is larger, and of opposite sign, so the net post-processing error in the case of exact thicknesses is in fact larger in the troposphere than for the other definitions of full-level temperature.

Formally, the standard scheme uses tension splines in $\ell n\eta$, where η is the hybrid vertical coordinate, to carry out the vertical interpolation from model half levels to pressure levels (Cline, 1974). However, at a late stage in this study it was realized (partly as a consequence of these results) that due to a programming error the tension factor was set so high that the interpolation method was essentially linear. The lower right panels of Fig. 3 compare (for the point-value definition of T_k) mean height errors for pure linear interpolation and for tension-spline interpolation using the intended tension factor of unity. Linear interpolation evidently gives results very close to those of the standard scheme, while the intended tension-spline interpolation gives a very different result. The predominant tropospheric error in this case arises from error in the integration of the hydrostatic equation to produce half-level heights, although the vertical interpolation is responsible for the oscillation in error from level to level.

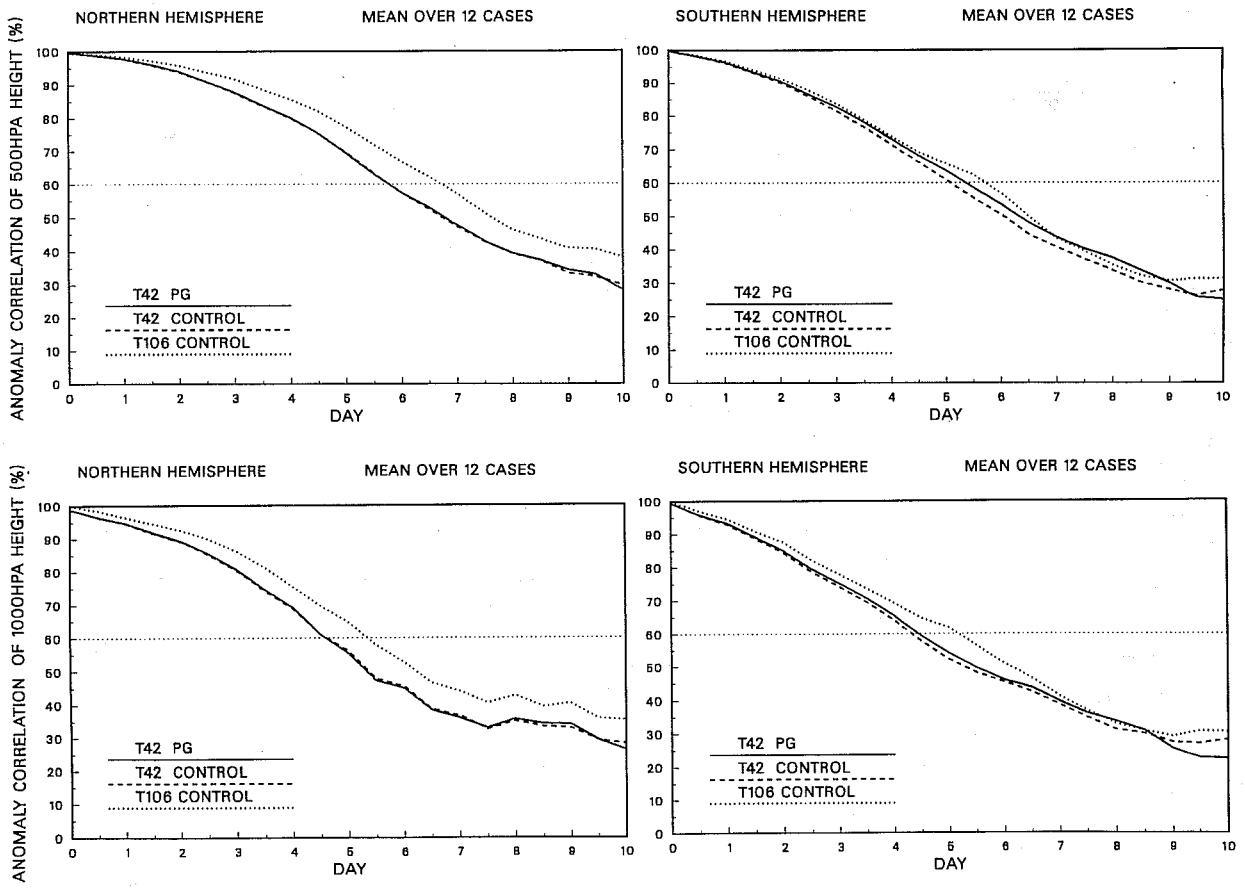

Fig. 5 Mean anomaly correlations of 500hPa (upper) and 1000hPa (lower) height forecasts for the extratropical northern (left) and southern (right) hemispheres. Results are shown for T106 and T42 resolution using the standard scheme, and T42 resolution using the PG scheme.

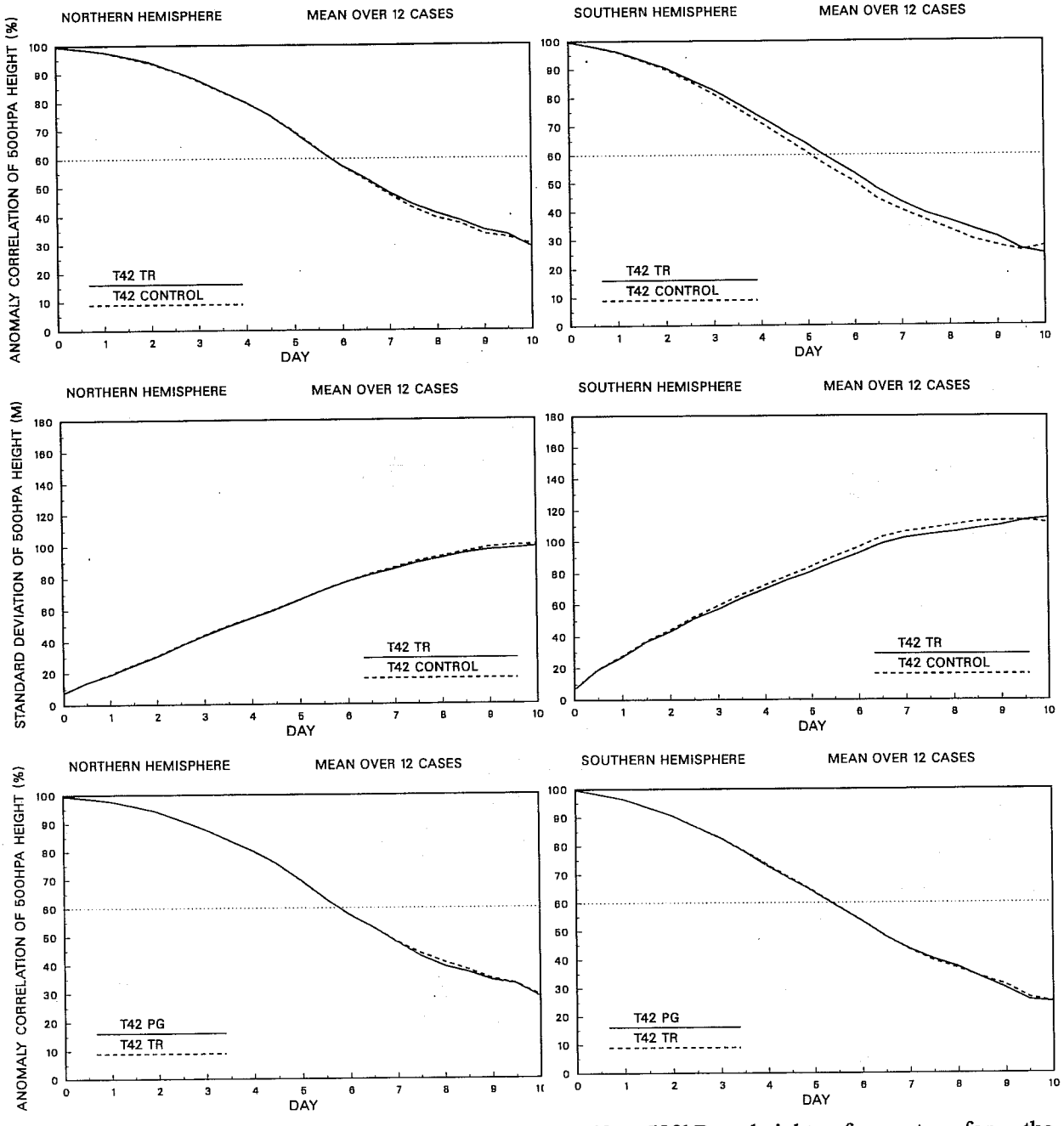

Fig. 4 Mean verification scores of 12 T42 500hPa height forecasts for the extratropical northern (left) and southern (right) hemispheres. Anomaly correlations (%) are presented in the upper and lower panels and standard deviations (m) in the middle panels. The upper and middle panels compare results from the standard and TR schemes, and the lower panels compare results from the standard and PG schemes.

the standard T106, or indeed T106 in general since it will be shown subsequently that the impact of the TR and PG schemes is much less at the higher resolution. This is particularly the case at 500hPa. At 1000hPa, the impact of the resolution increase is larger, and the impact of the change from the standard to the PG or TR scheme is smaller.

Since subjective assessment pointed to a particular sensitivity to the change in scheme at high latitudes, objective verification was also carried out separately for "Arctic" (north of 60°N), "Antarctic" (south of 60°S) and mid-latitude (20°-60°N;20°-60°S) regions. Comparisons of 500hPa height anomaly correlations for the TR and standard schemes, and for the PG and standard schemes, are presented in Fig. 6 for the Arctic and Antarctic regions. Differences are indeed larger than shown in the two preceding figures for the extratropical hemispheres. A small improvement can be seen at all forecast ranges for the Arctic, and improvement over the Antarctic region shows clearly in the short as well as medium range. The TR scheme appears to improve by a little more than the PG scheme late in the forecast range, although it will be seen from the following figure that the significance of differences in scores at this range is open to question.

Scatter diagrams showing 500hPa height anomaly correlations for individual PG and standard T42 forecasts are presented in Fig. 7. In these plots, a point lying above the diagonal indicates a case in which the PG forecast is more accurate than the standard forecast. The crosses denote the means for each set of forecasts, and the case of 15 September 1987 for which detailed study has been made is marked by a circle. These diagrams are shown for day 3 and day 7 for the Arctic and Antarctic regions, and for day 7 for the extratropical Northern and Southern Hemispheres.

At day 3 the signal seen in Fig. 7 for the Antarctic is particularly clear, with all points lying on or above the diagonal: in no case is the forecast with the standard scheme superior to the forecast with the PG scheme. The mean improvement at day 3 for the Arctic is much smaller, though only two of the cases are poorer with the PG scheme. Conversely, by day 7 there is a considerable scatter of points about the diagonal, and the significance of the mean differences is not obvious. An exception is perhaps the extratropical Southern Hemisphere as a whole, for which only two cases are below the diagonal.

The forecasts discussed above were all carried out using the hybrid vertical coordinate and envelope orography used routinely at ECMWF (Jarraud et al., 1988; Simmons et al., 1989). As any problem with the representation of the pressure gradient may be less with the hybrid coordinate than with the sigma coordinate, and greater with envelope orography than with the lower mean orography, T42 forecasts have been carried out for a sensitive case using mean orography (with the hybrid vertical coordinate) and using the sigma

of Fig. 4 for the TR and standard (labelled "control") schemes. Differences are small for the Northern Hemisphere, with the TR scheme producing a barely discernible improvement for days 1 to 3 and a more obvious improvement later in the forecast range, although the latter occurs after mean correlations have dropped below the 60% value which is usually taken as a limit below which forecasts cannot be generally regarded as useful (see, for example, Simmons, 1986). Conversely, for the Southern Hemisphere the TR scheme gives a much more substantial improvement over the standard scheme. This improvement occurs virtually throughout the forecast range.

Similar conclusions can be drawn from examination of the standard deviations of 500hPa height error presented in the middle panels of Fig. 4, and from objective verification of the temperature and wind fields (not shown). This overall agreement between different objective measures has been found for other comparisons made during this study, and for purposes of presentation in this report we restrict subsequent attention to anomaly correlations. These are shown for the 500hPa height field and the TR and PG schemes in the lower panels of Fig. 4. The two schemes give a very similar mean performance in both hemispheres. In particular, the similarity between the TR and PG curves implies that the PG scheme captures essentially the same improvement as the TR scheme for the Southern Hemisphere.

Fig. 5 compares results from the PG and standard schemes at T42 resolution with the standard T106 results. Anomaly correlations are presented for both 500 and 1000hPa height. Considering first the Northern Hemisphere, we note that the very small differences between the PG and standard schemes for T42 are quite negligible compared with the differences between T42 and T106 forecasts. The mean improvement of T106 over T42 in this 12-case sample is larger than reported by Simmons et al. (1989) for 24 cases drawn from T63 analyses for the period May 1983 to April 1985, using an earlier version of the model. It should also be noted, however, that the overall accuracy of forecasts from the more recent set shown here is substantially higher, so that the mean accuracy (as measured by the anomaly correlation) of the T42 forecasts presented here in fact matches that of the T106 forecasts in the set discussed by Simmons et al. (1989). It would require very substantial experimentation to quantify to what extent this reflects the many changes in data analysis (including use of a higher-resolution assimilating model) and in the model that have been made in recent years, since interannual variations in basic predictability could have influenced these results.

For the Southern Hemisphere, there is less difference between the standard T106 and T42 results, and more difference between the PG and standard results for T42. Thus introduction of the PG (or TR) scheme brings the T42 results significantly closer to those of

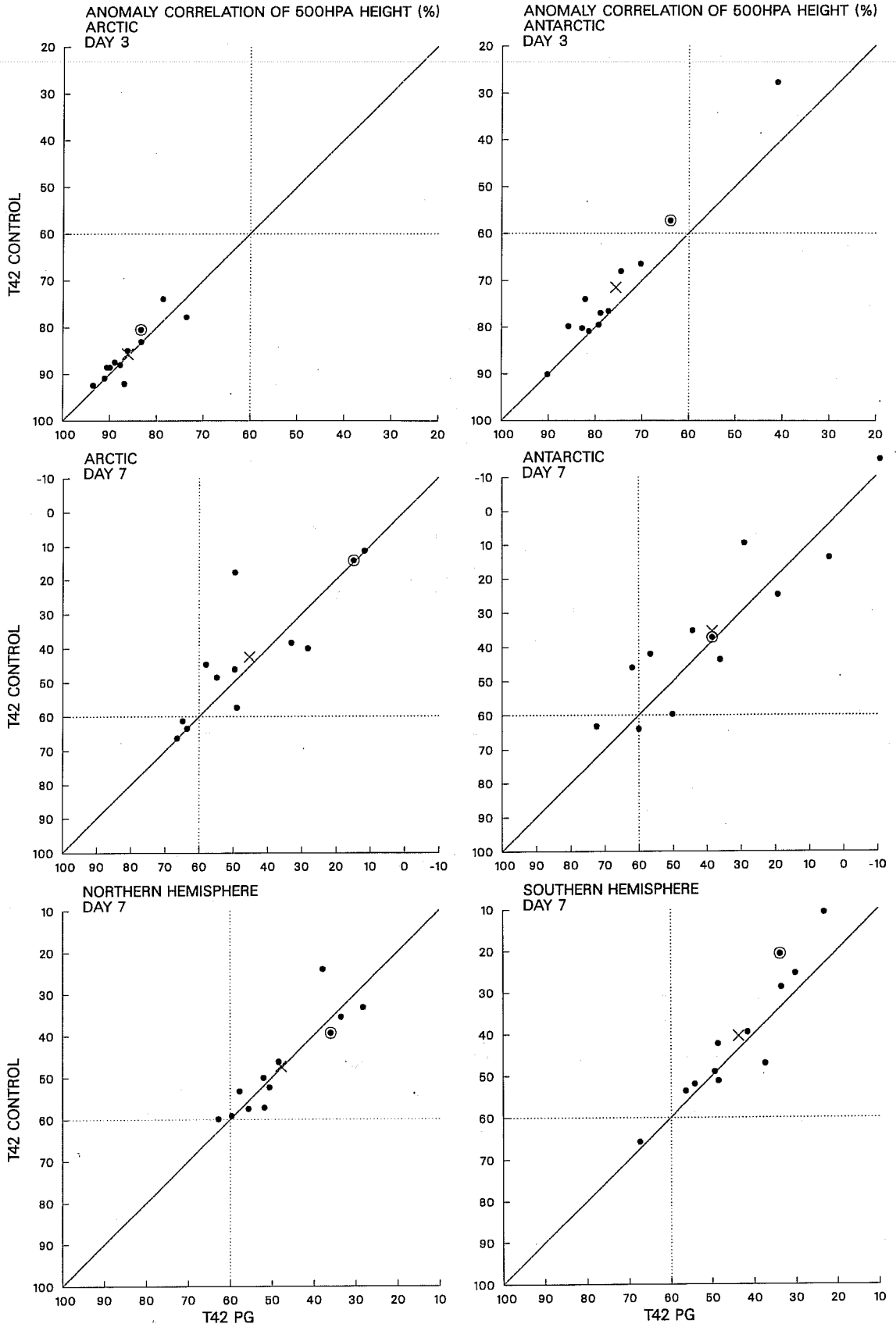

Fig. 7 Scatter diagrams showing anomaly correlations of the 500hPa height field for the 12 standard and PG forecasts at T42 resolution. Results are shown for the Arctic and Antarctic regions at days 3 and 7, and for the extratropical hemispheres at day 7.

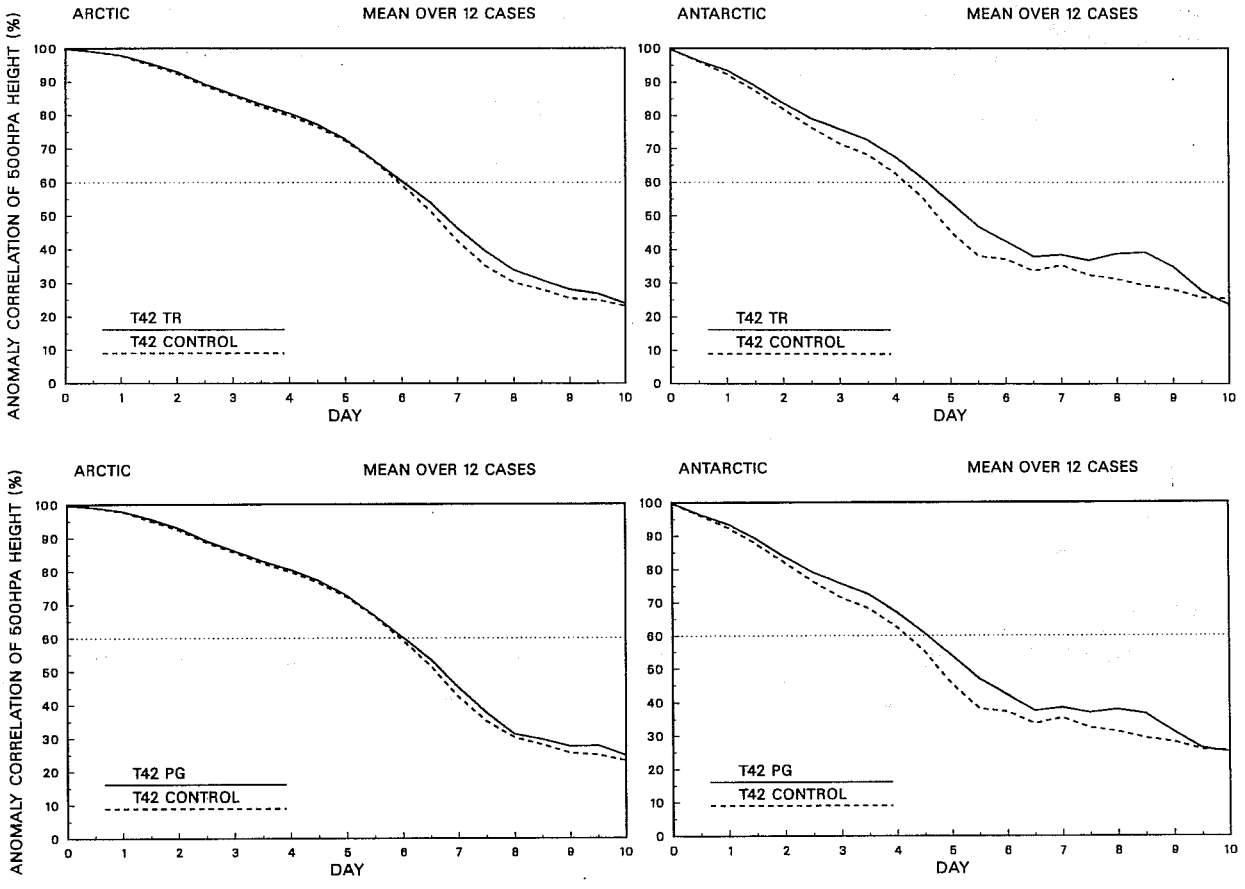

Fig. 6 Mean anomaly correlations of T42 500hPa height forecasts for the Arctic (left) and the Antarctic (right), comparing standard and TR results (upper) and standard and PG results (lower).

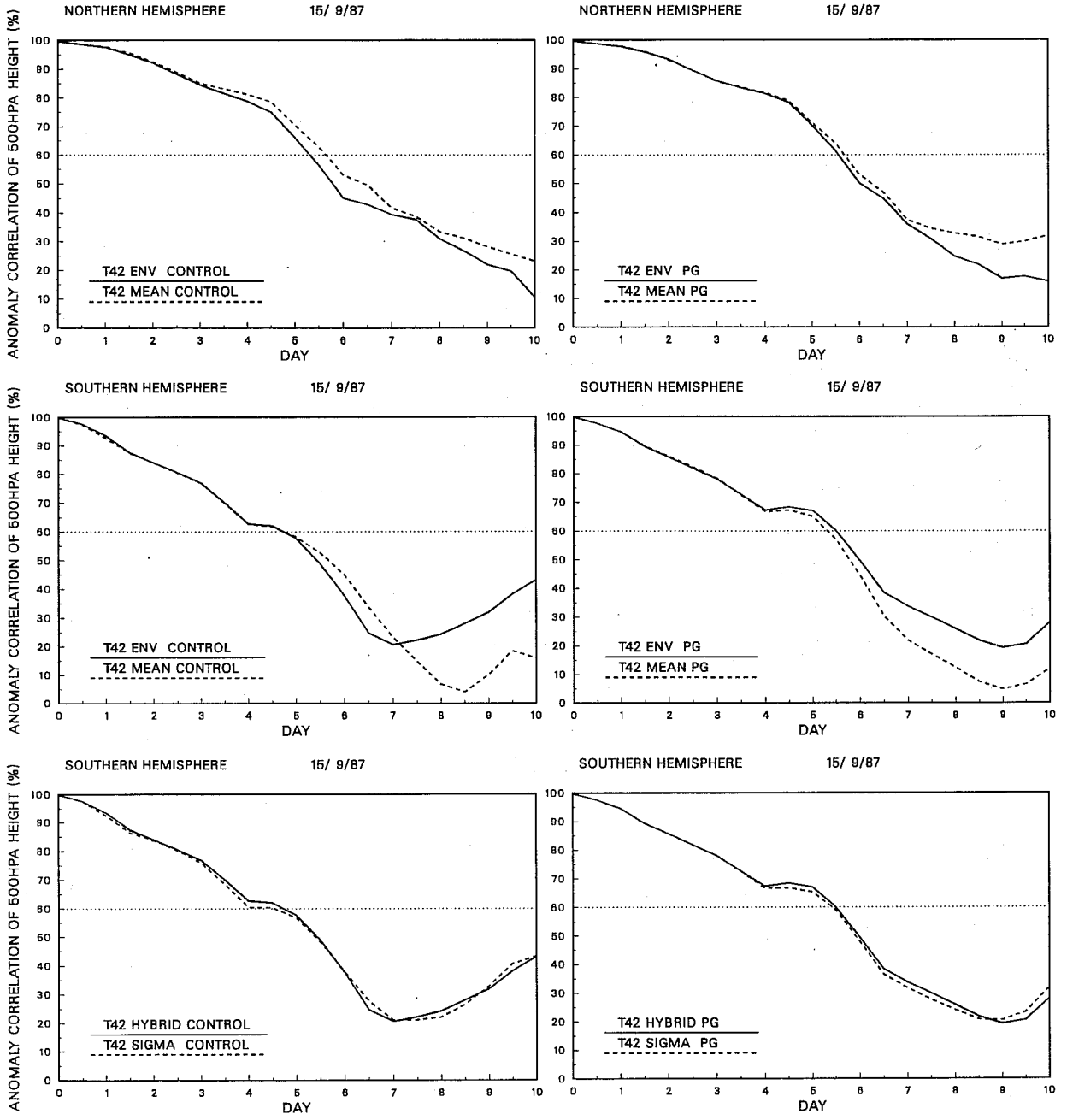

Fig. 8 Anomaly correlations of T42 500hPa height forecasts from 15 September 1987. Forecasts using the standard scheme are shown in the left-hand panels, and the right-hand panels are for the PG scheme. Mean- and envelope-orography forecasts are compared in the upper and middle panels, for the northern and southern hemispheres respectively. The lower panels compare hybrid- and sigma-coordinate forecasts for the Southern Hemisphere.

coordinate (with envelope orography, and sigma and hybrid levels coinciding for a pressure of 1013.2hPa). The forecasts were made both for the standard scheme and for the PG scheme. The case, 15 September 1987, was chosen as it was that for which the PG and TR schemes gave the biggest beneficial impact at day 5, as measured by the anomaly correlation of 500hPa height for the Southern Hemisphere. Synoptic maps from this case are presented in section 7.

The envelope- and mean-orography forecasts are compared for the two hemispheres in the upper and middle panels of Fig. 8, and the lower panels compare hybrid- and sigma-coordinate forecasts for the Southern Hemisphere. For the Northern Hemisphere, mean orography gives better forecasts than envelope orography for both the standard and PG schemes, as found on average for the May to October period at this resolution (Jarraud et al., 1988). However, the advantage of the mean over the envelope is much less with the PG scheme than with the standard scheme, at least for the time range over which the forecasts can be regarded as possessing useful skill. For the Southern Hemisphere, the PG scheme brings the mean-orography forecast up to the level of the envelope at day 1, but gives the envelope an advantage over the mean in the middle part of the forecast range. Here, for the period for which anomaly correlations are above 60%, the hybrid coordinate scores better than the sigma coordinate when the standard scheme is used, but the advantage of the hybrid coordinate is reduced when the PG scheme is used. It must be stressed that these are results for just one case, but they are largely consistent with expectations based on the sensitivity of pressure-gradient errors to the choice of vertical coordinate and orography.

c) T106 experiments

Mean anomaly correlations of 500hPa height for the extratropical hemispheres are shown in Fig. 9 for the 12 T106 cases. It is evident that there is much less improvement of the TR and PG schemes over the standard scheme than found for T42. A small improvement still exists for the Southern Hemisphere, albeit mostly at a time range when forecast quality is low. For the Northern Hemisphere there is very little difference in mean results between the TR and standard schemes, and an apparent slight worsening when the PG scheme replaces the standard scheme. There is reason, however, to doubt the significance of the latter result.

Fig. 10 presents scatter diagrams comparing the PG and standard T106 forecasts. Results are shown for the Arctic and Antarctic regions at day 5, and for the mid-latitude belt of each hemisphere for days 5 and 7. Considering first the Northern Hemisphere, no detrimental effect of the PG scheme can be seen in middle latitudes. For the Arctic, one case stands out as being quite substantially worse with the PG scheme at day 5, and this

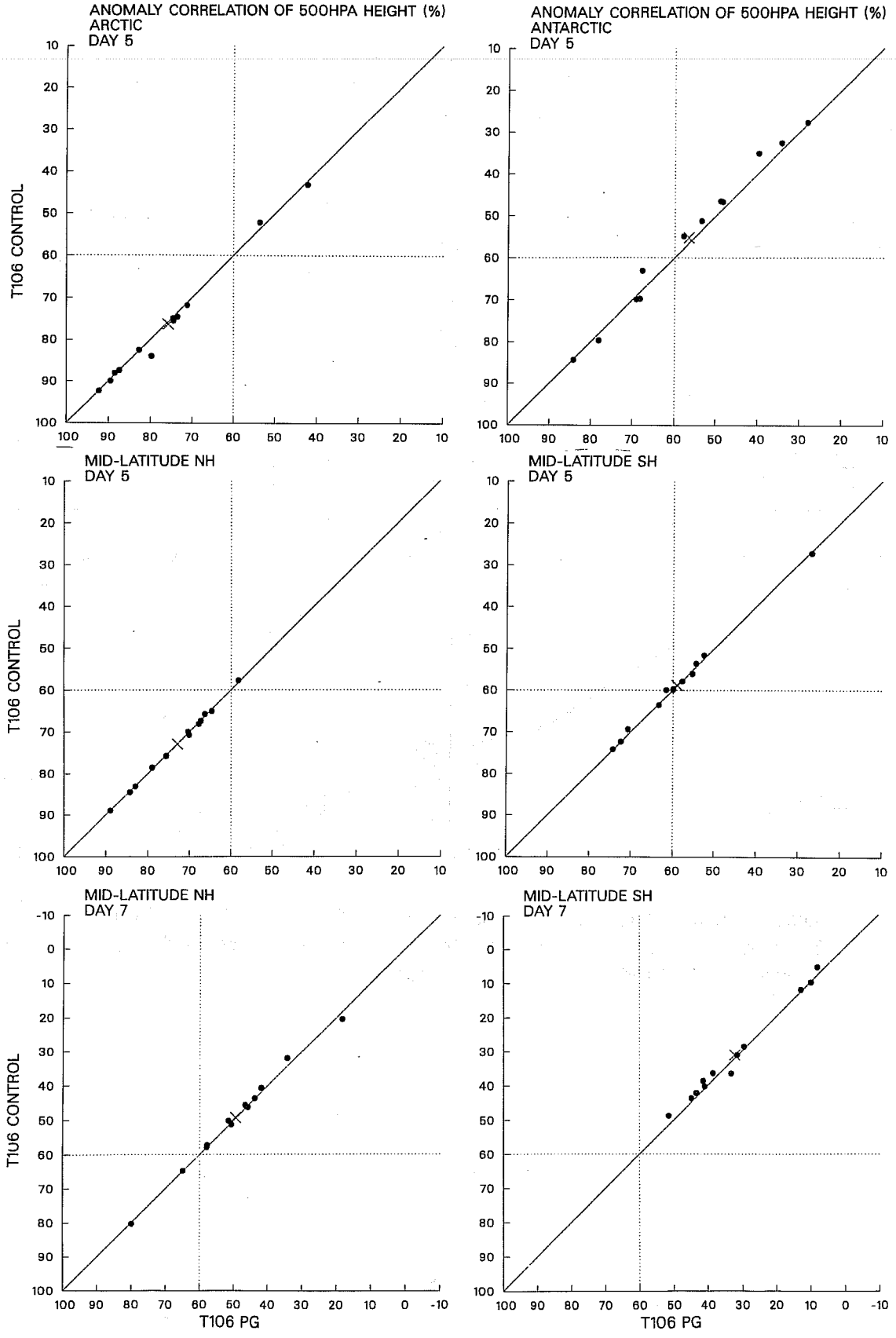

Fig. 10 Scatter diagrams showing anomaly correlations of the 500hPa height field for the 12 standard and PG forecasts at T106 resolution. Results are shown for the Arctic and Antarctic regions at day 5, and for the mid-latitude zones of each hemisphere at days 5 and 7.

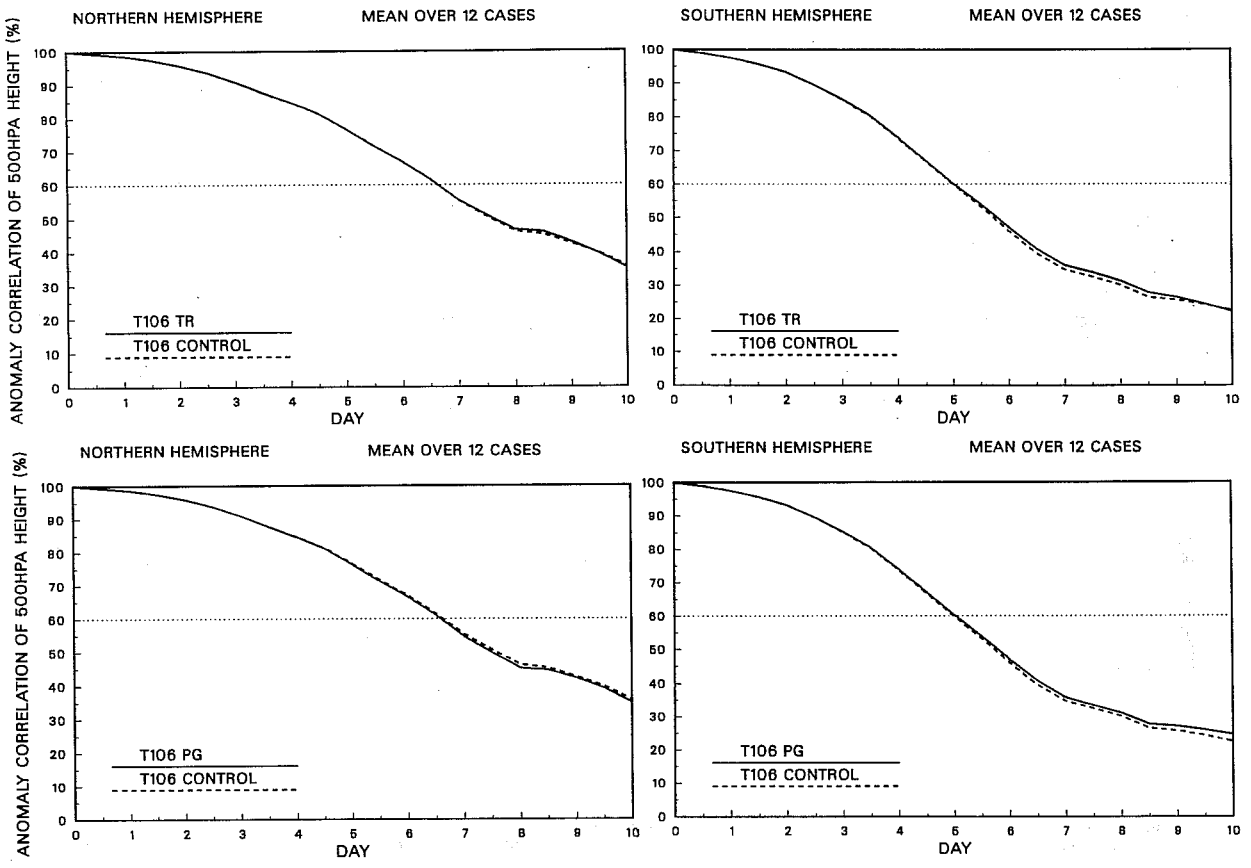

Fig. 9 Mean anomaly correlations of 500hPa height forecasts using T106 resolution for the northern (left) and southern (right) hemispheres, comparing standard and TR results (upper) and standard and PG results (lower).

7. SUBJECTIVE ASSESSMENT

a) A sensitive T42 case

As an example of synoptic impact at T42 resolution we choose the case of 15 September 1987 for which objective verification was presented in Fig. 8. Although this is the case that gives the largest advantage of the PG scheme over the standard scheme at day 5 as measured by the 500hPa height anomaly correlation for the Southern Hemisphere, it does not stand out particularly from several other cases showing clear improvement at this time range. The case is notable for a large beneficial impact of the TR and PG schemes at day 1 over Antarctica. Another case shows an even larger improvement at this range according to the 500hPa height anomaly correlation, although this does not show up as clearly in synoptic assessment.

Fig. 11 shows the 500hPa analysis over Antarctica for 16 September 1987, the 1-day forecasts with T106 and T42 resolution using the standard scheme, and the 1-day T42 forecast with the PG scheme. Also shown are two T42 forecasts using the standard scheme but different horizontal diffusions. The standard T42 forecast shows a vortex of quite spurious intensity centred over the boundary between the Ross Ice Shelf and the Antarctic plateau. No such vortex can be seen in the verifying analysis, and none was present in the initial conditions for the forecasts. There is only a weak low-pressure area, located further east, in the T106 forecast and in the T42 forecast with the PG scheme, and these latter forecasts verify quite well. Other differences between the T42 and T106 forecasts are comparatively minor, so use of the PG scheme removes the major discrepancy between the standard T42 and T106 forecasts, and the major error of the standard T42 forecast.

The ∇^4 horizontal diffusion used for the T106 forecasts has a coefficient $1 \times 10^{15} m^4 s^{-1}$ applied to the model variables vorticity, specific humidity and temperature, and a value 2.5 times larger is applied to the divergence field (Simmons et al., 1989). The T42 forecasts used for almost all forecasts reported here used a similar ∇^4 diffusion, with coefficients only twice as large as those used for T106. These coefficients have been assessed as about optimal for T63, and the use of similar values for T42 was based on a limited number of experiments with a very early version of the ECMWF forecasting system (Jarraud and Cubasch, 1979). The e-folding time of the diffusion on the smallest resolved scale is about 3.5 hours for T106, but is around 3 days for T42, suggesting that the diffusion has little effect at T42. Since error in the pressure-gradient calculation is likely to be largest for the smallest model scales, detrimental impact of the pressure-gradient error could be reduced with a more effective horizontal diffusion for T42.

The standard T42 forecast for the case of 15 September 1987 was thus repeated using the same e-folding time on the smallest resolved scale for T42 as for T106, though with no

becomes even more marked later in the forecast range. Had this one case been in favour of the PG scheme to a similar extent, the mean scores would likewise have favoured the PG scheme. As forecast error is influenced by a number of factors, which may be compensatory in any particular case, an isolated case of poorer performance may not be of significance. Also, there is an element of chance in the discovery of this sensitive case. The original intention in this experimentation was to run a set of just six cases, as little impact was expected. This would indeed have happened if the sensitive case had not been one of the initial six.

A different picture emerges for the Southern Hemisphere. For the Antarctic region, a clear majority of cases lies above the diagonal at day 5, indicating a small but probably significant improvement of the PG scheme over the standard scheme. At this time range there is little impact on the mid-latitude zone, but a slight tendency for points to be above the diagonal can be seen for day 7. At this later time, only one forecast is poorer with the PG scheme than with the standard scheme.

enhancement of diffusion of the divergence field. Forecasts were carried out using ∇^4, ∇^6 and ∇^8 forms for the horizontal diffusion (MacVean, 1983). The 1-day ∇^6 and ∇^8 forecasts are included in Fig. 11. The higher diffusion is evidently effective in reducing the intensity of the vortex, more so with the ∇^6 form than with the ∇^8 form, though neither forecast is as good as the PG scheme with much weaker diffusion. With the higher ∇^4 diffusion (not shown) the vortex over Antarctica was weaker still, but the larger damping on scales away from the limit of resolution could be seen to have detrimental impact elsewhere.

The region to the east of the Ross Ice Shelf is one where differences between T42 and T106 simulations commonly occur, and is one where particular sensitivity to the introduction of the PG or TR scheme is found. Further indication of this will be seen in several subsequent figures. It is thus of interest to consider briefly the geography of the region. Fig. 12 presents plots of the T42 and T106 envelope orographies used for these forecasts. The Ross Ice Shelf is enclosed on three sides by elevated terrain which is resolved quite well by T42 resolution, although not surprisingly the T106 resolution represents better the steep edge of the plateau. T106 resolution can give, however, only a slight indication of the mountains of the Transantarctic Range, which border the western and southern boundaries of the shelf, and which in reality reach heights in excess of 4000m in places. Nevertheless, the combination of the steep resolved orographic slopes and the strong temperature inversions that occur above the continent and ice shelf makes this a prime region for exposing problems in the representation of the pressure gradient in atmospheric models with terrain-following vertical coordinates.

Fig. 13 presents 1-day forecasts corresponding to those in the middle panels of Fig. 11, but for sigma coordinates (upper panels) and mean orography (lower panels). For the standard scheme, the intensity of the spurious vortex is even stronger with the sigma coordinate, and a more intense tongue of high pressure extends over the South Pole. With mean orography, the spurious low is less deep, but the high-pressure tongue is even more marked. It is striking how these erroneous features are removed by use of the PG scheme. With this scheme, the T42 forecasts are much more similar to each other, for mean and envelope orographies, and for hybrid and sigma coordinates.

Fig. 14 presents day-1 results in a different way, showing the T42 and T106 forecast errors for the standard scheme, and the differences between the standard T42 forecast and the T42 forecasts with the PG and TR schemes. Away from the plateau, the patterns of error are very similar for T42 and T106, with a tendency for somewhat smaller magnitudes for T106. The erroneous vortex shows as a region of large negative error near the Ross Ice Shelf for T42, and there is a tongue of erroneously high pressure on the opposite side of

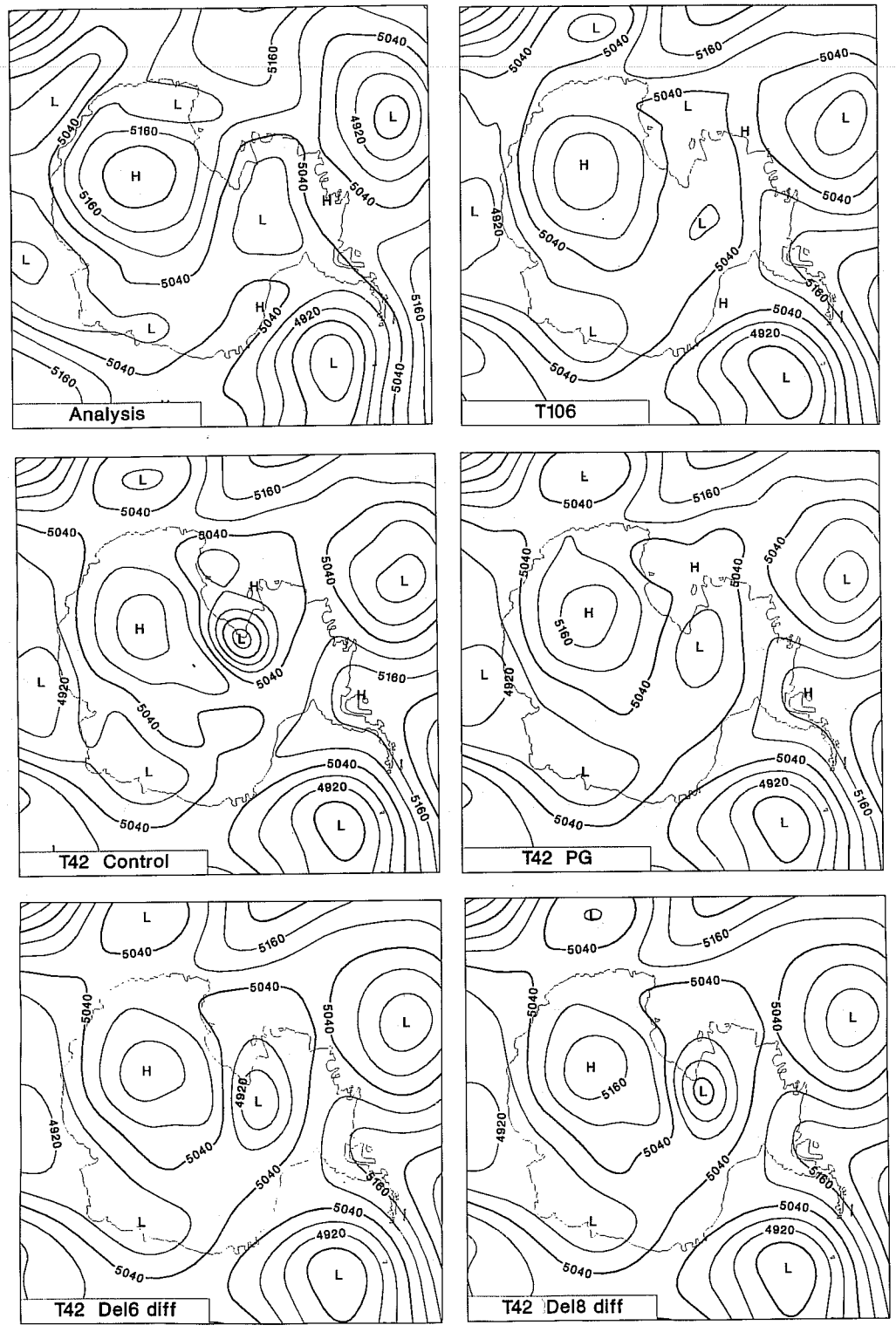

Fig. 11 The analyzed map (upper left) of 500hPa height (contour interval 60m) over Antarctica for 12UTC 16 September 1987, and one-day forecasts for this time using:

Upper right - T106 resolution and standard scheme
Middle left - T42 resolution and standard scheme
Middle right - T42 resolution and PG scheme
Lower left - T42 resolution and standard scheme with ∇^6 diffusion
Lower right - T42 resolution and standard scheme with ∇^8 diffusion

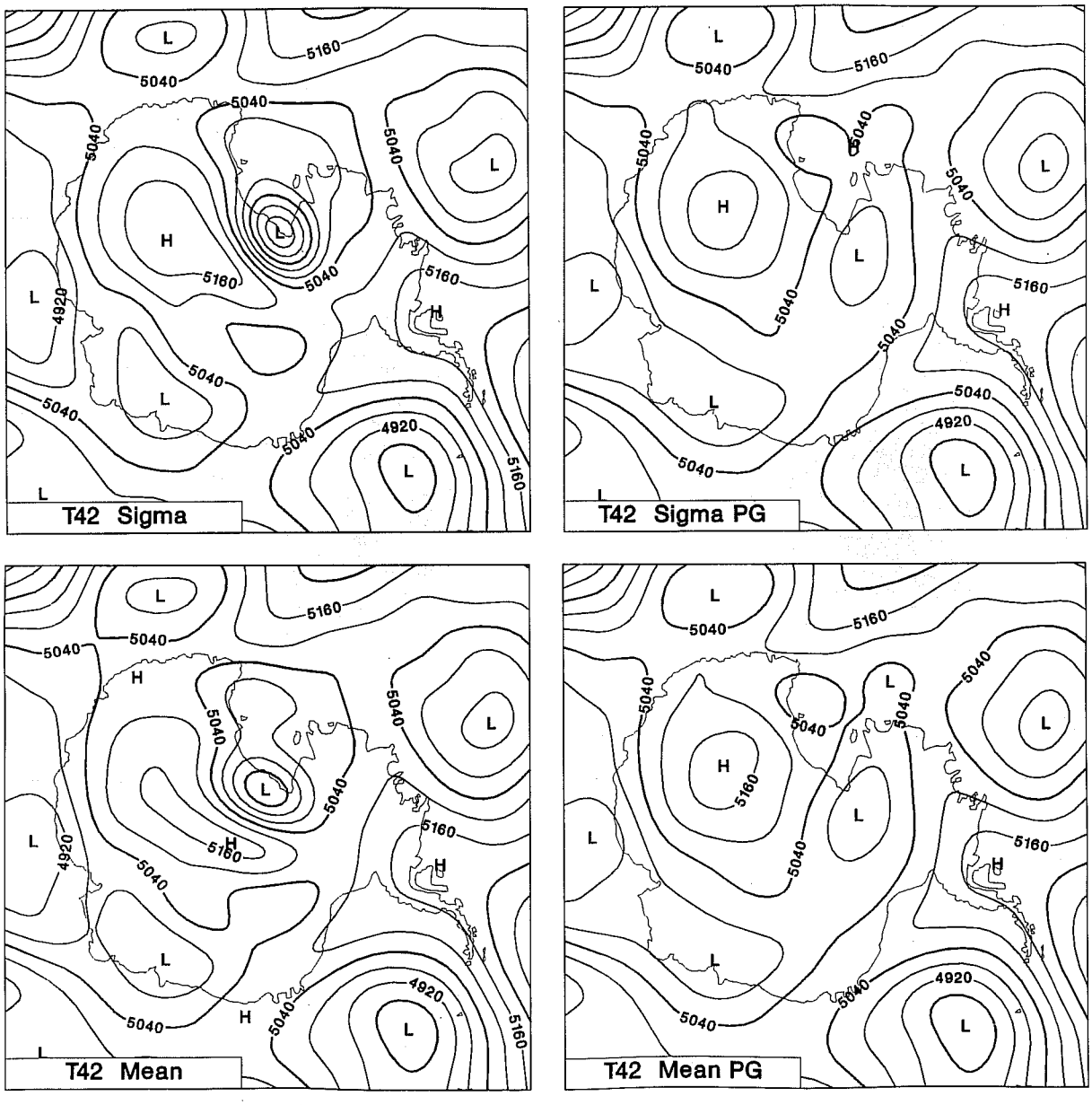

Fig. 13 One-day T42 500hPa forecasts for 12UTC 16 September 1987 using:
Upper left - Standard scheme, envelope orography and sigma coordinate
Upper right - PG scheme, envelope orography and sigma coordinate
Lower left - Standard scheme, mean orography and hybrid coordinate
Lower right - PG scheme, mean orography and hybrid coordinate

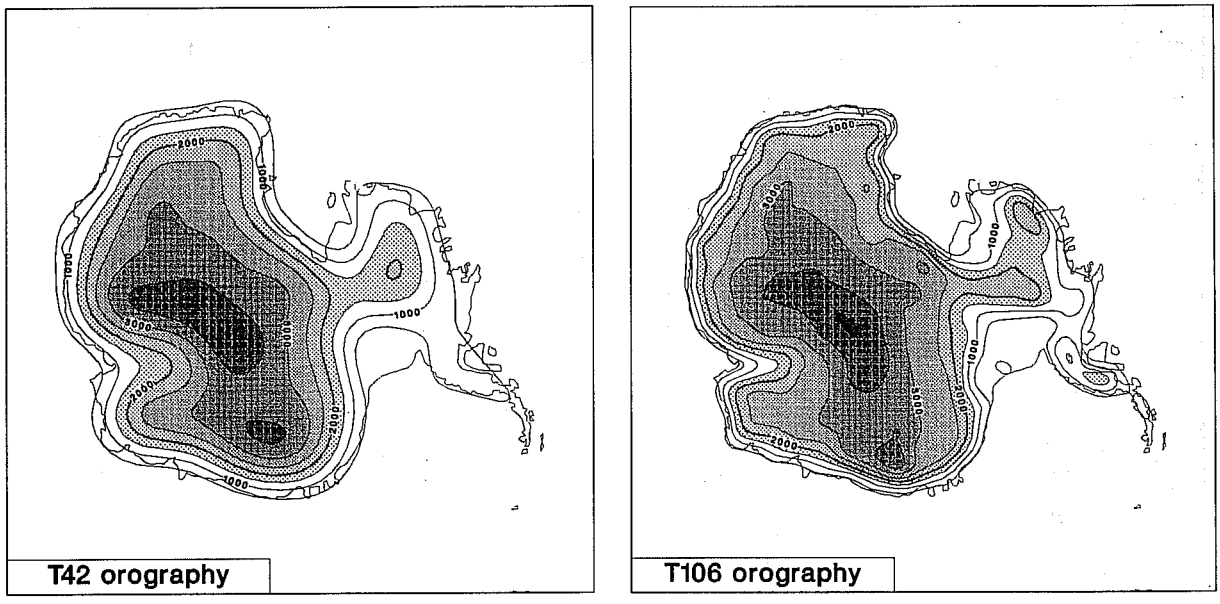

Fig. 12 The standard orographies used at T42 and T106 resolution. The contour interval is 500m.

the Pole. The difference maps show how the new schemes essentially remove this discrepancy in error pattern between the standard T42 and T106 forecasts. The similarity between the TR and PG forecasts is also evident. Larger differences between the standard and PG forecasts are found at day 1 from corresponding maps (not shown) for sigma coordinates and mean orography.

Fig. 15 shows similar maps for day 7, though over a larger domain. Away from Antarctica, error patterns remain very similar for the T42 and T106 forecasts, with still a tendency for smaller magnitudes at the higher resolution. The region of largest difference between the standard T42 and T106 forecasts is east of the Ross Ice Shelf, where heights are erroneously high with T42. Use of the TR or PG schemes reduces this error significantly, and also reduces the negative error in regions immediately to the north and downstream over the South Atlantic Ocean. High pressure east of the Ross Ice Shelf will be seen subsequently to be a systematic error of simulations with the standard scheme at lower horizontal resolutions.

Further difference maps for 7-day T42 forecasts are presented in Fig. 16. The upper panels indicate that the overall impact of the PG scheme is much the same for sigma as for hybrid coordinates, and much the same for mean as for envelope orography. The lower panels show how the forecasts with ∇^6 and ∇^8 diffusion and enhanced damping of the smallest scales also correct the principal error of the T42 forecast over Antarctica, without recourse to a change in formulation of the pressure gradient. Verified objectively over the Southern Hemisphere, these forecasts lie between the standard and PG forecasts in skill out to about 6 days, with the ∇^6 forecast better than the ∇^8. They exhibit higher anomaly correlations than both the standard and the PG forecasts beyond this time, but these correlations are below 60%. They also score substantially better over the Northern Hemisphere. Firm conclusions cannot be drawn from just one case, but the similarity of impact of the PG scheme and of the enhanced diffusion is striking with regard to the correction of the error which resembles the systematic deficiency over Antarctica.

An example of the smaller impact found over the Arctic due to the pressure-gradient change is shown in Fig. 17. The initial conditions are again 15 September 1987, and referring back to the upper left panel of Fig. 7 we note that the case is one of relatively low accuracy at T42, and of relatively large improvement due to the PG scheme. Fig. 17 shows the 500hPa height analysis for 12UTC 18 September 1987, the day-3 forecasts verifying at this time for T42 and T106 resolution with the standard scheme, and the T42 forecast with the PG scheme. The principal difference between the standard T42 and T106 forecasts is in the location and depth of the vortex which in reality is centred close to the North Pole, and which is quite well predicted using T106 resolution. Here the PG scheme produces a less

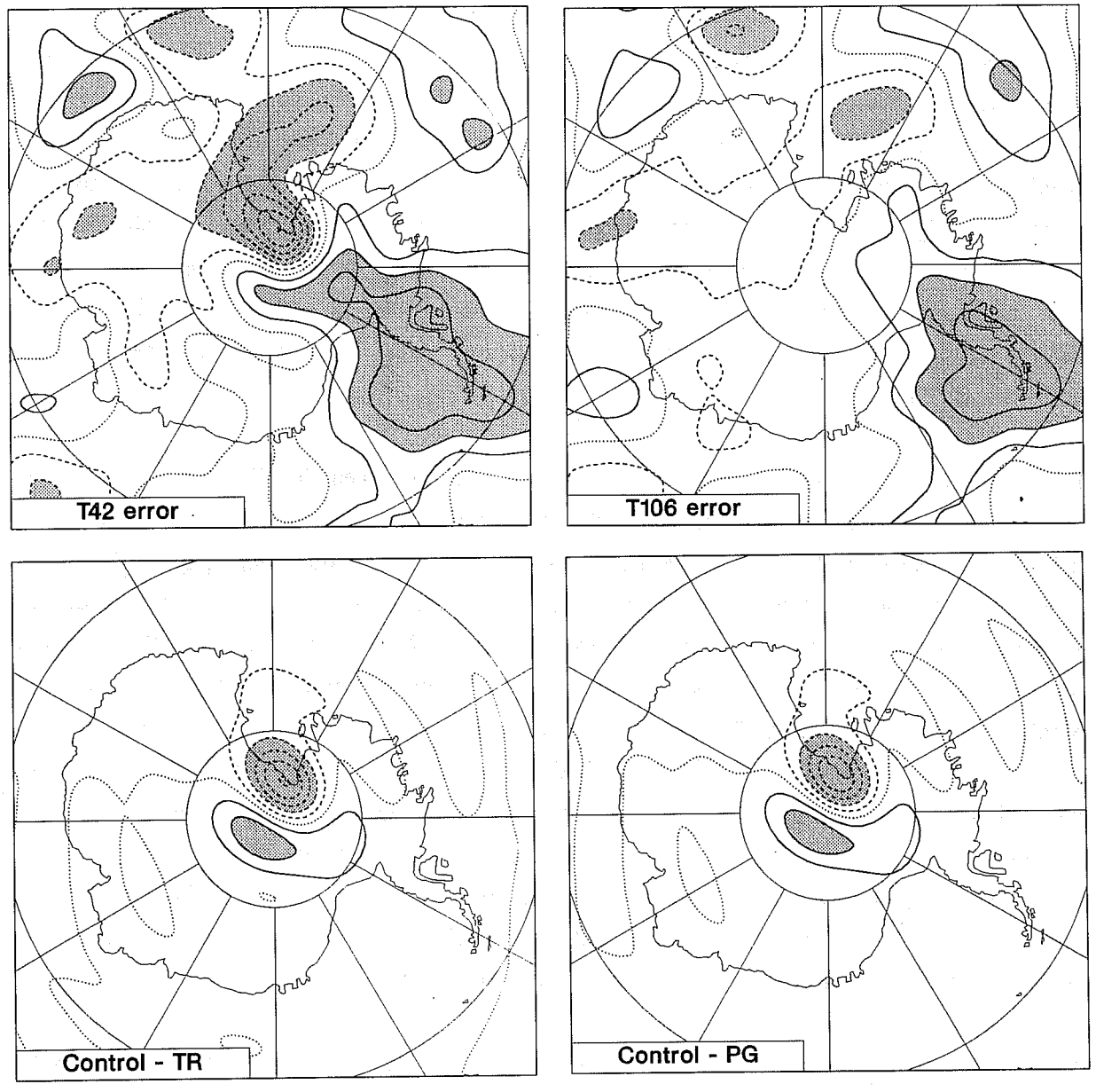

Fig. 14 One-day 500hPa forecast error for T42 (upper left) and T106 (upper right) resolutions, and the difference between the one-day standard T42 forecast and the TR (lower left) and PG (lower right) forecasts. The contour interval is 40m, and regions where differences exceed 80m are shaded.

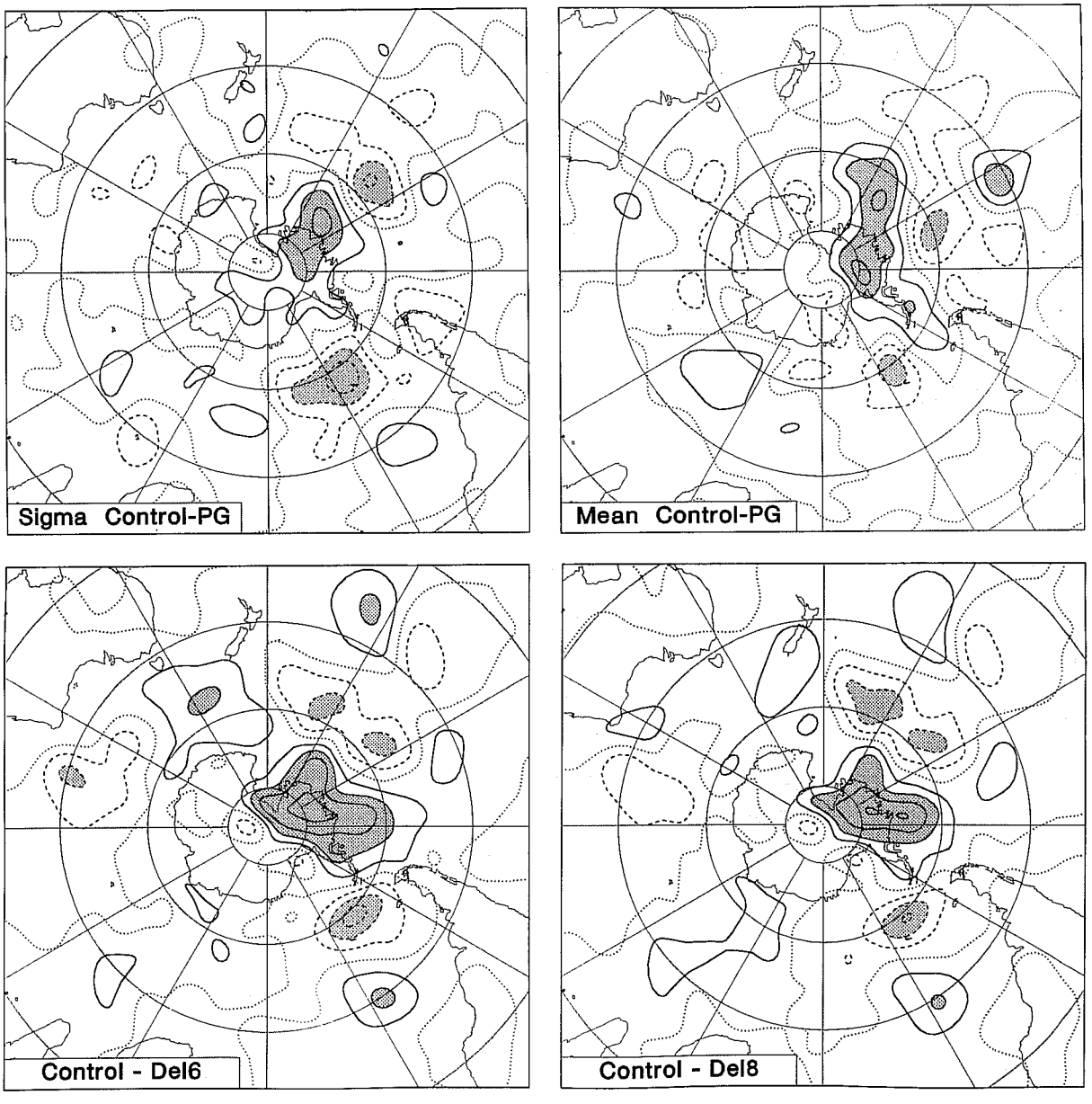

Fig. 16 Differences between 7-day 500hPa height forecasts (contour interval 80m, shading over 160m) using T42 resolution for:
Upper left - Standard and PG schemes for sigma coordinate
Upper right - Standard and PG schemes for mean orography
Lower left - Standard forecast and forecast with ∇^6 diffusion
Lower right - Standard forecast and forecast with ∇^8 diffusion

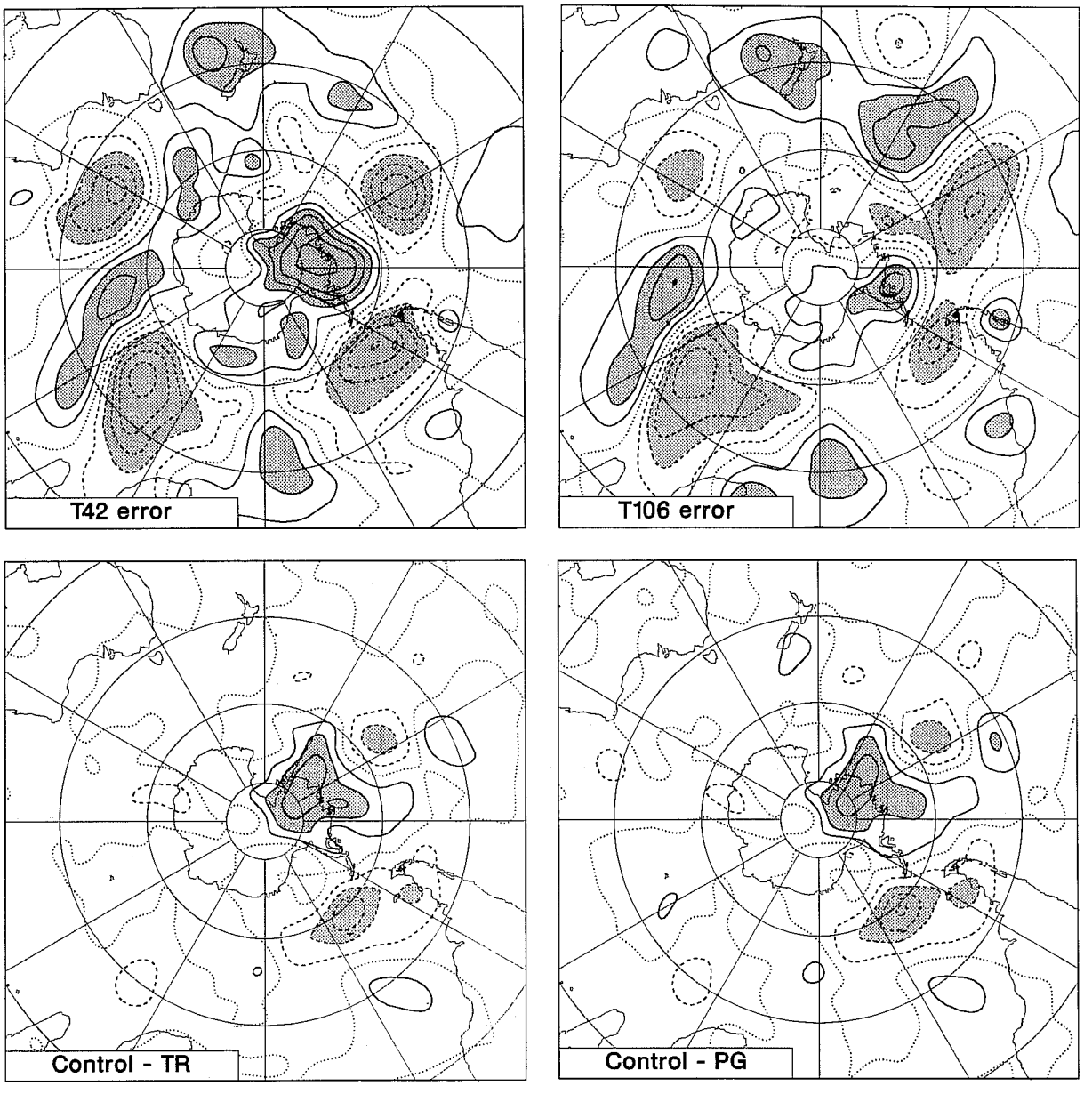

Fig. 15 7-day 500hPa forecast error for T42 (upper left) and T106 (upper right) resolutions, and the difference between the 7-day standard T42 forecast and the TR (lower left) and PG (lower right) forecasts. The contour interval is 80m, and regions where differences exceed 160m are shaded.

dramatic improvement than found over Antarctica. It nevertheless improves over the standard scheme at T42 resolution in showing less of an erroneous shift of the polar vortex towards Siberia, and in producing more of a trough extending down over Spitsbergen.

b) The T106 experiments

As expected from objective verification, examination of maps of 500 and 1000hPa height from the T106 forecasts revealed a high degree of similarity between the standard, TR and PG schemes. In the one sensitive case in which the PG scheme performed relatively poorly over the Arctic, small differences developed to the north of Greenland early in the forecast range. These subsequently propagated and amplified, and reached values in excess of 80m by day 7 over a region poleward of much of the northern coast of the USSR. These values are about one third of the largest difference shown in Fig. 16 for T42 over the Southern Hemisphere. Mean 500hPa heights for days 5-10 for this case show a peak difference approaching 100m between the PG and standard forecast, the latter being clearly the better. A second forecast produced mean differences of similar magnitude to the north and west of Greenland, but in this case neither the PG nor the standard scheme was generally the more accurate. Less extreme differences are found over the Antarctic, although there are more cases with intermediate levels of difference, and there is a tendency for larger errors with the standard scheme.

In addition to conventional synoptic assessment, the T106 forecasts have been subjected to a closer scrutiny in the vicinity of steep orography. One objective was to see whether any significant differences could be seen in the distribution of precipitation in the tropics and summer mid-latitudes, as the modified horizontal diffusion of temperature associated with the TR scheme could have given rise to changes in convective orographic precipitation. No systematic differences were evident. This was also the case for T42.

Maps of vertical velocity have also been examined. In a series for day 3, sensitivity was found over tropical South America, where the standard and PG schemes systematically produce a banded pattern of ascent and descent, aligned with the Andes, and spreading eastward over the Amazon basin and westward over the Pacific Ocean. These patterns are much less obvious with the TR scheme. Two marked examples, presenting the 3-day forecasts of 500hPa vertical velocity for the 15 March and 15 August cases, are shown in Fig. 18 for the standard and TR schemes. The vertical velocity produced by the PG scheme is very similar to that shown for the standard scheme in these two cases. Other time ranges have been examined for the two cases shown in Fig. 18, and generally similar results were found.

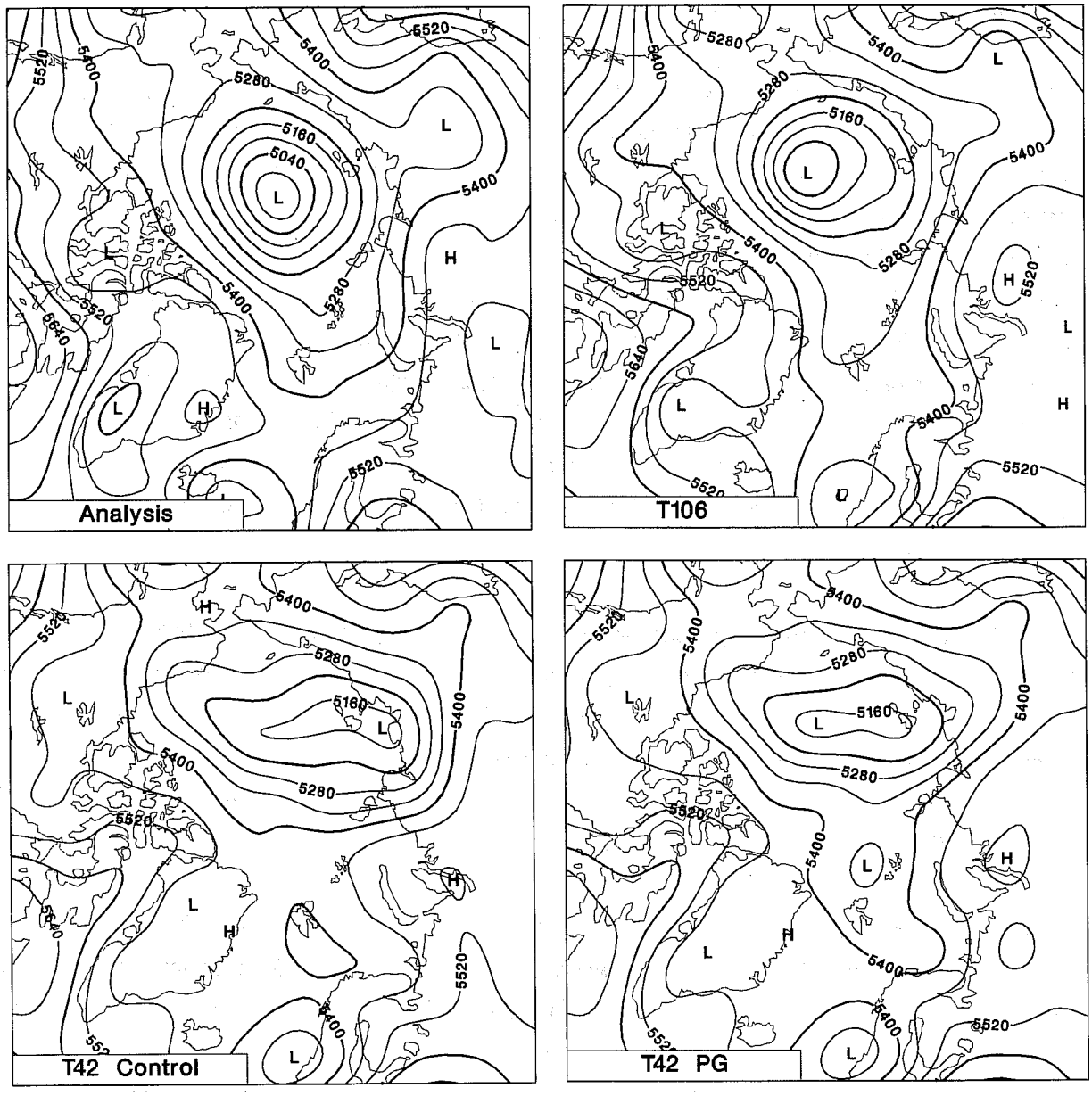

Fig. 17 The analyzed map (upper left) of 500hPa height (contour interval 60m) over the Arctic for 12UTC 18 September 1987, and 3-day forecasts for this time using:
Upper right - T106 resolution and standard scheme
Lower left - T42 resolution and standard scheme
Lower right - T42 resolution and PG scheme

c) Systematic errors

Systematic forecast errors and differences have been examined by calculating mean 500hPa heights for the final five days of the 10-day forecast range, and averaging these over the 12 cases studied. Fig. 19 shows the resulting systematic differences between the standard T42 ("control") and T106 forecasts, between the T42 forecast with the PG scheme and the standard T106, and between the T42 forecasts with the standard and PG schemes. These are shown for the high latitudes of both hemispheres.

For the Southern Hemisphere, mean differences between the T106 forecasts and the T42 forecasts with the PG scheme are clearly smaller than mean differences between the T106 and standard T42 forecasts. Differences between the two sets of T42 forecasts are largest in the immediate vicinity of the South Pole, but a region of relatively large reduction in heights due to use of the PG scheme can be seen to extend over the region east of the Ross Ice Shelf. Examining corresponding mean error maps for the three sets of forecasts (not shown) reveals that errors are generally low over Antarctica for T106 and T42 with the PG scheme, and much larger for T42 with the standard scheme. Elsewhere in the hemisphere, error patterns are similar for T42 and T106, with mostly slightly lower magnitudes for T106.

The mean impact of introducing the PG scheme is smaller for the Northern Hemisphere. The largest effect is in the immediate vicinity of the Pole, where the PG scheme again tends to produce smaller differences between T42 and T106 forecasts. Further from the Pole the mean differences between the two sets of T42 forecasts do not make one or other closer to the T106 set, but these differences are small and may not be of significance. In contrast to the Southern Hemisphere, the corresponding mean error maps show somewhat larger maxima for T106 than for the standard T42 forecasts, and mean T42 errors for the PG scheme are slightly larger than for the standard scheme.

Mean 500hPa fields have been similarly computed for the set of 12 cases carried out at T106 resolution using the standard and PG schemes. Maximum differences are found to be less than 20m in both hemispheres.

Study of the systematic errors of these forecasts was motivated by the recognition that the erroneously high pressures east of the Ross Ice Shelf seen in individual T42 forecasts with the standard scheme bore similarity to a systematic error of climate simulations carried out in Hamburg using an early T21 version of the ECMWF spectral model, reported by Xu et al. (1990). It is also of interest to compare with a set of 30-day forecasts carried out at T21, T42, T63 and T106 resolutions, which have been discussed more generally by Tibaldi et al. (1990). These used a version of the standard model which differed from that employed

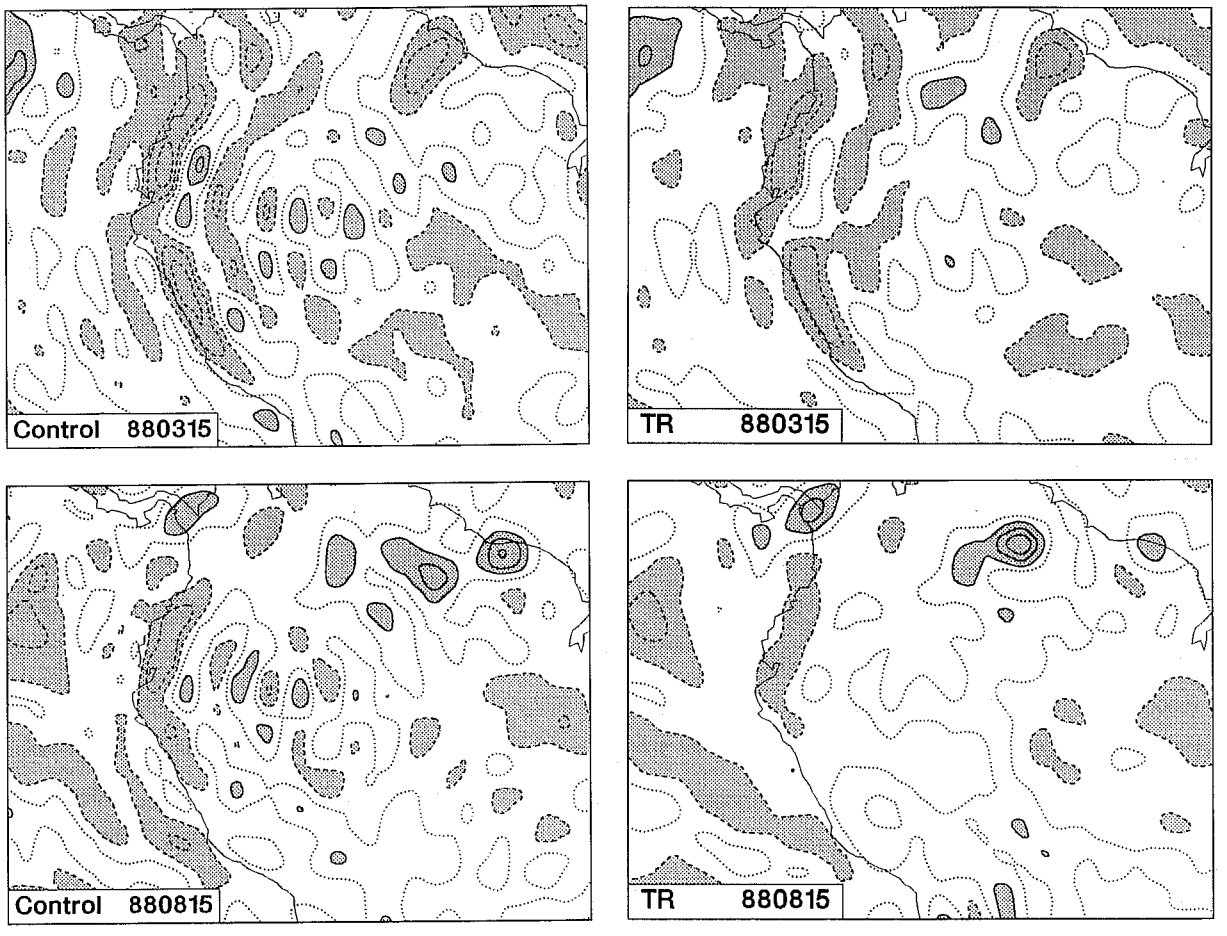

Fig. 18 The vertical motion over tropical South America in 3-day T106 forecasts. The contour interval is 0.1Pa/s, and values greater than this are shaded. Solid lines denote ascent, dashed lines descent, and the zero contour is dotted. Results are for two cases with the standard scheme (left) and the TR scheme (right).

for the present experiments principally in its use of 16-level vertical resolution, no parametrization of gravity-wave drag, and a very much larger vertical diffusion above the planetary boundary layer.

Some results from the experiments of Tibaldi et al. are presented in Fig. 20. The plots relate to 30-day means of the 500hPa height field averaged over 12 cases drawn from the "winter" season (October to March for the Northern Hemisphere; April to September for the Southern Hemisphere). The mean T42 errors and differences between T42 and T106 are shown for both hemispheres, and differences between T21 and T106, and T63 and T106, are shown for the Southern Hemisphere. For this hemisphere, the maximum T42 error indeed occurs east of the Ross Ice Shelf. This is also the region of maximum difference between T42 and T106, and the sign of the difference implies that error is smaller for T106. Differences between T106 and T63 are much smaller than between T106 and T42, and differences between T106 and T21 are very much larger. The latter difference exhibits a strong degree of zonal symmetry, but there is a pronounced error maximum for T21 which occurs in the vicinity of the ice shelf, somewhat to the west of the corresponding position for T42.

For the Northern Hemisphere, the largest T42 error occurs close to the pole, north of the Bering Strait. It can be seen in Fig. 20 that the principal difference between T42 and T106 also occurs in this region, and it corresponds to lower error for T106 than T42. In the near-polar region, the pattern of difference between T42 and T106 is similar to that found for the standard schemes in the 5-10 day range (Fig. 19), and similar to the pattern of difference found between the standard and PG schemes at T42 resolution.

The corresponding 30-day mean maps for the summer season (not shown) exhibit low errors over the Arctic for T42, and little difference between T42 and T106. Over Antarctica, essentially the same result is found as for the winter season. The amplitude of the maximum difference between T42 and T106 is only slightly less than in winter.

In order further to investigate systematic differences between schemes, two sets of 90-day T42 simulations were carried out. The initial dates chosen for these sets were 1 June and 1 December 1987. The standard, PG and TR schemes were used, the TR simulations being carried out both for ℓnp_s and p_s as the prognostic spectral variable.

The results for the summer season (the June initial conditions for the Northern Hemisphere and December initial conditions for the Southern Hemisphere) appear quite easy to interpret, and are shown in Fig. 21 in terms of differences in mean 500hPa heights for the 1-90 day period. Differences between the standard and PG simulations are evidently

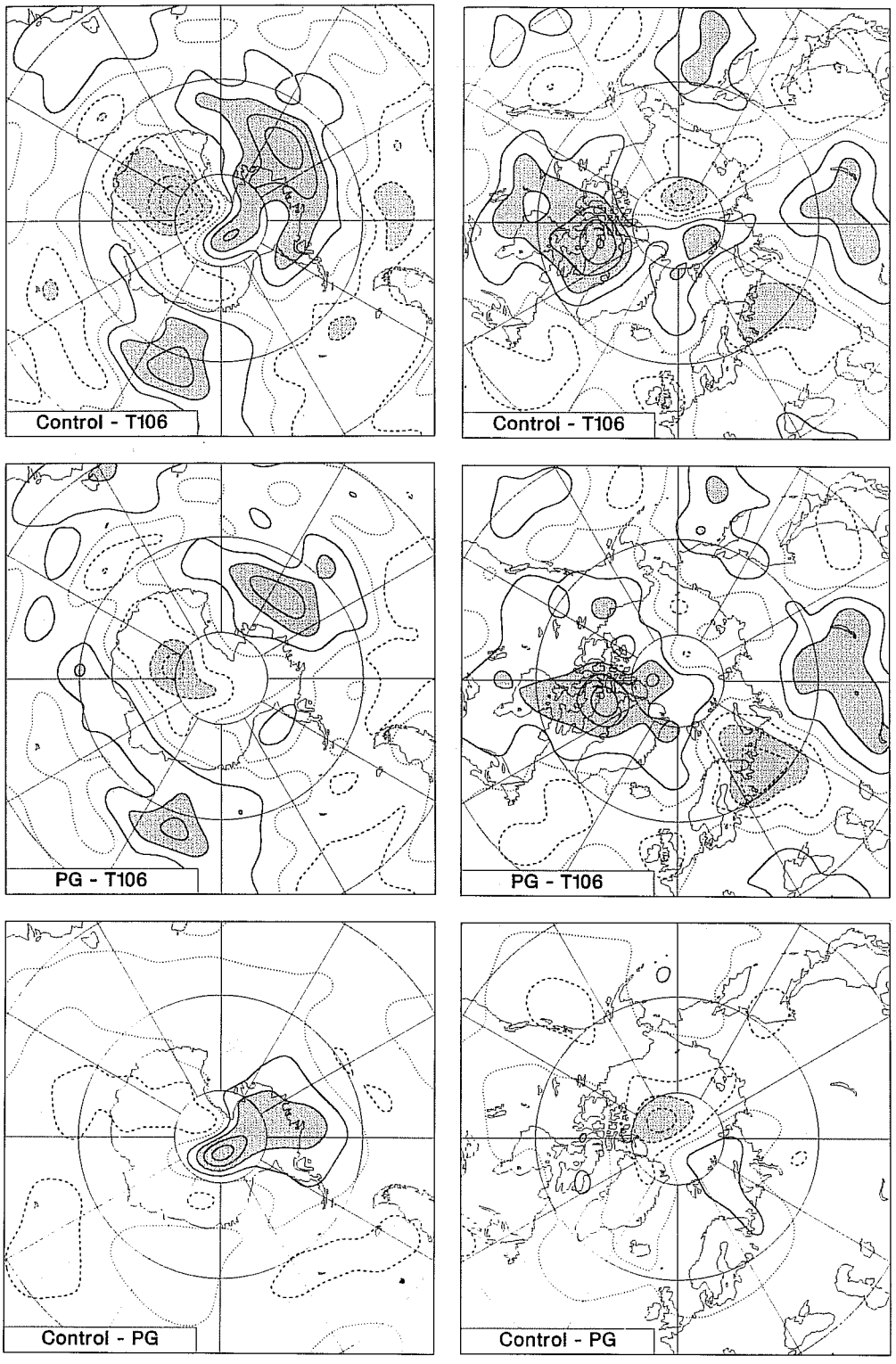

Fig. 19 Mean differences of 500hPa height forecasts, averaged over 12 cases and over 10 12-hourly forecast outputs from days 5.5 to 10, for the southern (left) and northern (right) hemispheres. The contour interval is 20m. The differences are between:

Upper - Standard T42 and T106 forecasts

Middle- T42 forecasts with the PG scheme and the standard T106 forecasts

Lower - T42 forecasts with the standard and PG schemes

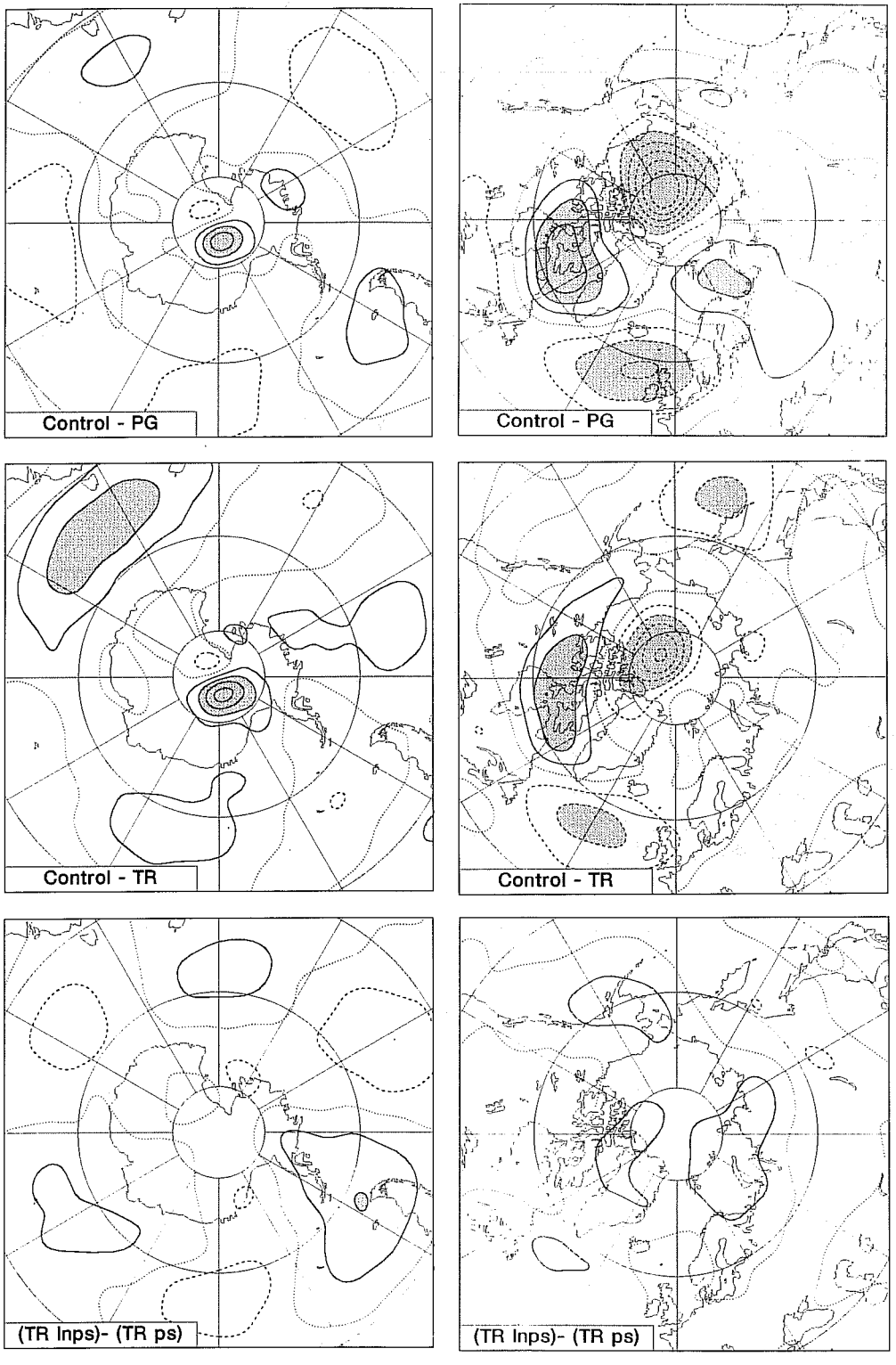

Fig. 21 90-day mean 500hPa height differences from summer T42 simulations. The contour interval is 20m. Differences are between:
Upper - Standard and PG forecasts
Middle- Standard and TR forecasts
Lower - TR forecasts using $\ell n p_s$ and p_s as the spectrally represented pressure variable.

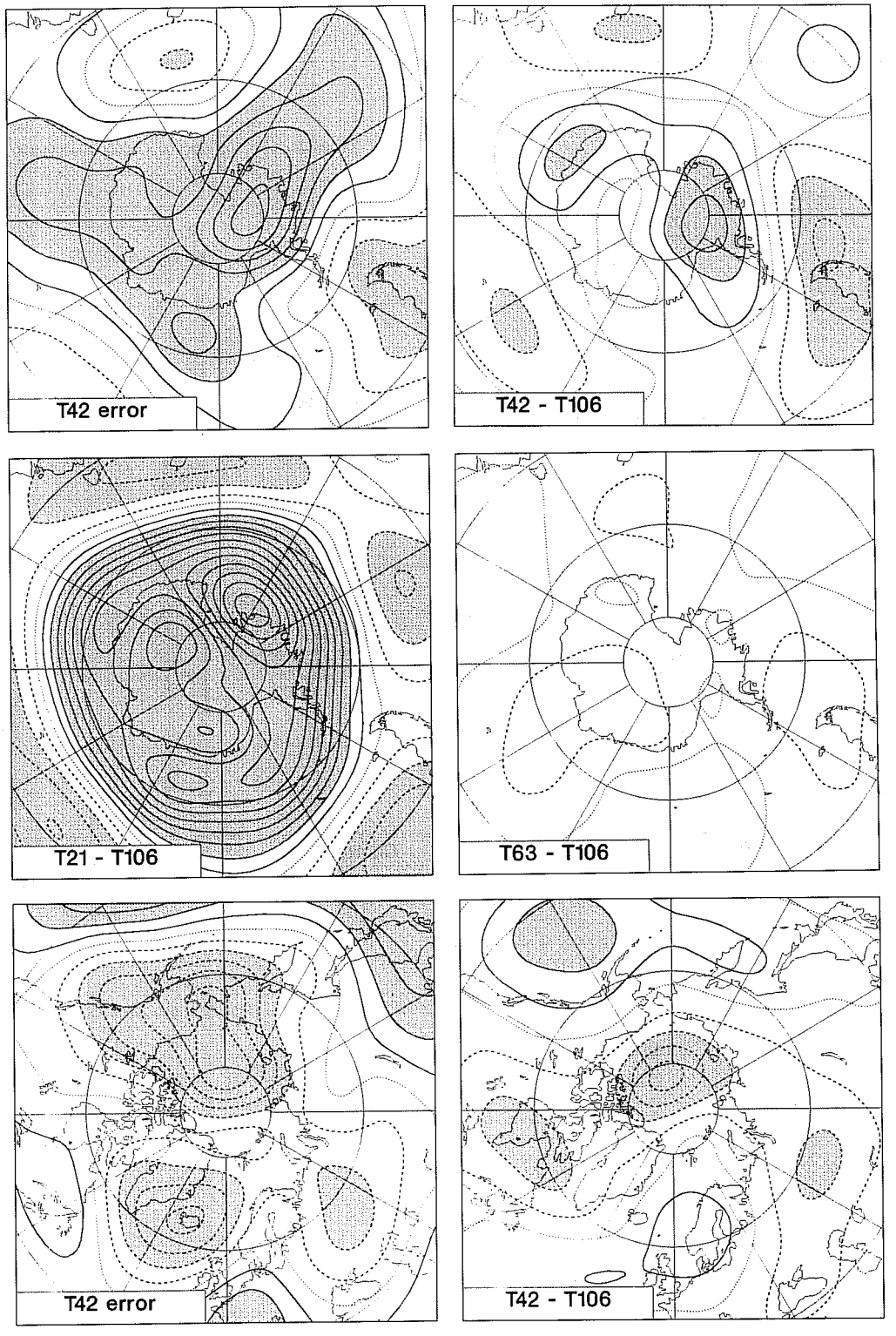

Fig. 20 500hPa height maps showing T42 forecast errors (upper and lower left) and differences between T106 forecasts and T21 (middle left), T42 (upper and lower right) and T63 (middle right) forecasts, averaged over 12 cases and over days 1 to 30 of integrations using the standard scheme. The contour interval is 20m.

similar to those between the standard and TR simulations. In the polar regions these differences are similar to those shown for the 5-10 day range in Fig. 19 (for which cases span the full year). The impact of changing from ℓnp_s to p_s as prognostic variable with the TR scheme is clearly less than that of changing from the standard to the TR or PG scheme.

Corresponding maps for the winter season are presented in Fig. 22. Differences are generally larger than for summer, and there is much more difference between the PG and TR simulations, and between the TR simulations using ℓnp_s and p_s as basic variable. Given the larger variance of the wintertime circulation, longer simulations are probably required to establish the true impact of the various changes in scheme considered here. However, near the poles the impact of changing from the standard to the PG and TR schemes is qualitatively as seen previously, with some measure of quantitative agreement between the TR and PG schemes for the Antarctic.

d) The reason for improved model performance

The PG and TR schemes remove analytically some of the cancellation between the $\nabla\varphi$ and $R_dT_v\nabla\ell np$ terms in the momentum equations, but it is not clear from idealized calculations of the net pressure-gradient error such as presented in section 5(a) why the scheme is so successful in improving lower-resolution forecasts. However, after completion of the experimentation described elsewhere in this report, and while developing the scheme for implementation within a new semi-Lagrangian version of the model, it became apparent that the high-latitude errors in model performance that are corrected by the PG and TR schemes did not occur when the model's usual semi-implicit treatment of vorticity advection (Simmons et al. 1989) was not used. This provides the following explanation for the improved model performance found with the new schemes.

The vorticity equation can be written in the form

$$\frac{\partial \xi}{\partial t} = \frac{1}{a(1-\mu^2)} \frac{\partial}{\partial \lambda} (F_v + P_v) - \frac{1}{a} \frac{\partial}{\partial \mu} (F_u + P_u) + K_\xi \qquad (16)$$

where

$$F_v = -(f+\xi)\, U - \dot{\eta} \frac{\partial V}{\partial \eta} - \frac{R_d T_v}{a} (1-\mu^2) \frac{\partial \ell np}{\partial \mu} \qquad (17)$$

and

$$F_u = (f+\xi)\, V - \dot{\eta} \frac{\partial U}{\partial \eta} - \frac{R_d T_v}{a} \frac{\partial \ell np}{\partial \lambda} \qquad (18)$$

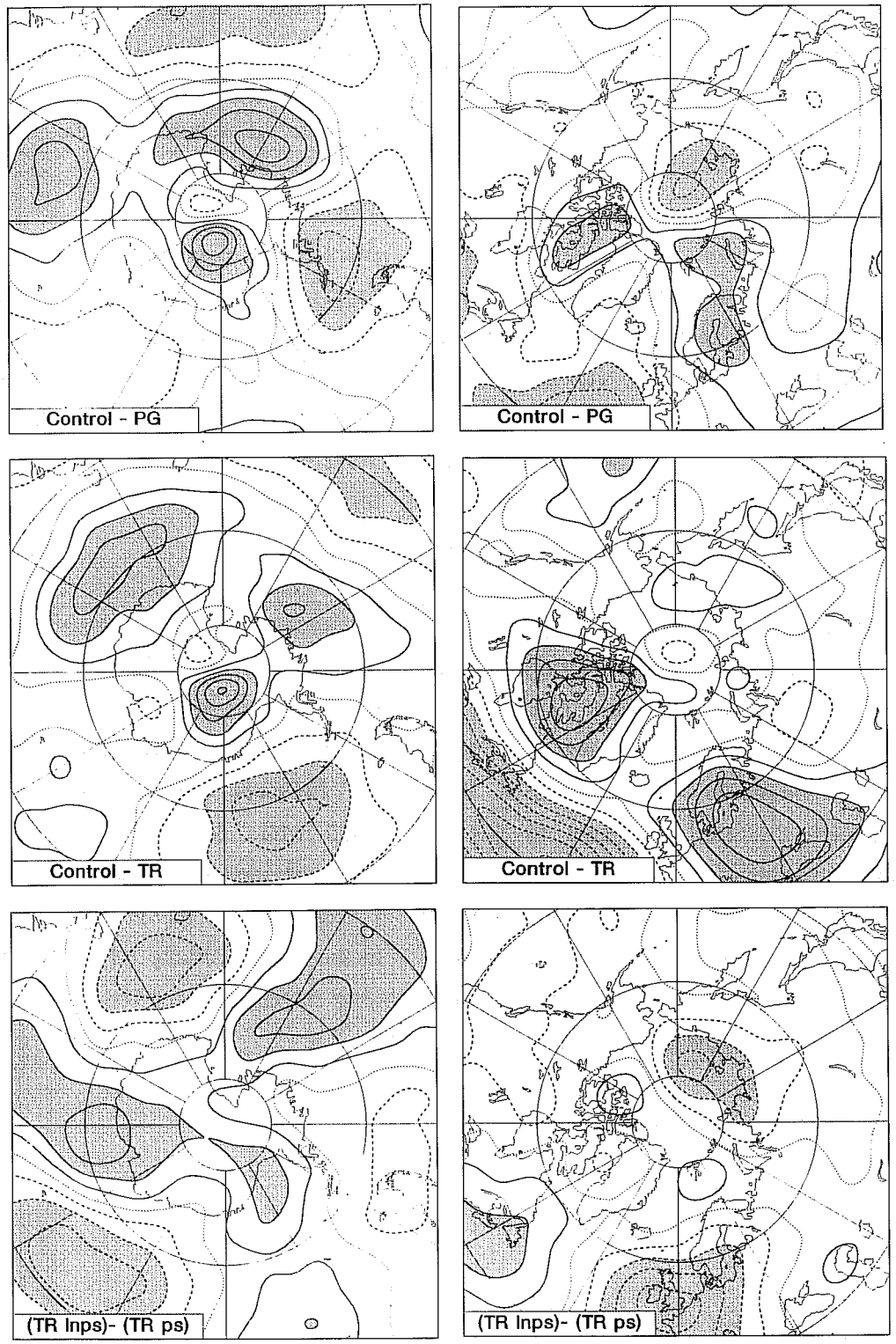

Fig. 22 As Fig. 21, but for winter simulations.

F_v and F_u are the dynamical tendencies of the cos(latitude)-scaled wind components V and U apart from the terms representing the gradients of the sum of the geopotential and kinetic energy density, which do not contribute to the vorticity tendency (in the true equations and in the model). P_v and P_u are the corresponding tendencies from parametrized processes, and K_ξ represents horizontal diffusion. F_v and F_u can be written in the forms

$$F_v = \tilde{F}_v - \frac{R_d T_r(p)}{a} (1-\mu^2) \frac{\partial \ell n p}{\partial \mu} \tag{19}$$

and

$$F_u = \tilde{F}_u - \frac{R_d T_r(p)}{a} \frac{\partial \ell n p}{\partial \lambda} \tag{20}$$

where $\tilde{F}_v$ and $\tilde{F}_u$ are as defined by Eqs. (17) and (18), but with T_v replaced by $\tilde{T}_v$, where $\tilde{T}_v = T_v - T_r(p)$.

The crucial point in the present context is that

$$\frac{1}{(1-\mu^2)} \frac{\partial}{\partial \lambda} \left(\frac{R_d T_r(p)}{a} (1-\mu^2) \frac{\partial \ell n p}{\partial \mu} \right) - \frac{\partial}{\partial \mu} \left(\frac{R_d T_r(p)}{a} \frac{\partial \ell n p}{\partial \lambda} \right) = 0 \tag{21}$$

This implies in particular that the pressure-gradient terms only directly influence the tendency of vorticity in the continuous equations through the deviation of virtual temperature from any reference distribution which is a function of pressure alone.

In spectral models it is usual to rely on the transform method to achieve the cancellation seen in Eq. (21). An accurate representation of this cancellation is important because the pressure-gradient terms are several orders of magnitude larger than the other terms comprising F_v and F_u in regions of steep orography. One source of inaccuracy is aliasing due to implementation of a semi-implicit treatment of vorticity advection. Use of the semi-implicit scheme means that the effective form of Eq. (21) is

$$imb_m(\mu) \left[T_r \frac{\partial \ell n p}{\partial \mu} \right]^m + \frac{\partial b_m}{\partial \mu} \left[T_r \frac{\partial \ell n p}{\partial \lambda} \right]^m - \frac{\partial}{\partial \mu} \left[b_m(\mu) T_r \frac{\partial \ell n p}{\partial \lambda} \right]^m = 0 \tag{22}$$

where $[\ ]^m$ denotes a Fourier component with zonal wavenumber m, and

$$b_m(\mu) = \left(1 + \frac{imU_r(\mu)\, \Delta t}{a\,(1-\mu^2)} \right)^{-1} \tag{23}$$

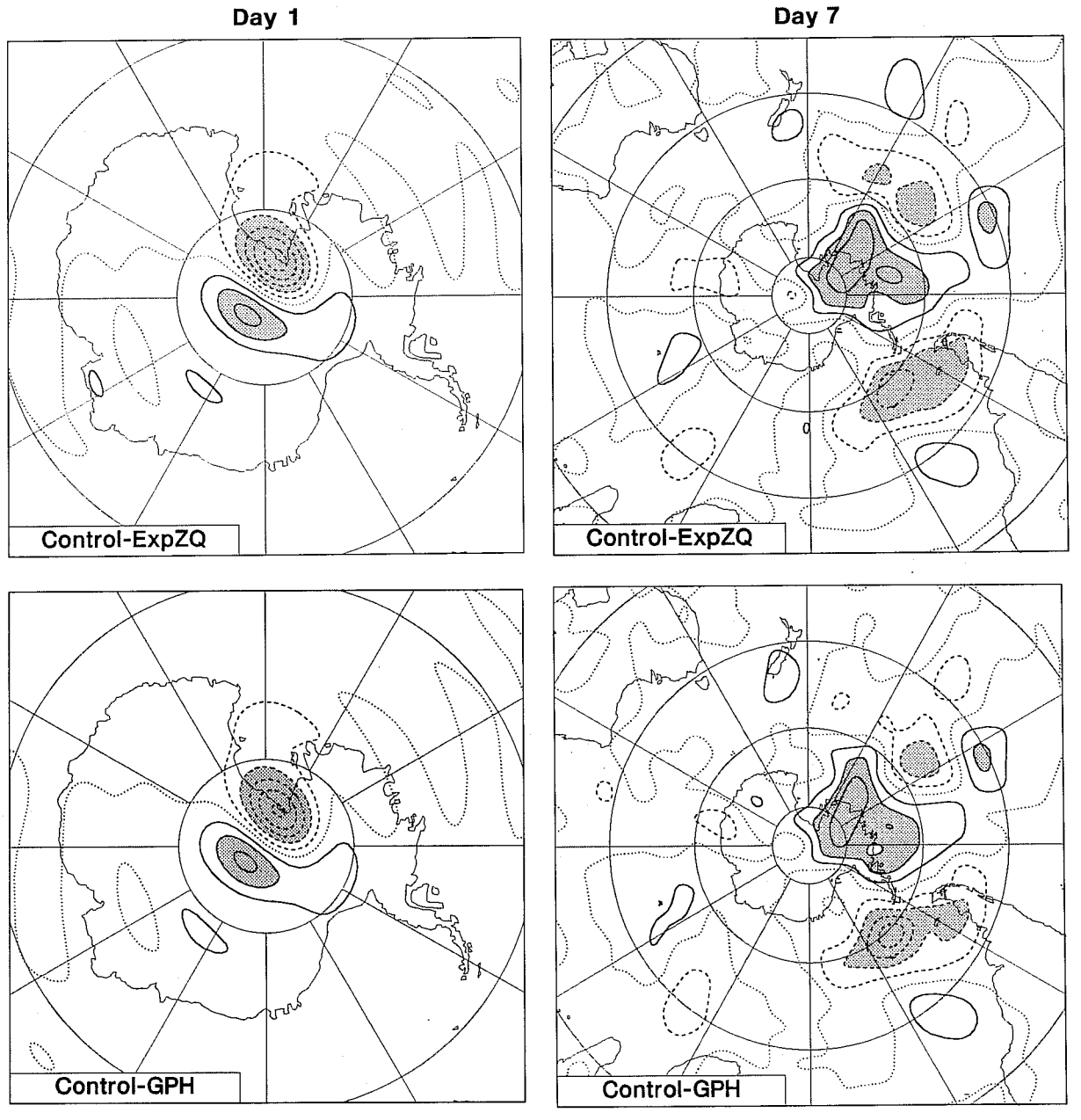

Fig. 23 Day-1 (left, contour interval 40m) and day-7 (right, contour interval 80m) forecast differences in 500 hPa height between standard forecasts and forecasts using the alternative treatments of the vorticity equation discussed in the text.

Here $U_r(\mu)$ is the reference advecting zonal flow (multiplied by the cosine of latitude) used in the semi-implicit scheme. In the ECMWF model it is chosen to be the arithmetic mean of the maximum and minimum values of the cosine-scaled zonal velocity component at the preceding timestep. As such, $b_m(\mu)$ can exhibit a sharp variation with latitude, and despite the Δt factor in (23), aliasing can apparently be a significant in the calculation of expression (22). The PG and TR schemes appear to be successful because the cancellation in equation (21) is imposed exactly when $T_r(p)$ is the chosen reference temperature profile.

Given that this is the source of improvement brought about by the PG scheme, an alternative can be suggested. It can be simply stated: explicitly include the geopotential-gradient terms in F_v and F_u. In regions of steep orography there is a strong degree of cancellation between the $\nabla\varphi$ and $R_d T_v \nabla \ln p$ terms, so the effect of the aliasing should be reduced.

Two further forecasts have been carried out at T42 resolution for the case of 15 September 1987 presented earlier. Maps at days 1 and 7 for the high-latitude Southern Hemisphere are shown in Fig. 23 for the differences between the standard forecast and the two new forecasts. Neither of the latter used the PG or TR scheme. The upper panels are from a forecast in which the semi-implicit scheme for vorticity (and humidity) advection was turned off (and the timestep reduced from its normal value of 36 minutes to 30 minutes). The lower panels are from a forecast which used the semi-implicit scheme and usual timestep, but which included the geopotential-gradient terms in F_v and F_u. In both cases the differences from the standard forecast are strikingly similar to those obtained with the PG or TR scheme (Figs. 14 and 15), and support the explanation given above. Further support is provided by objective verification (not shown).

8. DATA ASSIMILATION TESTS

In this section we discuss principally the results from two experimental data assimilations. Both were carried out for the two-day period from 12UTC 13 May 1989 to 12UTC 15 May 1989. The first experiment used the PG scheme in the assimilating model, but no change to the standard system for the calculation of pressure-level heights from model-level first-guess temperatures (the temperatures produced by a 6-hour forecast from the preceding analysis). The second assimilation used the same model changes and the PG version of the post-processing for the calculation of the pressure-level first guess in the analysis. The corresponding operational analyses and forecasts served as the controls for the experiments. The ECMWF data assimilation system is described by Shaw et al. (1987) and references therein. A feature of the data analysis that is basic to the discussion given here is that height rather than temperature is the analyzed thermodynamic variable.

A third data assimilation has also been carried out for the period in question. This differed from the second assimilation in that it used the corrected tension-spline interpolation discussed in section 5. Results from this assimilation will be mentioned where appropriate.

Some results on the mean fit to observations of various height fields from the standard and first two experimental assimilations are presented in Fig. 24. All are for 12UTC 15 May 1989, but for the most part similar pictures are found for other cycles of the assimilation. In these calculations model-level fields for the first guess and for the uninitialized and initialized analyses are post-processed to produce standard-level heights, and differences are computed between radiosonde measurements and these postprocessed heights. These differences are then averaged over all observations within the extratropical northern and southern hemispheres respectively. The observations are those used in each analysis, after quality-control, and the number used is shown to the right of each panel in Fig. 24. Where two figures are given a different decision has been made during the quality-control. The difference amounts, however, to no more than one observation. In this case the second of the figures shown is that for the control assimilation.

The top panels present first-guess biases for the northern (left) and southern (right) hemispheres from the control and first experimental assimilation. Changing just the assimilating model has little effect on the fits to observed data, but a small reduction in tropospheric bias can be seen for the Southern Hemisphere. There is a slight increase in bias in the stratosphere of the Northern Hemisphere. It should be noted that 10 of the 50 or so radiosondes used in the analysis of the extratropical Southern Hemisphere were located around the coastline of Antarctica, where the impact of the model change is largest.

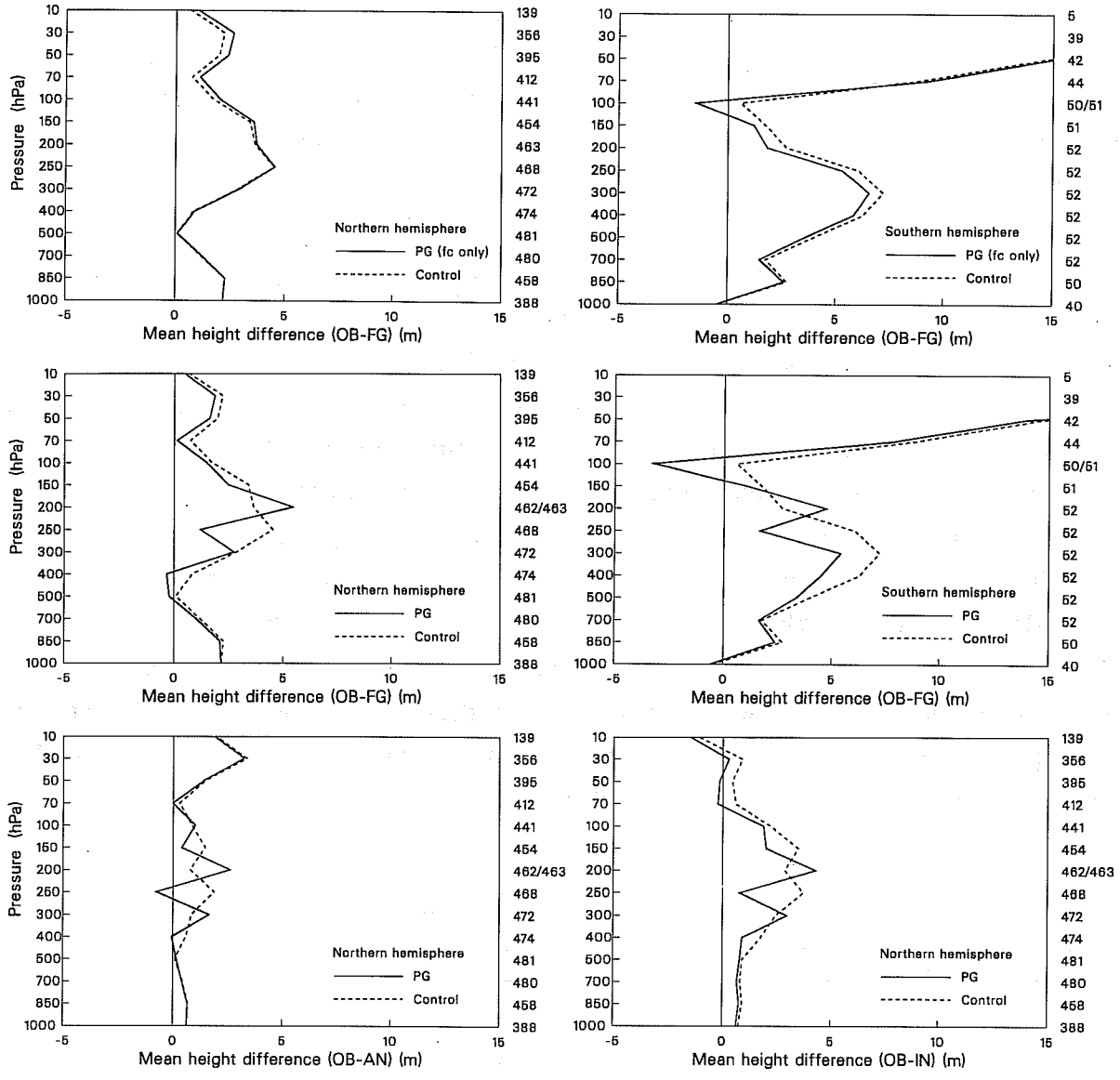

Fig. 24 Mean differences (m) between radiosonde height measurements and the first-guess heights (6-hour forecasts) used in the data analysis for 12UTC 15 May 1989, computed over the extratropical northern (left, upper and middle panels) and southern (right, upper and middle panels) hemispheres. The upper panels show the impact of changing just the assimilating model, and the middle panels the impact of changing both the model and the evaluation of the first guess at standard pressure levels. For the latter case, the lower panels show corresponding differences between observations and the uninitialized (left) and initialized (right) analyses for the Northern Hemisphere. The number of observations used is shown in the column to the right of each panel.

The remainder of Fig. 24 relates to the second assimilation in which the post-processing was also changed. The middle panels show first-guess biases for the two extratropical hemispheres, and the lower panels the biases of the uninitialized and initialized analyses for the Northern Hemisphere. These biases are generally lower for the experimental assimilation. This is particularly so for the first guess fields, but is true also for the analyses, discounting for the moment the oscillation between adjacent standard levels from 400 to 100hPa in the experimental assimilation. The reduction in bias is larger for the initialized than for the uninitialized analysis, which indicates that the new analysis is more consistent with the model. The same is the case for biases computed using radiosondes from the tropics.

The oscillation in bias from level to level between 400 and 100hPa is evidently larger (and opposite in phase) for the second experimental assimilation, but is not thought to be a cause for concern. It appears to be caused primarily by the initial shock to the experimental assimilation of starting it at 12UTC on 13 May using the operational model-level temperature field as the first guess. This temperature field had become adjusted over many assimilation cycles to compensate for the error in the postprocessing of geopotential, which from Fig. 3 can be seen to change sharply near the tropopause. As a result, a large oscillation in bias was set up at the beginning of the assimilation, and this diminished only rather slowly in time. Table 2 shows that the thickness bias for the 200-250hPa region approximately halves over the two-day course of the experimental assimilation. The oscillation is damped only slowly because of the particular distribution of model levels in the upper troposphere and lower stratosphere. Model full levels are close to standard levels in this region, whereas the analyzed changes to the first-guess heights are

Date	13 May		14 May			15 May		
Time	18	00	06	12	18	00	06	12
FG	1.35	0.88	0.99	0.73	0.85	0.88	0.79	0.64
AN	1.19	0.77	0.88	0.67	0.83	0.73	0.67	0.58
IN	1.18	0.81	0.86	0.74	0.79	0.81	0.66	0.61

Table 2 The bias in 200-250hPa thickness, expressed as a layer-mean temperature bias (K), of the first guess (FG), the uninitialized analysis (AN) and the initialized analysis (IN) for the second experimental assimilation for the period from 18UTC 13 May to 12UTC 15 May 1989. Biases were computed by comparing postprocessed model fields with radiosonde data for the extratropical Northern Hemisphere.

evaluated at half levels, prior to computation of full-level temperature changes. Height changes which alternate in sign from one standard level to another appear as rather small changes when evaluated at the model half levels. A much longer assimilation would be needed to establish whether or not the new scheme exhibits less of an oscillation than the standard scheme, but in view of the pattern of post-processing error in the standard scheme this might be expected to be the case. We note that the oscillation has been found to disappear in a standard assimilation when the vertical resolution of the assimilating model is approximately doubled in the upper troposphere and lower stratosphere (Undén, personal communication). Also, in the third experimental assimilation using the corrected tension-spline interpolation, the 200-250hPa thickness biases were reduced by about a third.

Given the two results that the height analyses agree in the mean to within a metre or so at most levels (Fig. 24) and that for identical temperature fields the standard and PG post-processing schemes give standard-level heights which differ by 5m or more (Fig. 3), the implication is that the initial temperature fields supplied to the forecast model differ significantly. This is illustrated in the left-hand panel of Fig. 25, which shows the global-mean differences between the temperature analyses for 12UTC 15 May 1989, and corresponding differences for the first-guess fields, for the standard and second experimental assimilation. Differences are shown for standard pressure levels, but similar differences are found for global means taken over model coordinate surfaces. Similar differences are also found at other analysis times. Mean temperatures at 700hPa are around 0.25K colder in the assimilation with the revised post-processing of geopotential, and upper tropospheric temperatures are almost 0.5K warmer. Middle- and upper-tropospheric differences vary in the horizontal by a few tenths of a degree above low ground, and there are larger variations of a degree or more linked to the distribution of orography, which causes significant variations in post-processing error for the standard scheme.

Somewhat smaller differences are seen for the first guess than for the analysis in Fig. 25. This is consistent with the larger standard-level height differences between the first guesses and the tendency of the model to evolve towards its preferred thermodynamic structure. Global budgets for standard forecasts characteristically show that evaporation is lower and convective precipitation higher in the short-range forecasts than at longer time ranges. Forecasts from the new assimilation show somewhat more initial evaporation and less convective precipitation, and reduce the imbalance in the hydrological budget by around 10 to 15% during the first few days of the forecast period.

There appears little doubt from comparison with radiosonde temperature measurements that it is the experimental assimilation that yields the more correct temperatures. The

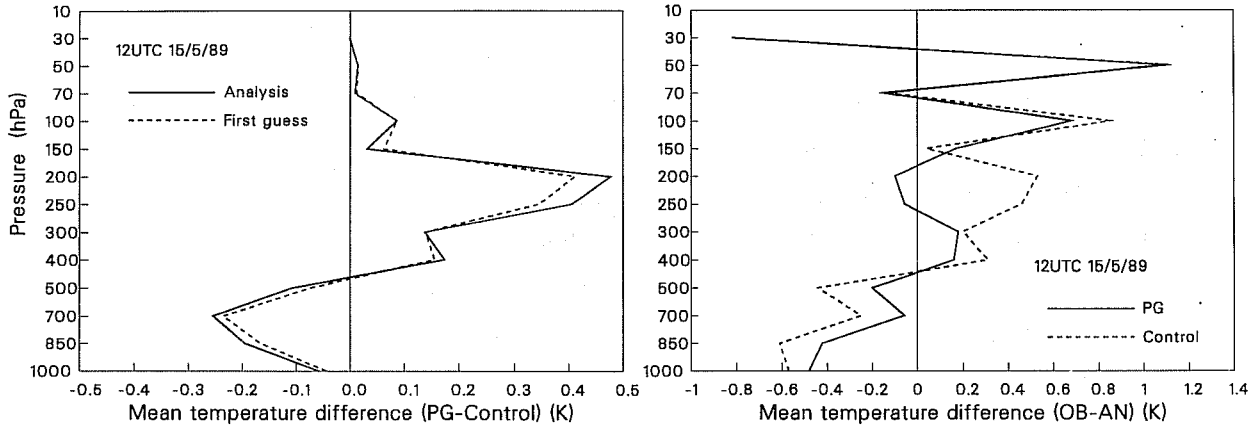

Fig. 25 Temperature changes brought about by use of the PG version of the model and first-guess evaluation, for 12 UTC 15 May 1989. The global-mean temperature differences at standard pressure levels between the first guesses (dashed) and between the uninitialized analyses (solid) are shown left, and the right-hand panel shows mean differences between radiosonde temperature measurements and the PG (solid) and standard (dashed) analyses.

right-hand panel of Fig. 25 shows the mean differences at standard levels between the observed temperatures and the temperature analyses produced by the two assimilations. These are averaged over all available radiosondes, and although these have a spatial distribution which is far from uniform over the globe, the difference in bias between the standard analysis and the analysis from the PG assimilation is consistent with the global-mean differences discussed above. The bias is significantly reduced at tropospheric levels in the new analysis. The oscillation in fit from level to level is also reduced in the troposphere, though both analyses suffer from a similar large oscillation near the top of the model. Here model levels are particularly close to standard pressure levels. An erroneous oscillation in temperature thus influences little the standard-level first-guess heights, and cannot be easily corrected by the analysis system. The oscillation is, however, reduced by use of tension-spline interpolation, although the latter gives a poorer fit at 200 and 250hPa.

Maps of 500hPa height are generally similar for the various analyses, and differ most in the polar regions. Fig. 26 shows differences between the standard and two experimental analyses for 12UTC 15 May 1989. The upper panels are for the first experimental assimilation in which only the model was changed. As expected from the forecast experiments with the PG scheme, the differences are largest over Antarctica. Indeed, pressures are lower in the PG analysis over just that region where pressure was systematically lower in the T42 PG forecasts (Fig. 19, lower left). There is only a small region over the Northern Hemisphere where differences exceed 4m, but this occurs as expected to the north of Greenland. The regions of principal difference found for the first assimilation are reproduced in the second (lower panels of Fig. 26), although there is a rather more widespread change in the latter case.

Ten-day forecasts have been carried out from 12UTC 14 and 15 May using initial analyses from the second experimental assimilation, and from 12UTC 15 May using the first assimilation. The PG version of the model was used in each case. Anomaly correlations of 500hPa height for the extratropics are presented in Fig. 27 together with the results for the standard (operational) forecasts from the standard assimilation. Inherent variations from day to day in the skill of operational forecasts make it difficult to draw firm conclusions as to impact on forecasts of a data assimilation change such as studied here, particularly at longer forecast ranges. The forecasts from the second assimilation are, however, generally better than the control forecasts out to day 4. The improvement is seen to occur almost entirely in the Southern Hemisphere for the 500hPa height correlations shown in Fig. 27, but other measures, particularly root-mean square wind errors at 850 and 200hPa, reveal that a slight improvement occurs also in the Northern Hemisphere in the

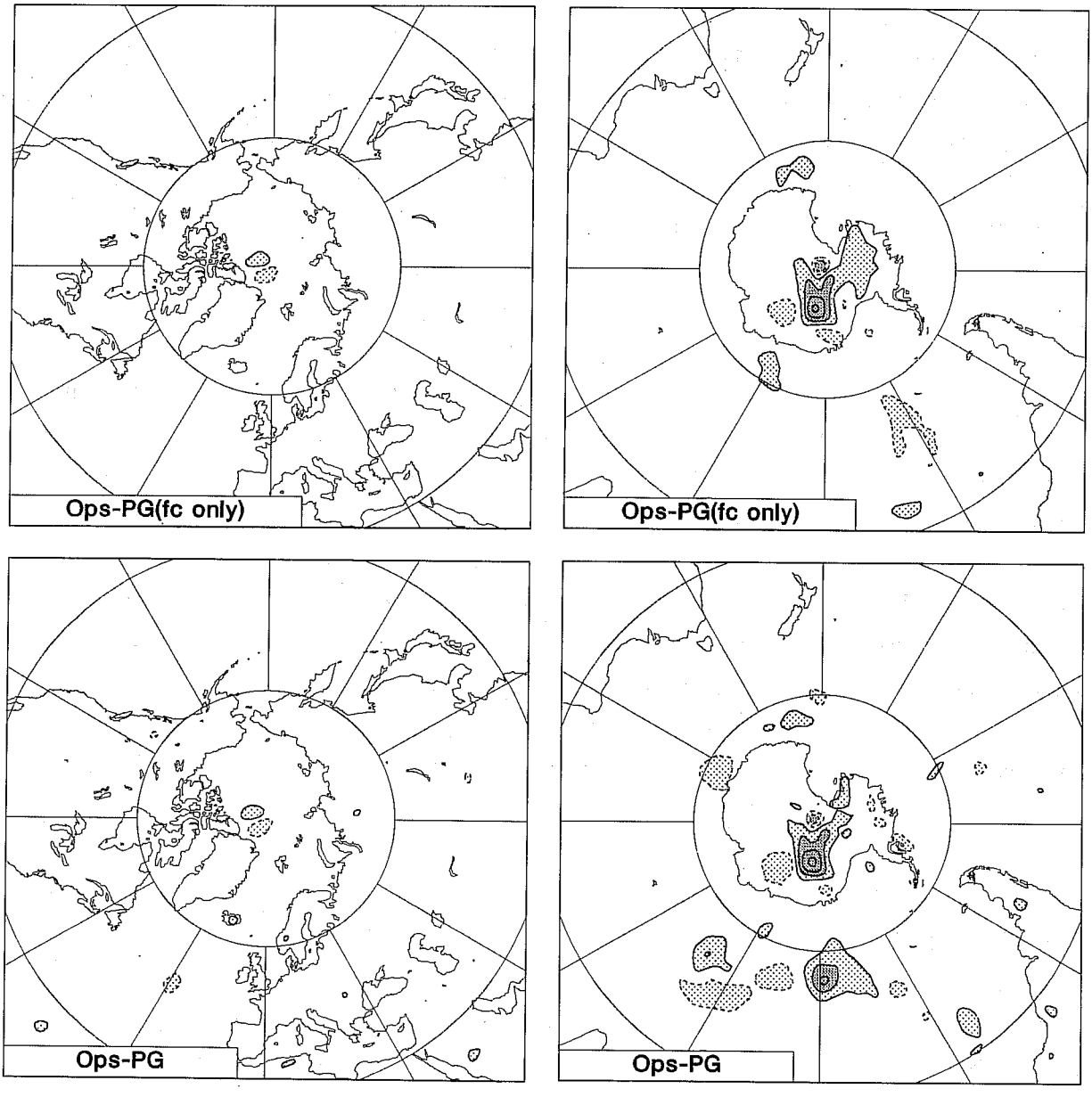

Fig. 26 Differences in 500hPa height for the northern (left) and southern (right) hemispheres, for 12 UTC 15 May 1989. The contour interval is 8m. Regions where differences are between 4m and 12m are lightly shaded, and heavy shading denotes differences greater than 12m. The upper panels show the impact of changing just the assimilating model, and the lower panels the impact of changing both the model and the evaluation of the first guess at standard pressure levels.

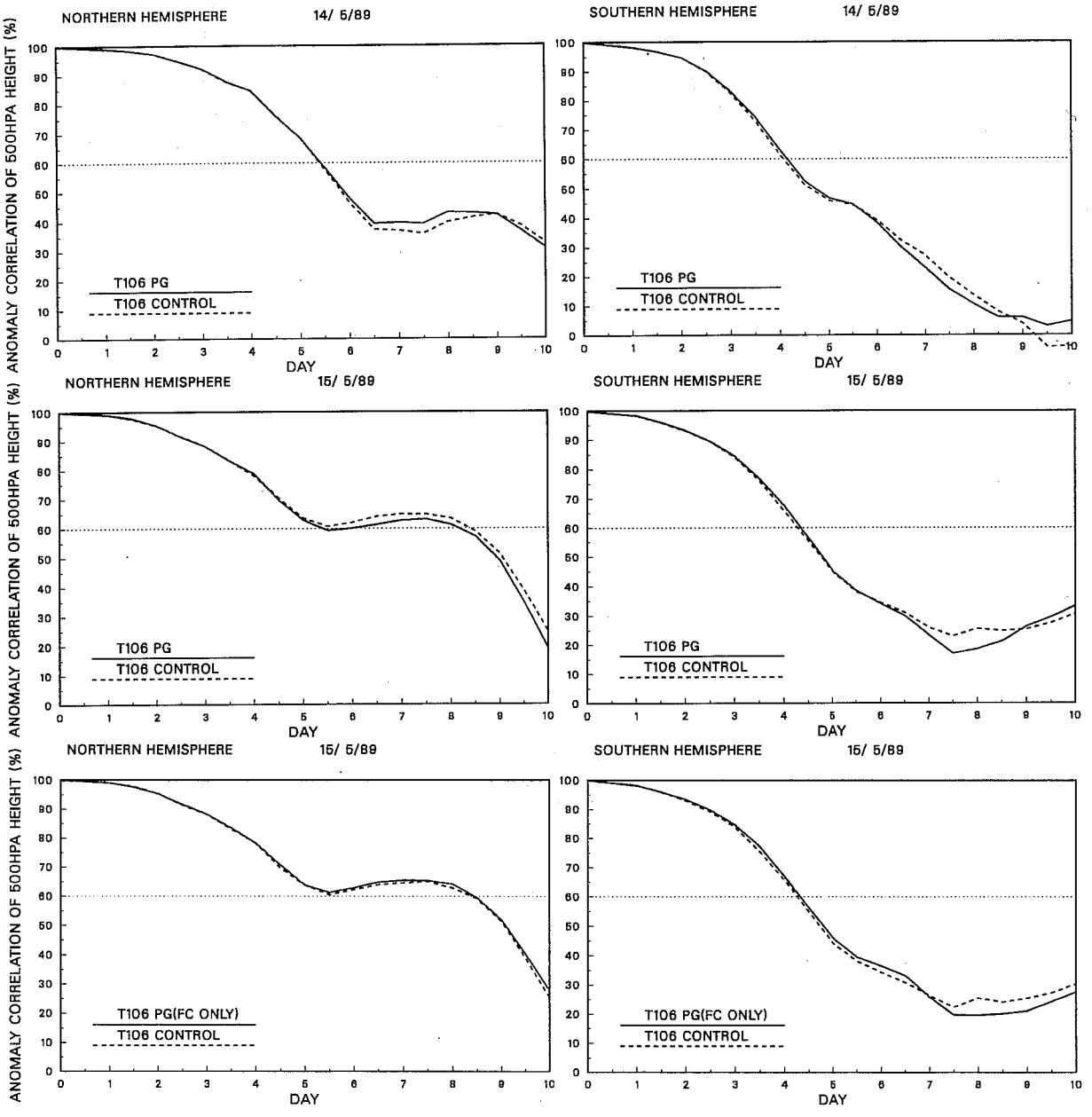

Fig. 27 Anomaly correlations of 500hPa height for T106 forecasts from analyses for 12UTC 14 May (upper panels) and 15 May (middle and lower panels), for the extratropical northern (left) and southern (right) hemispheres. The upper and middle panels compare standard forecasts with PG-scheme forecasts from the assimilation with the PG version of the model and first-guess post-processing. The PG-scheme forecast in the lower panels was from the assimilation in which only the model used the PG scheme.

first half of the forecast range. The same is true of verification scores for the tropics. There is no clear overall indication which set of forecasts is to be preferred later in the forecast range.

For the first assimilation, Fig. 27 shows there to be a small positive impact of the change to the PG scheme, at least while forecast accuracy remains high or moderate. A slight advantage occurs early in the range for the Southern Hemisphere, and comparison with scatter diagrams for the set of 12 T106 forecasts discussed previously shows a larger improvement at day 3 in this forecast from a consistent data assimilation than in any of the 12 forecasts carried out from the operational analyses.

9. EXPERIMENTS USING p_s AS PROGNOSTIC VARIABLE

Fig. 28 shows anomaly correlations of 500hPa height comparing forecasts with ℓnp_s and p_s as prognostic variable, using the TR scheme. Results are shown for the average of 12 T42 cases and 6 T106 cases. Mean forecast skill is evidently little sensitive to the choice of spectrally-represented pressure variable, at least for the time range over which forecasts can be regarded as useful. This lack of sensitivity is also seen in the verification of individual cases. The mean degradation in skill due to use of p_s seen beyond day 7 for the T42 forecasts for the Northern Hemisphere reflects a rather systematic trend, since only two of the 12 cases were in favour of p_s at day 10. There is no indication of this for T106, however.

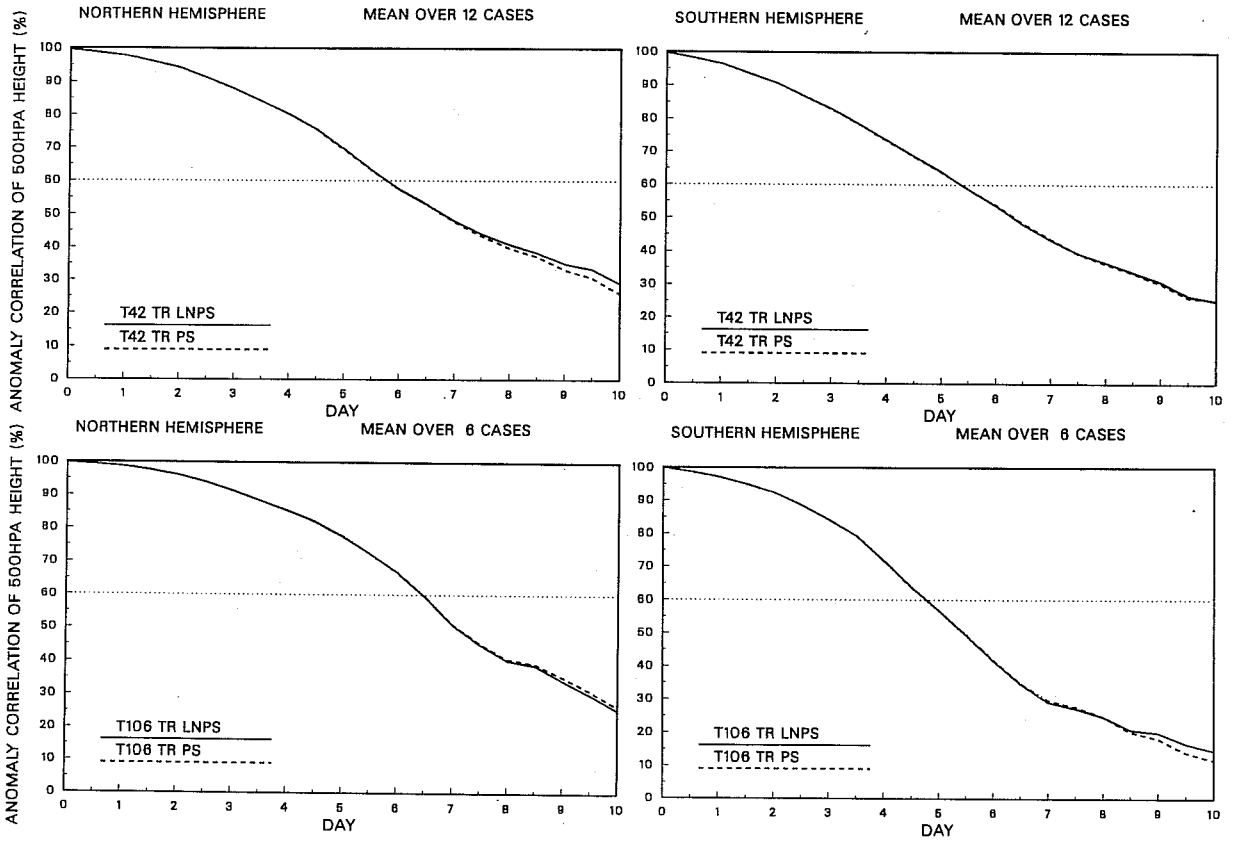

Fig. 28 Mean anomaly correlations of 500hPa height for the northern (left) and southern (right) hemispheres, comparing the use of ℓnp_s and p_s as the spectrally represented variable in the TR scheme. The upper panels are for averages of 12 T42 cases, and the lower panels are for 6 T106 cases.

Examination of synoptic maps confirms the basic similarity between the two sets of forecasts. In particular, the p_s version of the TR scheme captures all the improvement over the standard ECMWF scheme seen previously for T42 forecasts in the Southern Hemisphere. Fig. 29 shows day-1 and day-7 differences in 500hPa height between the standard T42 forecast and the TR-scheme forecast using the p_s version, for the case of 15 September 1987. Comparison with Figs.14 and 15 shows very close agreement with the corresponding maps for the ℓnp_s version of the TR scheme. For example, the forecasts from the two versions of the TR scheme are closer than those from the TR and PG schemes using ℓnp_s as the prognostic variable. Examination of vertical velocity maps from the T106 forecasts shows that the p_s version of the TR scheme matches the ℓnp_s version in giving a less noisy pattern of vertical motion over the South American region shown in Fig. 18.

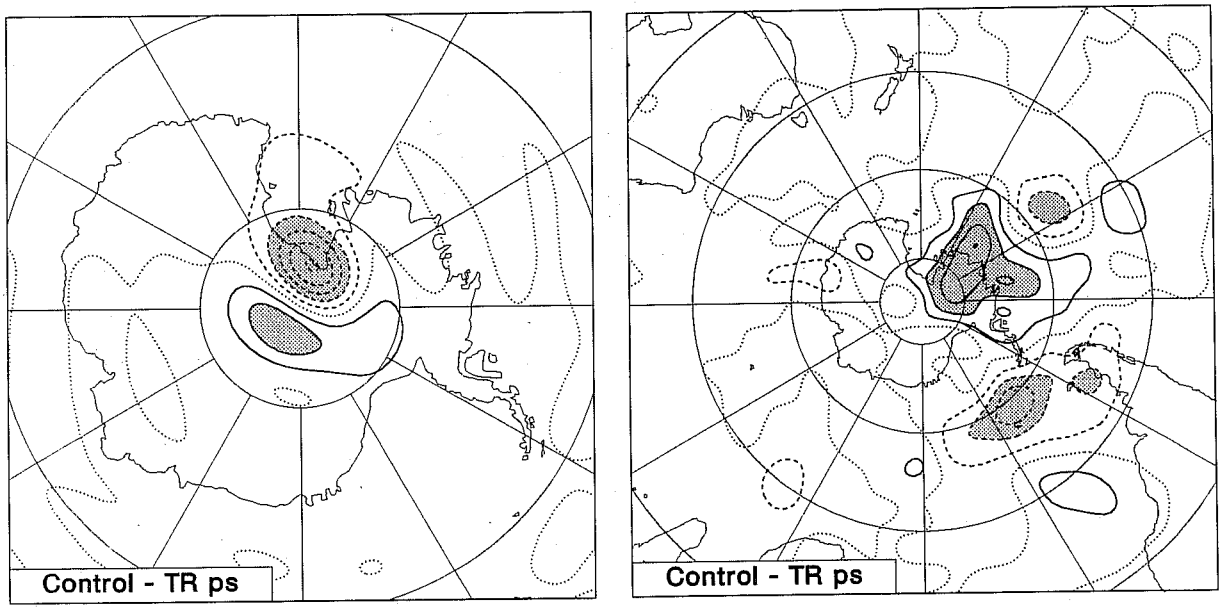

Fig. 29 500hPa height differences for one-day (left, contour interval 40m) and 7-day (right, contour interval 80m) forecasts from 15 September 1987. The differences are between the standard T42 forecast and the T42 forecast using p_s as the spectrally-represented variable in the TR scheme.

Maps have already been presented in Figs.21 and 22 from the 90-day T42 simulations. It was noted in the introduction that use of p_s as the spectrally represented pressure variable results in a mass-conserving model. This has been confirmed in practice, and figures relating to this are presented in Table 3. The ℓnp_s version of the TR scheme exhibits a spurious gain of about 1hPa in global-mean surface pressure in the course of the 90-day simulation for the December to February period. A smaller gain occurs for the June to August period. Similar results are found for the standard and PG simulations.

GLOBAL-MEAN SURFACE PRESSURE (hPa)

1 June 1987	ℓnp_s scheme	p_s scheme
Day 0	979.2661	979.2661
Day 90	979.6429	979.2661
1 Dec 1987	ℓnp_s scheme	p_s scheme
Day 0	978.9377	978.9377
Day 90	979.9353	978.9377

Table 3 The global-mean surface pressure of the model atmosphere for the initial day and day 90 of T42 integrations starting 1 June and 1 December 1987, using the TR scheme, for ℓnp_s and p_s as the spectrally represented prognostic variable.

10. CONCLUSIONS

It has been shown that the simulation of the high-latitude troposphere in the ECMWF spectral model is sensitive to the form chosen for the representation of pressure-gradient terms, when the model is run using its standard 19-level vertical resolution and T42 horizontal resolution. In particular, changing the standard calculation of the pressure gradient to that of the PG scheme reduces erroneously high pressures east of the Ross Ice Shelf over Antarctica, a deficiency noted previously in T21 simulations. Little impact from the model change alone is found at the T106 resolution currently used for operational prediction, but the revised pressure-gradient formulation brings about a minor improvement in southern polar latitudes, and use of the full TR scheme reduces noise in the tropics.

The results concerning the pressure-gradient formulation apply to those spectral models that incorporate the semi-implicit treatment of the vorticity equation as developed originally for the ECMWF model. They are likely to be of most direct relevance for climate modelling, which typically employs lower horizontal resolution than routine weather prediction. This should be especially the case when the interest is principally in behaviour at high latitudes, for example in studies of sea-ice changes. We note that Roeckner et al. (1989) report a significantly improved representation of the Southern Hemisphere from a new version of a T21 climate model. This model was derived from the ECMWF forecast model, and the new version included the PG scheme whose development is reported here.

The idealized calculations of error in the standard scheme used at ECMWF for the calculation of geopotential at standard pressure levels reveal a bias towards erroneously low tropospheric heights. Correction of this by use of a reference temperature profile in the post-processing causes a clear improvement in the mean fit of the first-guess and analyzed heights to observed heights in a data assimilation experiment. Comparison with observations also shows a quite substantial improvement in the overall temperature structure of the analyses. The new initial states appear to be more consistent with the model dynamics and physics, since there is a reduction in the bias introduced by initialization and in the initial imbalance of the hydrological budget. A small beneficial impact from the revised pressure-gradient calculation in the assimilating model is also found. Forecasts are improved out to about the 4-day range, and results are rather inconclusive for longer time ranges.

The post-processing biases of the standard version depend on the vertical integration scheme for the model hydrostatic equation, on the method of interpolation from model to standard pressure levels, and on the disposition of model levels. It is thus difficult to assess the importance of these results for other forecasting systems.

The experiments using p_s as the spectrally-represented prognostic variable do not produce compelling evidence for a change from using ℓnp_s for medium-range prediction, since the impact of the change in variable on forecast quality appears to be extremely small, and there is a greater risk of instability of the semi-implicit time scheme in the version tested here. This p_s version may be a worthwhile option for models for long-term integration, in which case mass conservation becomes more important.

In view of the results presented in this report, the PG versions of the model and post-processing were introduced into operational forecasting in May 1990. The data assimilation test using the corrected tension-spline method for the vertical interpolation did not yield results which were generally superior, so at the same time the vertical interpolation was set to be generally linear, with quadratic interpolation for geopotential in the top layer of the model.

Acknowledgements

We are grateful to Per Undén for much advice on aspects of the data assimilation experiments, and Mats Hamrud for discussion and debugging of the tension-spline interpolation.

References

Arakawa, A. and M.J. Suarez, 1983: "Vertical differencing of the primitive equations in sigma coordinates". Mon. Wea. Rev., 111, 34-45.

Boer, G.J., N.A. McFarlane, R. Laprise, J.D. Henderson and J.-P. Blanchet, 1984: "The Canadian Climate Centre spectral atmospheric general circulation model". Atmos.-Ocean, 22, 397429.

Chen, J., Ji L. and Wu W., 1987: "Design and test of an improved scheme for global spectral model with reduced truncation error". Advances in Atmos. Sci., 4, 156-168.

Chen, J. and A.J. Simmons, 1990: "Sensitivity of medium-range weather forecasts to use of a reference atmosphere". Submitted to Advances in Atmos. Sci..

Cline, A.K., 1974: "Scalar- and planar-valued curve fitting using splines under tension". Communications of the ACM, 17, 218-220.

Corby, G.A., A. Gilchrist and R.L. Newson, 1972: "A general circulation model of the atmosphere suitable for long period integrations". Quart. J. Roy. Meteor. Soc., 98, 809-832.

Fels, S.B., D.J. Mahlman, M.D. Schwarzkopf and R.W. Sinclair, 1980: "Stratospheric sensitivity to perturbations in ozone and carbon dioxide. Radiative and dynamical response". J. Atmos. Sci., 37, 2265-2297.

Gary, J.M., 1973: "Estimate of truncation error in transformed coordinate, primitive equation atmospheric models". J. Atmos. Sci., 30, 223-233.

Gordon, H.B., 1981: "A flux formulation of the spectral atmospheric equations suitable for use in long-term climate modelling". Mon. Wea. Rev.,109, 56-64.

ICAO, 1964: "Manual of the ICAO Standard Atmosphere". U.S. Government Printing Office, Washington, D.C..

Janjic, Z.I., 1977: "Pressure gradient force and advection scheme used for forecasting with steep and small scale topography". Contrib. Atmos. Phys., 50, 186-199.

Jarraud, M., and U. Cubasch, 1979: "Horizontal diffusion experiments with the ECMWF spectral model". ECMWF Technical Memorandum No. 8, 17pp.

Jarraud, M., A.J. Simmons and M. Kanamitsu, 1988: "Sensitivity of medium range weather forecasts to the use of an envelope orography". Quart. J. Roy. Meteor. Soc., 114, 989-1025.

Kurihara, Y., 1968: "Note on finite difference expressions for the hydrostatic relation and pressure gradient force". Mon. Wea. Rev., 96, 654-656.

Laprise, R., 1985: "Mass correction in a spectral GCM". Research Activities in Atmospheric and Oceanic Modelling, Report No. 8, WMO, Geneva, 3.12- 3.13.

Laprise, R. and C. Girard, 1989: "A spectral general circulation model using a piecewise-constant finite-element representation on a hybrid vertical coordinate system". J. Climate, in press.

Lorenz, E.N., 1955: "Available potential energy and the maintenance of the general circulation". Tellus, 7, 157-167.

MacVean, M.K., 1983: "The effects of horizontal dissipation on baroclinic development in a spectral model". Quart. J. Roy. Meteor. Soc., 109, 771-783.

Mechoso, C.R., M.J. Suarez, K. Yamazaki, J.A. Spahr and A. Arakawa, 1982: "A study of the sensitivity of numerical forecasts to an upper boundary in the lower stratosphere". Mon. Wea. Rev., 110, 1984-1993.

Mesinger, F., 1982: "On the convergence and error problems of the calculation of the pressure gradient force in sigma coordinate models". Geophys. Astrophys. Fluid Dyn., 19, 105-117.

Mesinger, F., 1984: "A blocking technique for representation of mountains in atmospheric models". Riv. Meteor. Aeronautica, 44, 195-202.

Mesinger, F., Z.I. Janjic, S. Nickovic, D. Gavrilov and D.G. Deaven, 1988: "The step-mountain coordinate: Model description and performance for cases of Alpine lee cyclogenesis and for a case of Appalachian redevelopment". Mon. Wea. Rev., 116, 1493-1518.

Mesinger, F. and Z.I. Janjic, 1987: "Numerical techniques for the representation of mountains". Proceedings of 1986 ECMWF Seminar on Observation, Theory and Modelling of Orographic Effects, Vol.2, 29-80.

Nakamura, H., 1978: "Dynamical effects of mountains on the general circulation of the atmosphere. I: Development of finite-difference schemes suitable for incorporating mountains". J. Meteor. Soc. Japan, 56, 317-340.

Palmer, T.N., G.J. Shutts and R. Swinbank, 1986: "Alleviation of a systematic westerly bias in general circulation and numerical weather prediction models through an orographic gravity-wave drag parametrization". Quart. J. Roy. Meteor. Soc., 112, 1001-1039.

Phillips, N.A., 1957: "A coordinate having some special advantages for numerical forecasting". J. Meteor., 14, 184-185.

Phillips, N.A., 1973: " Principles of large scale numerical weather prediction". Dynamic Meteorology, P. Morel (Ed.), D. Reidel Publishing Co., Dordrecht, 1-96.

Roeckner, E., L. Dümenil, E. Kirk, F. Lunkeit, M. Ponater, B. Rockel, R. Sausen and U. Schlese, 1989: The Hamburg version of the EMCWF model (ECHAM). Research Activities in Atmospheric and Oceanic Modelling, 13, 7.1-7.4, WMO, Geneva.

Shaw, D.B., P. Lönnberg, A. Hollingsworth and P. Undén, 1987: "The 1984/85 revisions of the ECMWF assimilation system". Quart. J. Roy. Meteor. Soc., 113, 533-566.

Simmons, A.J., 1986: "Numerical prediction: Some results from operational forecasting at ECMWF". Advances in Geophysics, 29, 305-338.

Simmons, A.J., 1987: "Orography and the development of the ECMWF forecast model". Proceedings of 1986 ECMWF Seminar on Observation, Theory and Modelling of Orographic Effects, Vol.2, 129-163.

Simmons, A.J. and D.M. Burridge, 1981: "An energy and angular-momentum conserving vertical finite-difference scheme and hybrid vertical coordinates". Mon. Wea. Rev., 109, 758-766.

Simmons, A.J., and R. Strüfing, 1983: "Numerical forecasts of stratospheric warming events using a model with a hybrid vertical coordinate". Quart. J. Roy. Meteor. Soc., 109, 81-111.

Simmons, A.J., B.J. Hoskins and D.M. Burridge, 1978: "Stability of the semi-implicit time scheme". Mon. Wea. Rev., 106, 405-412.

Simmons, A.J., D.M. Burridge, M. Jarraud, C. Girard and W. Wergen, 1989: "The ECMWF medium-range prediction models. Development of the numerical formulations and the impact of increased resolution". Meteor. Atmos. Phys., 40, 28-60.

Sundqvist, H., 1976: "On vertical interpolation and truncation in connexion with use of sigma system models". Atmosphere, 14, 37-52.

Tibaldi, S., T. Palmer, C. Brankovic and U. Cubasch, 1990: "Extended range predictions with ECMWF models. II Influence of horizontal resolution on systematic error and forecast skill". Submitted to Quart. J. Roy. Meteor. Soc..

Wallace, J.M., S. Tibaldi and A.J. Simmons, 1983: "Reduction of systematic forecast errors in the ECMWF model through the introduction of an envelope orography". Quart. J. Roy. Meteor. Soc., 109, 683-717.

Xu, J.S., H. von Storch and H. van Loon, 1990: "The performance of four spectral GCMs in the southern hemisphere: The January and July climatology and the semi-annual wave". J. Climate, 3, in press.

Zeng, Q., 1963: Characteristic parameters and dynamical equations of atmospheric motion. Acta Meteorologica Sinica, 33, 472-483 (in Chinese).

Zeng, Q., 1965: On the design of finite difference schemes for solving the primitive equations. Technical Report, Institute of Geophysics and Meteorology, Academica Sinica (in Chinese).

Zhang, D., H. Seng and L. Ji, 1990: Development and test of hydrostatic extraction scheme in spectral model. Advances in Atmos. Sci., 7, 142-153.

TECHNICAL REPORTS

No. 1 A case study of a ten day prediction.
K. Arpe, L. Bengtsson, A. Hollingsworth and Z. Janjic. September, 1976

No. 2 The effect of arithmetic precision on some meteorological integrations.
A.P.M. Baede, D. Dent and A. Hollingsworth. December, 1976

No. 3 Mixed-radix fourier transforms without reordering.
C. Temperton. February, 1977

No. 4 A model for medium range weather forecasts - adiabatic formulation.
D.M. Burridge and J. Haseler. March, 1977

No. 5 A study of some parameterisations of sub-grid processes in a baroclinic wave in a two dimensional model.
A. Hollingsworth. July, 1977

No. 6 The ECMWF analysis and data assimilation scheme: analysis of mass and wind field.
A. Lorenc, I. Rutherford and G. Larsen. December, 1977

No. 7 A ten-day high-resolution non-adiabatic spectral integration; a comparative study.
A.P.M. Baede and A.W. Hansen. October, 1977

No. 8 On the asymptotic behaviour of simple stochastic-dynamic systems.
A. Wiin-Nielsen. November, 1977

No. 9 On balance requirements as initial conditions.
A. Wiin-Nielsen. October, 1978

No. 10 ECMWF model parameterisation of sub-grid scale processes.
M. Tiedtke, J-F. Geleyn, A. Hollingsworth, and J-F. Louis. January, 1979

No. 11 Normal mode initialization for a multi-level grid-point model.
C. Temperton and D.L. Williamson. April, 1979

No. 12 Data assimilation experiments.
R. Seaman. October, 1978

No. 13 Comparison of medium range forecasts made with two parameterisation schemes.
A. Hollingsworth, K. Arpe, M. Tiedkte, M. Capaldo, H. Savijarvi, O. Akesson and J.A. Woods. October, 1978

No. 14 On initial conditions for non-hydrostatic models.
A.C. Wiin-Nielsen. November, 1978

No. 15 Adiabatic formulation and organization of ECMWF's spectral model.
A.P.M. Baede, M. Jarraud and U. Cubasch. November, 1979

No. 16 Model studies of a developing boundary layer over the ocean.
H. Okland. November, 1979

No. 17 The response of a global barotropic model to forcing by large scale orography.
J. Quiby. January 1980.

No. 18 Confidence limits for verification and energetic studies.
K. Arpe. May, 1980

No. 19 A low order barotropic model on the sphere with orographic and newtonian forcing.
E. Kallen. July, 1980

No. 20 A review of the normal mode initialization method.
Du Xing-yuan. August, 1980

No. 21 The adjoint equation technique applied to meteorological problems.
G. Kontarev. September, 1980

No. 22 The use of empirical methods for mesoscale pressure forecasts.
P. Bergthorsson. November, 1980

No. 23 Comparison of medium range weather forecasts made with models using spectral or finite difference techniques in the horizontal.
M. Jarraud, C. Girard and U. Cubasch. February, 1981

No. 24 On the average error of an ensemble of forecasts.
J. Derome. February, 1981

No. 25 On the atmospheric factors affecting the Levantine Sea.
E. Ozsoy. May, 1981

No. 26 Tropical influences on stationary wave motion in middle and high latitudes.
A.J. Simmons. August, 1981

No. 27 The energy budgets in North America, North Atlantic and Europe based on ECMWF analysis and forecasts.
H. Savijarvi. November, 1981

No. 28 An energy and angular momentum conserving finite-difference scheme, hybrid coordinates and medium range weather forecasts.
A.J. Simmons and R. Strüfing. November, 1981

No. 29 Orographic influences on Mediterranean lee cyclogenesis and European blocking in a global numerical model.
S. Tibaldi and A. Buzzi. February, 1982

No. 30 Review and re-assessment of ECNET - A private network with open architecture.
A. Haag, F. Konigshofer and P. Quoilin. May, 1982

No. 31 An investigation of the impact at middle and high latitudes of tropical forecast errors.
J. Haseler. August, 1982

No. 32 Short and medium range forecast differences between a spectral and grid point model. An extensive quasi-operational comparison. C. Girard and M. Jarraud
August, 1982

No. 33 Numerical simulations of a case of blocking: The effects of orography and land-sea contrast.
L.R. Ji and S. Tibaldi. September, 1982

No. 34 The impact of cloud track wind data on global analyses and medium range forecasts.
P. Kallberg, S. Uppala, N. Gustafsson and J. Pailleux. December, 1982

No. 35 Energy budget calculations at ECMWF. Part 1: Analyses 1980-81.
E. Oriol. December, 1982

No. 36 Operational verification of ECMWF forecast fields and results for 1980-1981.
R. Nieminen. February, 1983

No. 37 High resolution experiments with the ECMWF model: a case study.
L. Dell'Osso. September, 1983

No. 38 The response of the ECMWF global model to the El-Nino anomaly in extended range prediction experiments.
U. Cubasch. September, 1983

No. 39 On the parameterisation of vertical diffusion in large-scale atmospheric models.
M.J. Manton. December, 1983

No. 40 Spectral characteristics of the ECMWF objective analysis system.
R. Daley. December, 1983

No. 41 Systematic errors in the baroclinic waves of the ECMWF model.
E. Klinker and M. Capaldo. February, 1984

No. 42 On long stationary and transient atmospheric waves.
A.C. Wiin-Nielsen. August, 1984

No. 43 A new convective adjustment scheme.
A.K. Betts and M.J. Miller. October, 1984

No. 44 Numerical experiments on the simulation of the 1979 Asian summer monsoon.
U.C. Mohanty, R.P. Pearce and M. Tiedtke. October, 1984

No. 45 The effect of mechanical forcing on the formation of a mesoscale vortex.
G-X. Wu and S-J. Chen. October, 1984.

No. 46 Cloud prediction in the ECMWF model.
J. Slingo and B. Ritter. January, 1985

No. 47 Impact of aircraft wind data on ECMWF analyses and forecasts during the FGGE period, 8-19 November, 1979.
A.P.M. Baede, P. Kallberg and S. Uppala. March, 1985

No. 48 A numerical case study of East Asian coastal cyclogenesis.
Shou-jun Chen and L. Dell'Osso. May, 1985

No. 49 A study of the predictability of the ECMWF operational forecast model in the tropics.
M. Kanamitsu. September, 1985

No. 50 On the development of orographic cyclones.
D. Radinovic. June, 1985

No. 51 Climatology and system error of rainfall forecasts at ECMWF.
F. Molteni and S. Tibaldi. October, 1985

No. 52 Impact of modified physical processes on the tropical simulation in the ECMWF model.
U.C. Mohanty, J.M. Slingo and M. Tiedtke. October, 1985

No. 53 The performance and systematic errors of the ECMWF tropical forecasts (1982-1984).
W.A. Heckley. November, 1985

No. 54 Finite element schemes for the vertical discretization of the ECMWF forecast model using linear elements.
D.M. Burridge, J. Steppeler and R. Strüfing. January, 1986

No. 55 Finite element schemes for the vertical discretization of the ECMWF forecast model using quadratic and cubic elements.
J. Steppeler. February, 1986

No. 56 Sensitivity of medium-range weather forecasts to the use of an envelope orography.
M. Jarraud, A.J. Simmons and M. Kanamitsu. September, 1986

No. 57 Zonal diagnostics of the ECMWF 1984-85 operational analyses and forecasts.
C. Brankovic. October, 1986

No. 58 An evaluation of the performance of the ECMWF operational forecasting system in analysing and forecasting tropical easterly wave disturbances. Part 1: Synoptic investigation.
R.J. Reed, A. Hollingsworth, W.A. Heckley and F. Delsol. September, 1986

No. 59 Diabatic nonlinear normal mode initialisation for a spectral model with a hybrid vertical coordinate.
W. Wergen. January, 1987

No. 60 An evaluation of the performance of the ECMWF operational forecasting system in analysing and forecasting tropical easterly wave disturbances. Part 2: Spectral investigation.
R.J. Reed, E. Klinker and A. Hollingsworth. January, 1987

No. 61 Empirical orthogonal function analysis in the zonal and eddy components of 500 mb height fields in the Northern extratropics.
F. Molteni. January, 1987

No. 62 Atmospheric effective angular momentum functions for 1986-1987.
G. Sakellarides. February 1989.

No. 63 A verification study of the global WAM model. December 1987 - November 1988
L. Zambresky. Date required.

No. 64 Impact of a change of radiation transfer scheme in the ECMWF model.
J-J. Morcrette. Date required.

No. 65 The ECMWF analysis-forecst system during AMEX
K. Puri, P. Lönnberg and M. Miller. May 1990.